A NEW SOLID-STATE NMR METHOD REVEALS THE INFLUENCE OF CHAIN STRUCTURE AND THERMAL HISTORY ON THE CRYSTAL-AMORPHOUS INTERFACE IN POLYETHYLENES

By
ARIFUZZAMAN TAPASH

Bachelor of Science in Applied Chemistry & Chem. Tech.
University of Dhaka
Dhaka
2005

Masters of Science in Applied Chemistry & Chem. Eng.
University of Dhaka
Dhaka
2006

Submitted to the Faculty of the
Graduate College of the
Oklahoma State University
in partial fulfillment of
the requirements for
the Degree of
DOCTOR OF PHILOSOPHY
May, 2016

A NEW SOLID-STATE NMR METHOD REVEALS THE

INFLUENCE OF CHAIN STRUCTURE AND THERMAL HISTORY ON

THE CRYSTAL-AMORPHOUS INTERFACE IN POLYETHYLENES

Dissertation Approved:

Dr. Jeffery L. White

Dissertation Adviser

Dr. Frank D. Blum

Dr. Toby Nelson

Dr. Jimmie Weaver

Dr. Rob Whiteley

Name: ARIFUZZAMAN TAPASH

Date of Degree: MAY, 2016

Title of Study: A NEW SOLID-STATE NMR METHOD REVEALS THE INFLUENCE OF CHAIN STRUCTURE AND THERMAL HISTORY ON THE CRYSTAL-AMORPHOUS INTERFACE IN POLYETHYLENES.

Major Field: CHEMISTRY

Abstract: Clear understanding of polymer morphology is important as it is directly related to the final properties. A simple solid-state NMR method is presented in this contribution to quantitatively determine the distribution of solid polyethylene chain segments in different morphological regions. The rigid chain in the crystalline phase with all-trans chain conformations, the non-crystalline (amorphous) mixed trans-gauche chains undergoing essentially isotropic reorientation, all-trans chains with higher mobility (mobile all-trans), and non-crystalline chains with limited mobility (constrained amorphous) fractions were reliably quantified using a new double-acquisition solid-state ^{13}C NMR experiment. A wide range of well-characterized PE samples was studied, which reveals that the amount of interface region increases with the chain length of linear metallocene-PE. Topologically different polyethylenes that contain short-chain branches (SCB), long-chain branches (LCB), and LCB's with SCB's exhibit unique morphological behavior relative to the linear PE's of similar M_w. The method also reveals the variations in morphology due to different thermal histories. Thermally quenched polyethylene was found to have higher interface content than that of the annealed or untreated PEs. Phase composition results obtained by this simple experiment are quantitative, reliable and reproducible as all of the data was collected in a single experiment. The results suggest a route to large-scale design and control of interfacial morphology in polyethylenes and related properties.

In a separate project, a ^{1}H NMR experiment based on slow/fast magic-angle spinning (MAS) and a spin-counting strategy are presented to quantitatively determine the amount of soft and hard phase of styrene-butadiene gradient copolymers in component specific resolution. The experiments provide bulk rigidity and the amount of polybutadiene (or polystyrene) partitioned into both soft and hard phases. It was found that the partitioning of each comonomer depends on the synthesis conditions and we propose that the hard-soft interface is responsible for the differential partitioning.

Both experimental methods presented here can also be used to study different polymer systems.

TABLE OF CONTENTS

LIST OF TABLES

LIST OF FIGURES

CHAPTER 1

1 MOTIVATION

Polyethylene (PE) is the major type of polyolefins on the market, and their demand continues to increase due to their excellent physical and mechanical properties, chemical inertness, non-toxicity, energy efficient production, low cost and readily available raw materials. It contributes more than 50% of all polyolefin global consumption.[1] So many products around us ranging from our necessities such as soft plastic bags, storage bottles, and containers, home furniture, children's toys, etc., to special applications like gas and water pipelines, automotive applications, bullet-proof vest, and biomedical implants are made from polyethylene. Because of its usefulness, PE is of considerable industrial importance and is produced by millions of tons each year. Its versatility makes it an attractive commodity to produce. Often it has been predicted that polyethylene would lose market shares to new high-performance plastics, but this has never happened because of the continuous improvements in their performance by extensive research.[2]

The extensive and still increasing usage of polyethylene is due to their unique and widely variable physical and mechanical properties. The properties of solid polyethylene depend on the structural organization of the polymer chains in the solid state, including morphology, local structure, phase behavior, and chain dynamics.[3] It is a very old polymer, and numerous research has been done to understand its morphology and properties in different conditions.[4] However, most of the studies mainly focused on crystalline or amorphous phase. Recently it was found that the crystalline-amorphous

interface has an significant effect on controlling the final properties.[5] To improve and optimize macromolecular behavior and mechanical properties, it is very important to understand the structure-property relationship, and to understand the microscopic and molecular parameters in solid state, the focus needs to be on the development of modern experimental techniques.

Various experimental techniques can be used to probe the microscopic properties of polymers.[6] Fourier transform infrared (FT-IR)[7] and Raman spectroscopy[8] can determine the molecular-scale characterization. Small angle X-ray scattering (SASX),[9] wide-angle X-ray scattering (WAXS), neutron diffraction,[10] electron scattering and electron microscopy[11] (TEM, SEM), AFM[12] techniques can be used to characterize the local order of macromolecules.

Different NMR methods, such as, proton FID study, relaxation experiments, spin diffusion, cross polarization, deuterium NMR, etc. have successfully been applied to polyethylene which provide structural and dynamic information about their morphology that subsequently can be correlated with the macroscopic properties.[4b, 13] However, those methods are incapable of providing reliable and quantitative data about the crystalline-amorphous interface. So, to clearly understand the behavior of crystal-amorphous interface of polyethylene and to correlate the phase composition with the synthesis conditions and the final properties, it is necessary to develop an experimental technique which can provide complete, quantitative and reliable information of polyethylene morphology without affecting the microstructure in solid-state.

The aim of this doctoral research is to develop a robust experimental method based on solid-state nuclear magnetic resonance (NMR) spectroscopy to study the distribution of polyethylene (PE) chain in different morphological regions, and to investigate the influence of chain length and chain architecture, as well as the different thermal histories, on the phase composition of PE's. In a separate project, slow/fast

magic-angle spinning (MAS) ^{1}H NMR experimental method is developed and applied to study the component specific heterogeneity of styrene-butadiene gradient copolymer.

This dissertation is documented in the following format:

It begins with *Chapter 2* that presents a brief discussion of the historical background of polyethylene and theoretical discussion on polyethylene morphology, as well as the theoretical background of nuclear magnetic solid-state NMR spectroscopy. Its objectives are to help the reader build some fundamentals related to the studies undertaken by the author.

Chapter 3 will discuss in detail about the solid-state NMR experimental method that was developed and used to study the morphology of polyethylenes in this research.

In *Chapter 4,* the results of the study on the 'as synthesized' polyethylene samples are discussed and the influence of chain length and chain architecture on crystalline-amorphous interface composition is reported.

Chapter 5 will discuss the thermal history effect on the polyethylene morphology. A wide variety of linear polyethylene samples of different molecular weight and different thermal histories were characterized by the developed method, and the findings are reported in *Chapter 5.*

Chapter 6 will focus on a different project. In *Chapter 6,* a slow/fast MAS proton solid-state NMR method will be introduced which reveals the morphological heterogeneity of styrene-butadiene gradient copolymer, and the results of the study will be presented. A summary of the complete dissertation is given in Chapter 7.

Since Chapter 4 and 6 have been written as manuscripts for publication in a scientific journal, the corresponding sections are essentially “manuscript-based,” and therefore, certain materials may be repeated in the different chapters.

CHAPTER 2

2 INTRODUCTION AND THEORETICAL BACKGROUND

2.1 Historical Background of Polyethylene

The earliest report on the polyethylene synthesis was made in 1898 by Von Pechmann when he observed a white substance that formed when diazomethane was dissolved in ether.[14] Later, Bamberger and Tschirner[15] produced and characterized the compound from the same technique as Pechmann. The macromolecule they produced was a waxy, white solid substance containing simple and long repeating methylene units, thus, Pechmann named this composition as "polymethylene". Unlike polyethylene, which must contain an even number of repeating carbon atoms, polymethylene can have any number of repeating carbon atoms. They stated that its structure was $(CH_2)_n$, and it had a melting point of 128 ^oC.

The industrial development for the synthesis of polyethylene took place in the early 1930's after a small amount of polyethylene was accidently produced at British company, Imperial Chemical Industries (ICI). ICI established a research program with the goal of investigating the high-pressure chemistry of selected organic compounds which also include ethylene.[6a] Peacock[6a] reports that on 29th March 1933, Eric Fawcett and Reginald Gibson discovered a sub-gram quantity of a white waxy polymer of ethylene lining the reaction vessel of a failed experiment in which ethylene and benzaldehyde had been reacted. The development of a reproducible set of polymerization conditions was not found until December 1935 by a fellow ICI chemist, Michael Perrin. The first set of experimental conditions yielded eight grams of the

highly ductile polyethylene having a melting point in the range of 110 ^{o}C. His discovery is the basis for all future low-density polyethylene materials produced to date.[6a]

The advent of World War II (WWII) led ICI to secure the first manufacturing patent in 1936.[16] The first high-pressure production plant in 1937 demonstrated the successful development of polyethylene, and by the outbreak of WWII, ICI was commercially producing polyethylene. At that time, the inherent flexibility and chemical inertness of this new material were investigated for potential electrical insulating and barrier materials. The impact of polyethylene was most extensively seen in the areas of insulator materials, and by the end of the war, polyethylene was utilized in insulating radar components, submarine communication cables, and telecommunication cables linking France and England. The benefits brought about by using polyethylene materials were so great that both Union Carbide and the DuPont companies bought the rights from ICI to commercially produce polyethylene in the United States. Commercial output of polyethylene began in 1943 overtaking the initial production by Great Britain.[6a]

The expansion of products made from polyethylene opened new markets for molding small parts and extruded cable wire insulation. Despite the numerous applications and good mechanical properties, polyethylene production and expansion into other various markets had been limited. One major problem was the requirement of high pressure for polyethylene manufacture which needs high energy input. Moreover, the ICI polyethylene was highly branched materials with low tensile strength, flexibility, and softening temperature. Subsequent landmarks in polyethylene's history were the modification and control of these factors influencing the overall behavior and performance of this simple material.

In 1953, Karl Ziegler and his group discovered that zirconium and titanium salts produce polyethylene of high molar masses when combined with an aluminum co-catalyst.[17] Meanwhile, Giulio Natta found out that isotactic polypropylene (iPP) can be synthesized with certain conditioning and

preparations of the catalyst. Both these discoveries led to widespread commercialization of some key thermoplastics such as linear low-density polyethylene, high-density polyethylene, and polypropylene. Both Ziegler and Natta were awarded the Nobel Prize for chemistry in 1963 for their contributions.[17a, 18] Later on, Kaminsky and Sinn discovered several catalyst systems based on metallocene complexes that are highly active in ethylene polymerization reactions. They also discovered enormous increases in the activity of the metallocene catalysts when methylaluminoxane (MAO) was used as a co-catalyst.[19] These new catalysts offer more control in molecular stereo-regulation as well as uniformity in comonomer insertion as compared to Ziegler-Natta catalysts.

2.2 Main Types of Polyethylenes

Although polyethylene is a chemically simple polymer, different manufacturing conditions, catalysts used, and the post-synthetic treatments can produce many different types of PE based on molecular weight, branch types, and branch contents. Final properties can vary significantly. Polyethylene can be classified into many types such as ultra-high-molecular-weight polyethylene (UHMWPE), ultra-low-molecular-weight polyethylene (ULMWPE or PE-WAX), high-molecular-weight polyethylene (HMWPE), high-density polyethylene (HDPE), medium-density polyethylene (MDPE), linear low-density polyethylene (LLDPE), low-density polyethylene (LDPE) and very-low-density polyethylene (VLDPE). However, LDPE, LLDPE and HDPE (Figure 2.1) are the most important in terms of commercial output.[20]

2.2.1 Low-density polyethylene (LDPE)

Low-density polyethylene (LDPE) is the homopolymer of ethylene and is manufactured using high pressures usually ranging between 82 and 286 MPa and temperature in the range of 132 to 332 ^{o}C.[20e] The density or the crystallinity of the resultant resin can be controlled by the manufacturing temperature and conditions. The molar mass and the molar mass distribution depend upon the pressure used as well as

the concentration of the chain transfer agents. One important feature that characterizes the molecular structure of LDPE is long chain branching (LCB). Long chain branching gives LDPE a more complex structure as compared to LLDPE or HDPE. Molar mass increases with decreased temperature or increased pressure and LCB increases with temperature. It is extremely difficult to control the level of long chain branching and batches may vary significantly. A small amount of oxygen or organic peroxide is used as an initiator for the reaction. Molar masses are usually in the range of 10,000 to 50,000 g/mol.[21] The density of LDPE ranges from 0.910 – 0.925 g/cm^3. The biggest challenges in LDPE manufacture include the high capital investment for commercial plant construction, high-pressure operation requirement, and high energy consumption in production.[20e] Until recently, the production of LDPE has been limited to free radical process only.[22]

2.2.2 Linear low-density polyethylene (LLDPE)

Linear low-density polyethylenes (LLDPEs) are made through the copolymerization of ethylene and a α-olefin, for example, 1-butene, 1-hexene, 1-octene, and 4-methyl-1-pentene.[1, 23] The α-olefin introduces short chain branches (SCB) on the polymer chain backbone. The average distance between these branches along the main chain is approximately 25 – 100 carbon atoms. The methylene sequences between these branches can fold and arrange themselves into lamellae while the branches protrude into the amorphous regions. In the absence of the comonomer, the crystallizable sequences are longer and form thicker lamellae, resulting in resins with high crystallinities. The type of branch on the central

backbone chain is controlled by using appropriate type comonomer in LLDPE synthesis. LLDPEs can be produced using Ziegler-Natta,[24] Phillips, or single-site metallocene catalysts.[25] However, such resins cannot be produced by free radical polymerization.[19] Of these catalysts, Ziegler-Natta heterogeneous catalysts are widely used, and the resins produced by these catalysts are characterized by considerable heterogeneity regarding of molar mass and chemical composition. This results in heterogeneity in the melting behavior.[23] On the other hand, metallocene catalyst produces LLDPE resins with uniform molecular structures (i.e. narrow molar mass and chemical composition distributions).[2a, 26] A more uniform arrangement of comonomer units allows for better predictability of LLDPE resin properties. Crystallizable methylene sequences of almost uniform length can be obtained as opposed to when Ziegler-Natta type catalysts are used.

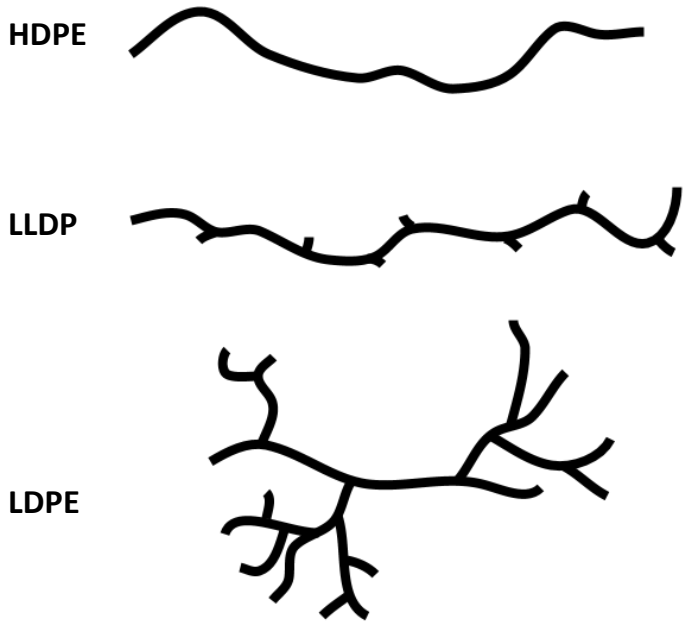

Figure 2.1. Schematic representation of different types of polyethylene chains; high - density polyethylene (HDPE), linear low-density polyethylene (LLDPE) and low-density polyethylene (LDPE).

The linearity of the copolymer chains in LLDPE (as opposed to LDPE) provides strength while branching provides toughness.[27] LLDPE has higher tensile strength, puncture resistance, tear properties

and elongation than LDPE.[28] Density of LLDPE is typically 0.915 – 0.930 g/cm^3.[19] General advantages of LLDPE over LDPE are improved chemical resistance, improved performance at low and high temperatures, higher surface gloss, higher strength at a given density, better heat sealing properties and a greater resistance to environmental stress in some applications.[27]

2.2.3 High-density polyethylene (HDPE)

HDPE is one of the largest volume commodity plastics produced in the world.[20e] Commercial production of HDPE was started in 1956 by Phillips Petroleum Co. (United States) and by Hoechst (Europe). HDPE is a linear, nonpolar thermoplastic with up to 80% crystallinity.[20e] The density of HDPE ranges from 0.942 – 0.965 g/cm^3. Due to its linear structure, molecules tend to align themselves in the direction of flow, and this makes the tear strength of the film much lower as compared to LDPE or LLDPE. HDPE can be produced by solution, slurry or gas phase processes.[29]

2.3 Catalysts Used in Polyethylene Manufacture

Since the accidental discovery of olefin polymerization, the development of catalysts has been fuelled by the need for more control over the molecular architecture and properties of polyethylene at a molecular level. Catalysts that have been developed to date offer varying controls over molar mass, its distribution, and comonomer insertion.

2.3.1 Ziegler – Natta catalysts[17b, 30]

Catalyst systems used for Ziegler – Natta polymerizations consist of a co-catalyst or activator and the catalyst itself. Commonly used Ziegler – Natta catalysts are $TiCl_3$ and $TiCl_4$. Active sites of Ziegler – Natta catalysts are formed due to the interaction between a transition metal compound and an organometallic co-catalyst. This is true for metallocene catalysts as well. Common co-catalysts include

triethylaluminum (TEA), diethylaluminum chloride (DEAC), and triisobutyaluminium (TIBA). The presence of the many types of active sites in the Ziegler- Natta catalyst systems produce polyolefin resins with broad chemical and molar mass characteristics.

2.3.2 Metallocene catalysts[6a, 19, 30a]

Metallocene catalysts are also referred to as single site catalysts because all their metal cation active sites are assumed to be identical during polymerization reactions. Therefore, the homogeneity of active sites in metallocene catalysts results in very narrow chemical compositions and molar mass distributions. Development of these catalysts is primarily attributed to the work of Kaminsky and Sinn. Metallocene catalysts are organometallic compounds in which metal centers are sandwiched between aromatic ligands. Ligands that are usually used are dicyclopentadienyl, indenyl or fluorenyl groups and these have a significant influence on the molar mass, polymerization activity, comonomer insertion as well as the overall microstructure of the polyolefin produced. The metal centers also greatly affect the yields and the molar masses of the resins produced.

2.3.3 Phillips catalysts[31]

The Phillips catalyst is a chromium-based catalyst supported on silica. These type of catalysts were discovered by Hogan and Banks in 1951.[31a] Since their discovery, there is still no consensus on issues regarding the oxidation state of the active site, molecular structure of the catalyst and the polymerization mechanism. While propagation and termination steps for ethylene are well understood, the same cannot be said about the initiation step with the Phillips catalysts. Supported Phillips catalysts are used to produce 40-50% of the world's HDPE.[31c] These catalysts are also able to copolymerize ethylene with various 1-olefins, but the comonomer incorporation is random. Also, the molecular weight distribution of the

polyethylenes produced is significantly larger than that of the resins produced by metallocene as well as Ziegler – Natta type catalysts.

2.4 Polyethylene Morphology

Polyethylene consists of a backbone of a great number of covalently linked carbon atoms (Figure 2.2). It is now well known that, polyethylene is a semi-crystalline thermoplastic polymer which can be considered to be a composite of dense crystalline segments embedded within an unorganized amorphous matrix. The morphology of polyethylene has been extensively studied over the past four decades, and excellent books[32] and review papers[33] on this topic are available. The following discussion provided aims to familiarize the readers with the morphological basis of semi-crystalline polyethylene.

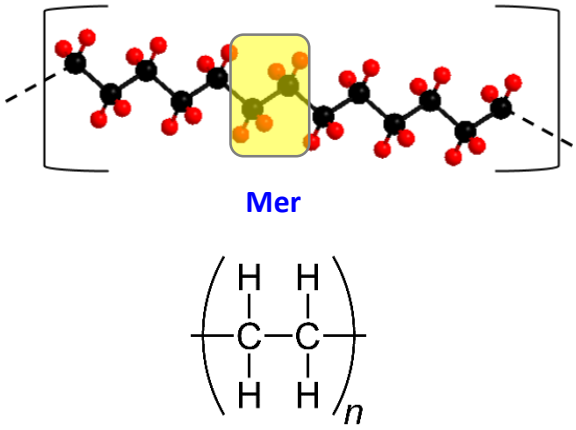

Figure 2.2. Chemical structure of the polyethylene chain.

2.4.1 Crystalline lamellae

It is now universally accepted that polymers with flexible chains crystallize as thin lamellae with the advent of chain folding. Although this idea was initially reported by Sauter and Stork in the 1930s,[34] the concept of folding macromolecules was dismissed and believed to be unlikely due to molecular entanglements. In the linear polyethylene, due to the small atomic volume of hydrogen, the steric effects

between alkane units against the chemical bond rotation is the lowest. The uniform nonpolar molecular chains eliminate intra- or intermolecular electrostatic interactions. Therefore, long polyethylene chains are highly flexible. Also, due to the total symmetric structure along the backbone, these n-alkane chains actively intent to fold back to themselves in regular arrays.[35] Figure 2.3(a) shows a regular tight chain folding model, in which the chains form 180^{o} folds then re-enter into the nearest adjacent neighboring site in the (001) plane. This type of fold is known as the adjacent re-entry model.[35-36]

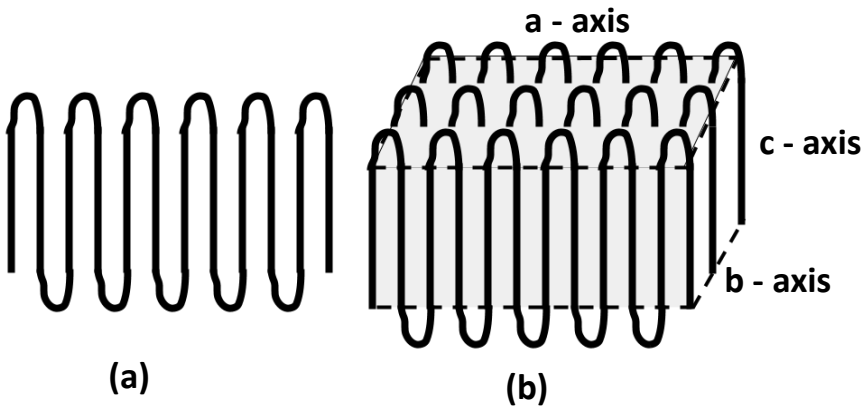

Figure 2.3. Schematic representation of, (a) the regular tight chain folds on polyethylene, and (2) the lamella structure with stacks of dense chain arrays.

A single regular array is not able to exist stably due to the high surface energy. Thus, either some arrays tend to pack themselves together in a stack, or the free chains on the array surface continue the folding procedure at the adjacent positions.[37] The above processes enable the arrays to grow in a third dimension, resulting in a layered structure with a certain thickness, as shown in Figure 2.3(b). This structure is conventionally known as a lamella, and it is the basic building block for the larger morphologies, such as spherulites, row-structures, transcrystalline layers, or dendrites, etc., observed in crystalline macromolecules. The above spontaneous assembly steps are the fundamental reasons for the

formation of the crystalline structures in PE.[38] The direction along the molecular chains in the lamella is commonly defined as the 'c' axis.

Herrmann *et al.* in 1930 postulated a fringe-micelle crystallization model which proposes that a single, chain-extended polymer stem can contribute to several different crystalline and amorphous domains.[39] The concept did predict the observed mechanical properties of polyethylene; however, the model was unable to associate the fine details (tie molecules and loops) seen with spherulites of helix formation in polypropylenes.

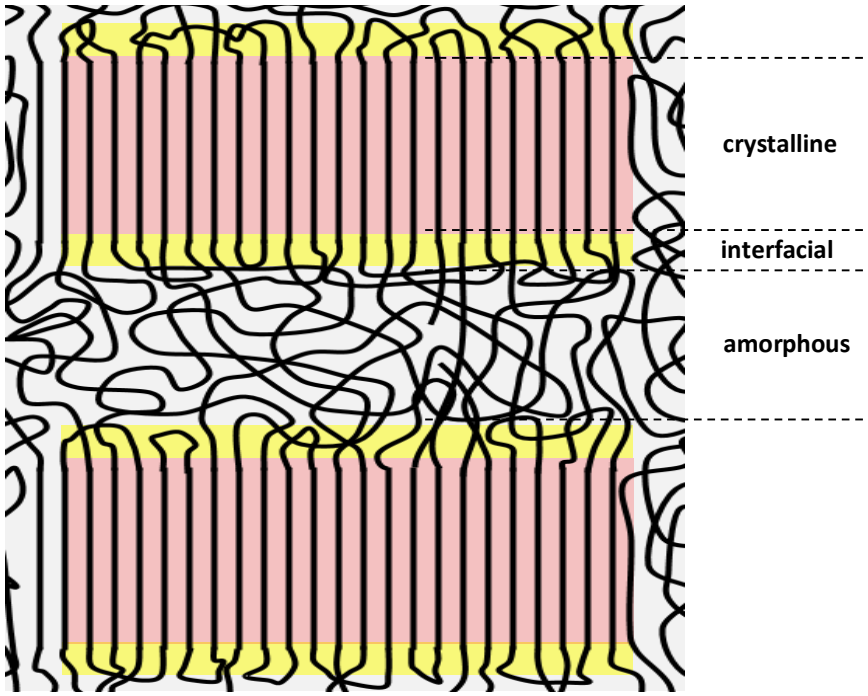

Figure 2.4. The three-component phase model of polyethylene. The pink region represents the crystalline phase, the gray region represents the amorphous phase, and the yellow region is for the interface.

Several groups[40] in the 1950s showed it was possible to grow single crystals of polymeric materials. After that, Keller[35], Fischer[38], and Till[41] independently published the first evidence for a chain-folded, solution grown polyethylene. The most recognizable switchboard model was proposed by Flory.[42]

The collection of present-day observations produce a crystallization model that can be represented in terms of a three-phase model as outlined in Figure 2.4. The model constitutes a well-defined highly ordered phase surrounded by a 'liquid-like' disordered phase. The crystalline and the amorphous phases are connected through an intermediate phase which is called the 'interface'. Although the nature of this interface is not well understood, Figure 2.4 represents the presently accepted model.

To understand the crystal structure, Alex Muller[43] completed the most exhaustive study on n-paraffins obtaining the single crystal diffraction pattern for $C_{29}H_{60}$ in the mid-1920s. It was concluded that the material packed in parallel zigzag planes, in the orthorhombic crystal structure. Later the similar structure was also observed for linear polymeric alkanes, such as polyethylene.[44] The mapping of individual cells was categorized by Vand in accordance with the repeating methylene sequences.[45] By far, Vand's rendition of the orthorhombic unit cell, outlined for the *ab* face in Figure 2.5, is the most common structural representation encountered in aliphatic polymers.

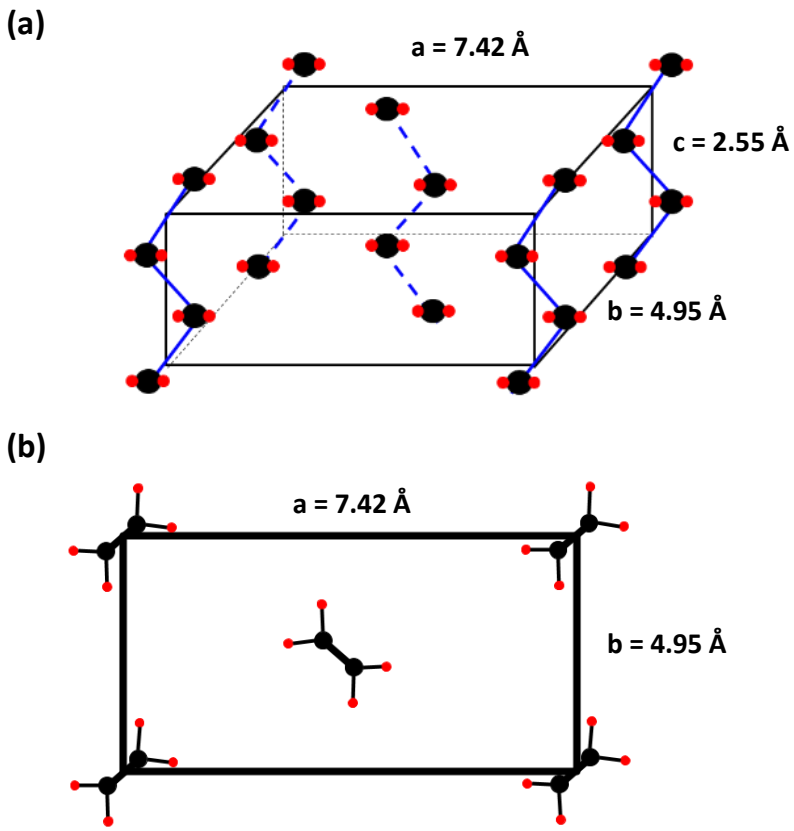

Figure 2.5. Polyethylene orthorhombic crystal lattice, (a) orthogonal view, and (b) along the c-axis.

2.4.2 Phase composition and chain types

In total, polyethylene bulk is believed to be consist of many crystalline microdomains embedded in the amorphous matrix. Between the crystalline and amorphous phases, a third phase exists which structure is not clearly understood yet. In the crystalline phase, the PE chains exist as in all-trans conformation. Due to the highly ordered orientation of all-trans chains in the crystal unit cell, the chain mobility is highly restricted. However, Spiess and Schmidt-Rohr[46] showed that chain diffusion can occur from the crystalline region to the amorphous region through the interface. The PE chains in the amorphous phase are highly mobile, and because of entanglement between chains, those are in a mixed trans-gauche conformation. It is believed that the amorphous chains undergo isotropic reorientation maintaining an equilibrium trans-gauche density along the chains. Besides the rigid all-trans chains in the

crystalline phase and the highly mobile trans-gauche chains in the amorphous phase, two different types of chains were reported in the literature, mobile all-trans chain, and constrained amorphous chain.[4c, 47] The interface regions are believed to be composed of these two types of chains. During the 180^{o} tight fold, parts of the chain segment have to stay out of the crystalline lamella before chains re-enter into the adjacent positions. This protruded segment of the chain might be the source of constrained trans-gauche chain which mobility is restricted due to tight folding. In fact, adjacent re-entry is not the only manner applicable during the chain packing**.** The continuous chains from the crystalline phase can be connected to an adjacent lamella, which is called tie chains; or it can fold back on themselves to the original one but not re-enter at the adjacent position forming a loop; or the chain can terminate as chain ends forming cilia (Figure 2.4).[48] These different types of chain extension from the crystalline region, like loose loops, ties, and cilia, form the amorphous regions where the chains are loosely packed. The part of the cilia and tie chains which are near to the crystal surface might be the highly mobile chains which are in all-trans conformation.

The coexistence of the three phases with different chain conformations and molecular properties, their interactions and connection with each other, make PE desirably stiff and meanwhile tough for applications. Many physical properties of PE such as stiffness, toughness, tensile strength, and impact strength are related to the phase composition. Therefore, to understand the mechanical behavior and to tailor the applications of PE, it is essential to characterize the phase composition precisely.

2.5 Polyethylene Molecular Dynamics[49]

In addition to the different types of chain order, the intrinsic phase differences in the semi-crystalline polymers are associated with different molecular dynamics. The molecular dynamics is related

to the specific chain motions and relaxations which allow classifying the phases by different analytical techniques.

2.5.1 Translation and rotation in the crystalline phase[49]

The chain mobility in the crystalline phase is highly restricted due to the compact arrangements. The chain motions in this region are accomplished by the coordinated movements with other repeat units in the lamella. Figure 2.6(a) describes the typical molecular motions in the crystalline phase, in which two different movements, translation, and rotation, are exhibited. The rotation movement, also known as 180^{o} flip, is achieved by a screw rotation of the whole chain segment about the `c' axis. Both the rigid and flexible rotations accompany by a half repeat unit shift along the `c' axis and cause one end of the chain segment to translate out of the lamella, as shown in Figure 2.6(a).

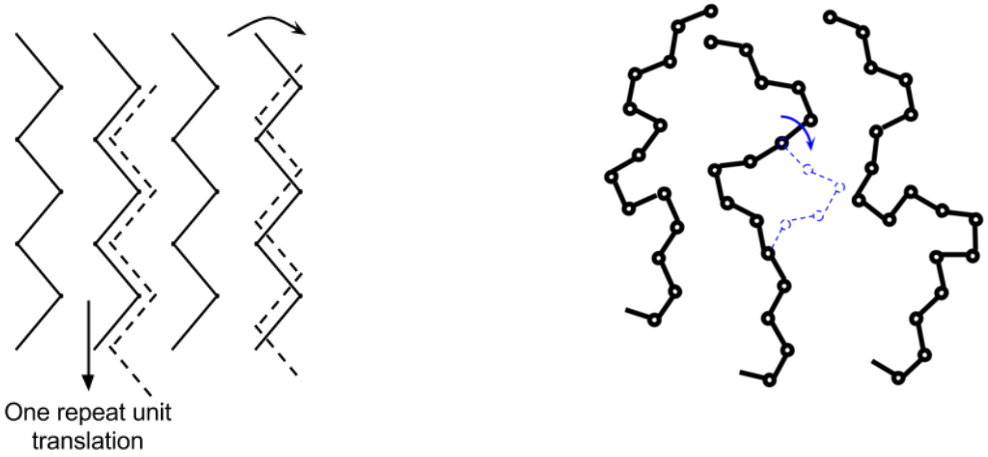

Figure 2.6. Schematic diagram showing the chain dynamics in polyethylene, (a) the chain translation and rotation in the crystalline phase, and (b) the crankshaft motion in the amorphous phase.

In translation movement, the chain segments in the lamella translate in such a way that the phases of the chain segment before and after the movement are equivalent, while the whole chain segment shifts along the `c' axis. The energy barrier of such movement is also proportional to the number of repeat units involved. Enough energy must be accumulated for the translation of one repeat unit out of the crystal in a fine lamella structure.

2.5.2 Crankshaft motion in the amorphous phase

In the amorphous phase, when the temperature is above the glass transition temperature (Tg) of the polymer materials, the chain segments are highly flexible because of the loose chain packing.[50] Extra space caused by the random chain arrangement, known as free volume (V_f), consists of the holes in the polymer matrix.[51] When the system has sufficient energy, the movements can lead the chain segments to jump into the holes by collaborative bond rotation with several repeat units, but without disturbing the stem polymer chains,[52] as shown in Figure 2.6(b). A series of such motions enables the polymer chains to change their positions completely. These segmental movements in the amorphous phase are known as crankshaft motions.[53]

2.5.3 Cooperative motion in the interface[54]

The interphase is a transitional phase between the crystalline phase and the amorphous phase, which makes the chain motions in this region more complicated and arbitrary. On one side, the chains continue from the crystalline phase and have at least one of their terminal attaches on the axial cross-section of the lamella. Thus, the chain motions are partially constrained by the crystalline structure. On the other side, the chain segments are also the extensions from the amorphous phase with high flexibility. Furthermore, the segmental mobility's are also decided by the re-entry types, adjacent or random re-entry. Therefore, the chain motions in the interphase display a wide range of varieties. In fact, most of the

chain segments move cooperatively with the chain motions from either the lamella or the amorphous region.

2.6 Physical and Mechanical Properties of PE[6a]

Polyethylene is the most useful commodity plastic, and its principal value lies in its excellent balance of physical properties in the solid state and its chemical inertness. These qualities in combination with its low cost and ready processability make it the material of choice for a wide variety of uses. The physical and mechanical properties of polyethylene can be controlled by tuning the synthesis conditions and the post-synthetic processing. The properties of polyethylene are determined by its semi-crystalline nature. Many of its most important properties are attributable to a combination of the characteristics of its crystalline and non-crystalline components and the connections linking them. PE in the crystal, the chain segments are well ordered which provide the desirable stiffness and tensile strength for applications. However, PE consisting of only crystals would be a friable material with poor toughness and impact strength which is mechanically undesirable.

On the positive side, polyethylene is a tough, flexible material that is chemically inert and has a high electrical resistance. However, it's dimensional instability under prolonged load, and its relatively low softening temperature is undesirable for many purposes. Polyethylene is thus very useful in short-term or non-critical applications such as food wrapping, storage containers, and piping but ineffective as an engineering resin or where high-temperature stability is required, such as in structural components or under-hood automotive applications. The chemical inertness of PE and its excellent electrical resistance stem from the covalent nature of its carbon-carbon and carbon-hydrogen bonds. From electronic polarity standpoint, the two primary types of bonds in polyethylene are well matched with a little dipole moment. For this reason, polyethylenes are largely resistant to chemical attack and little affected by electrical fields.

The melt rheological properties of polyethylene are controlled by its molecular characteristics. These characteristics include the distribution of molecular lengths and the number and type of branches. Moreover, there is very little interaction between adjacent polyethylene chains in the melt. The combination of limited chain interaction and a flexible backbone of carbon-carbon bonds results in polymer melts that are highly mobile on a local scale.

2.7 Historical and Theoretical Background of NMR Spectroscopy[55]

NMR spectroscopy is the study of molecules by recording the interaction of radiofrequency (rf) electromagnetic radiation with the nuclei of molecules placed in a strong magnetic field. Zeeman first observed the strange behavior of certain nuclei subjected to a strong magnetic field at the end of the last century, but practical use of the so-called “Zeeman effect” was made only in the 1950s when NMR spectrometers become commercially available.

Since the first NMR experiments were carried out shortly after the Second World War, this branch of spectroscopy has developed at a rapid and accelerating pace. Today the subject has expanded so that it is of equal importance with the older-established vibrational (infrared) and electronic (ultraviolet) branches of spectroscopy. Indeed, in many areas, NMR is superior to IR and UV, but the cost of instrumentation in usually greater. Moreover, the NMR experiment causes only a slight perturbation of the system in contrast to optical spectroscopy experiments as there are only very small energy changes involved in the transition between nuclear spin energy levels. So, the NMR experiments are non-destructive which is very useful in many cases.

In present days, the modern NMR has become an excellent physical tool for investigating the matter. Its range is staggering, encompassing such diverse areas as brains, bones, ceramics, inorganic chemistry, liquid crystals, protein folding, surfaces, zeolites, blood flow, drug development, polymers,

natural products, electrophoresis, geology, colloids, catalysis, food processing, cement, paint, wood, phase transitions, membranes, plants, micelles, grains, soil, explosives detection, coal, quantum computing, rubber, glasses, oil wells and Antarctic ice.[55a]

2.8 The Development of NMR[55b]

NMR spectroscopy was discovered around 75 years ago; however, it is a field that has come from centuries of scientific development. Pieter Zeeman (Nobel Prize, 1902) and Sir Joseph Larmor (knighted around 100 years ago in 1909) worked on magnetism, charge and radiation long before intrinsic angular momentum was hypothesized or even the proton was discovered. Since then to fourth decades of the nineteenth century, significant progress was made toward the discovery of nuclear magnetic resonance. Otto Stern found the nuclear spin in 1933, by using his molecular beam technique to measure the magnetic moment of the proton. Isidor Rabi (Nobel Prize, 1944) is credited with being the first person to observe nuclear magnetic resonance. Technological advances in the radio made during World War II allowed Felix Bloch and Edward Purcell (both shared the Nobel Prize, 1952) to invent a simpler method of magnetic resonance. In December 1945, Purcell, Torrey, and Pound detected weak radio-frequency signals generated by the nuclei of atoms in paraffin wax.[56] Almost simultaneously, Bloch, Hansen and Packard independently performed a different experiment in which they observed radio signals from the atomic nuclei in water.[57] These two experiments were the birth of the field we now know as nuclear magnetic resonance (NMR).

NMR spectroscopy of solid sample was made possible by introducing magic angle spinning by Andrew and Lowe at around 1958.[58] It was found that rotating the sample at a certain angle (54.74^{o}) to the static magnetic field removes the dipolar broadening and enhances the resolution of the solid-state NMR spectra. Ernst (Nobel Prize, 1991) and Anderson provided a full treatment of the Fourier

transformation method.[59] Throughout the next several decades after its first discovery, NMR spectroscopists mostly utilized a technique known as continuous wave (CW) spectroscopy. The limitation of this technique is that it probes each of the frequencies in succession, resulting in a poor signal-to-noise ratio.

Pulsed NMR took another leap forward with Haeberlen and Waugh's treatment on coherent averaging effects.[60] During the 1970s, the combination of cross-polarization (CP) with magic-angle spinning (MAS) by Schaefer, Stejskal and Buchdahl[61] introduce the modern era, with pulsed NMR under MAS being favored over continuous-wave static experiments.[62] A factor of ~1000 improvement in signal gained by FT-CPMAS has undoubtedly changed the world of organic chemistry, amongst other fields, forever.

In addition to that, it was found that the signal-to-noise ratio can be improved by the signal averaging method which increases the signal-to-noise ratio by the square-root of the number of signals scanned. The FT-NMR technique has been made more practical with the development of modern computers capable of performing the computationally intensive mathematical transformation of the data from the time domain to the frequency domain, to produce a spectrum. In modern NMR spectroscopy, very specific information about a complex system can be obtained by using of pulses of various shapes, frequencies, and durations, in specially designed patterns, called pulse program.

2.9 Basics of NMR[55, 63]

In NMR spectroscopy, when a sample is placed in a static magnetic field, the nuclei in the molecule generate a bulk macroscopic magnetization. To collect the NMR spectra, a radiofrequency pulse is applied to perturb the system from the equilibrium and then the response of the system to the disturbance is observed. It is mathematically proved that nuclei have a property known as *spin.* According to quantum

mechanics, this nuclear spin is characterized by a nuclear spin quantum number, *I,* which may be integral or half-integral or zero. The nucleus with an odd mass number have half-integral spin, with an even mass number and an even charge number have zero spin, and with an even mass number but an odd charge number have integral spin. A nuclear state with spin the *I* is (2*I* + 1)-fold degenerate. Normally, in the absence of any static magnetic field, there is no net magnetization in any direction as the spins are randomly oriented. But when a magnetic field is applied, the degeneracy is broken, and the splitting of

the nuclear spin levels is called the *nuclear Zeeman splitting*. NMR is the spectroscopy of the nuclear Zeeman sublevels.

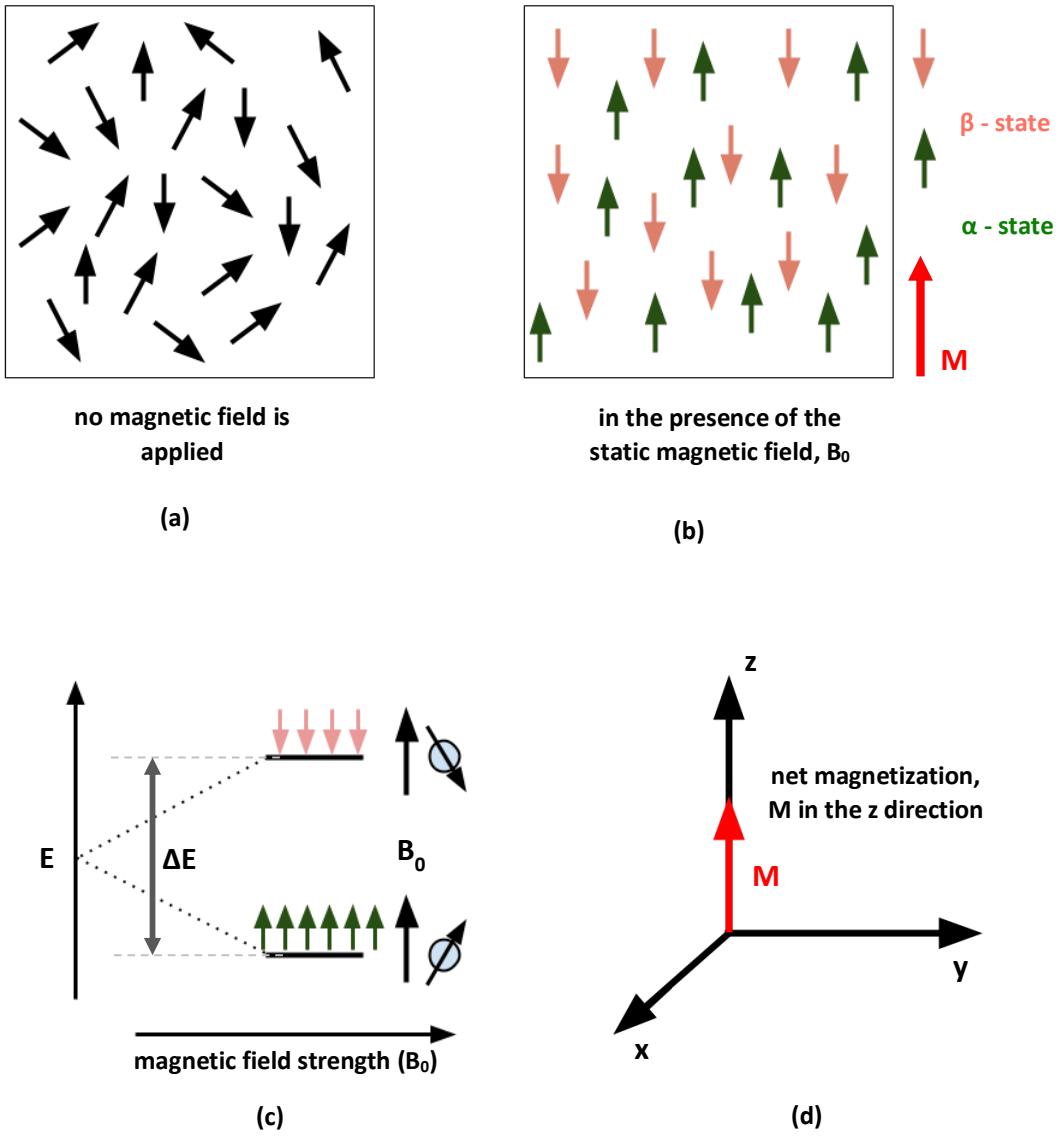

Figure 2.7. Schematic representation of, (a) a random orientation of spin magnetization in absence of external magnetic field, (b) in presence of B_0 field, spins are oriented producing a net magnetic vector along the B_0 field, (c) Zeeman splitting in presence of static magnetic field (B_0), and (d) the vector representation of net magnetic field.

In this dissertation, we are going to deal with ^{1}H and ^{13}C, and both of which are half-integral nuclei. A spin-half nucleus when interacts with a magnetic field, gives rise to two energy levels. These are

characterized by another quantum number *m* which quantum mechanics tells us is restricted to the values –*I* to *I* in integer steps. So, in the case of a spin-half, there are only two values of m, - ½ and + ½. By tradition in NMR the energy level (or state, as it is sometimes called) with m = ½ is denoted α and is sometimes described as "spin up". The state with m = - ½ is denoted β and is sometimes described as "spin down". For the nuclei described in this dissertation, the α-state is the one with the lowest energy. These two energy states are separated by an amount ΔE, which is field dependent.

$$\Delta E = \frac{h\gamma B_0}{2\pi} \qquad \textbf{(1)}$$

Where, ϒ is the magnetogyric ratio and B_0 is the magnitude of the applied static magnetic field.

2.9.1 The vector model[55a, 63a]

In NMR spectroscopy, only energy levels and selection rules cannot describe how the most basic pulsed NMR experiment works. Although NMR experiments can clearly be described by quantum mechanics or product operator formalism, for simple understanding *vector model* is a nice tool for visualization the spin interactions. The vector model should not be considered to be a complete theoretical description of NMR but rather a useful method of viewing the events which take place during an NMR experiment.

In the vector model of NMR, we will only consider the net nuclear spin magnetization coming from the nuclei in the sample and its behavior in magnetic fields. As mentioned above, the magnetic moments in a sample, in the absence of any static magnetic field, is randomly oriented (Figure 2.7(a)), and there is no net magnetic field in any direction. When a sample is first placed in a magnetic field there is no bulk magnetization along the applied magnetic field (commonly denoted as z-axis); rather, it takes a

finite time for this magnetization to build up. If we wait long enough, the magnetization reaches a steady value, and this steady state is called *equilibrium magnetization* state. At equilibrium state, although both 'spin up' and 'spin down' state of nuclei are present, but the population of 'spin up' state will be slightly higher than the other. Thus, a net magnetic field is build up along the z-axis (Figure 2.7(b) and (d)), which can be denoted by M. The net magnetization aligned with the applied magnetic field will remain there unless the system is disturbed in some way. If we could somehow misalign the induced magnetization from the applied field, there would be a force developed on M by B_0. The magnetization is generated from the nuclear spins and, as a consequence, it behaves in much the same way as a gyroscope behaves in a gravitational field. The force generated by B_0 on M is a torque which will cause M to precess about B_0. This motion is known as Larmor precession. The Larmor precession frequency can be written in equation as-

$$\omega_0 = \Upsilon B_0 \text{ radians/second} \quad \textbf{(2)}$$

The frequency ω_0 is called the Larmor precession frequency of the nuclear spins, Υ is the magnetogyric ratio of the nuclei, and B_0 is the applied magnetic field strength. If ω_0 has the traditional units of rad/sec and the magnetic field B_0 has units of Tesla (1 T = 10^4 Gauss), the magnetogyric ratio Υ will have the units of rad/sec-T. Thus, the proton Larmor frequency in the applied magnetic field B_0 will be ω_0 = 2.6751 * 10^8 B_0 rad/sec. Since NMR spectroscopists like to use ν_0 (units is Hz) instead of ω_0 (rad/sec) for the Larmor precession frequency, the above equation can be defined as:

$$\nu_0 = \frac{\gamma B_0}{2\pi} \; hertz \quad \textbf{(3)}$$

Here, the proton Larmor frequency will be $\nu_0 = 42.575\ B_0$ MHz, where units of B_0 is still Tesla. For example, when $B_0 = 7.03$ Tesla, the proton Larmor frequency, ν_0, will be around 300 MHz.

2.9.2 Boltzmann distribution and the spin temperature[64]

When a sample containing NMR active (spin ½) nucleus is placed in a high static magnetic field B_0, an energy difference between the 'spin up, α' and 'spin down, β' states are created. The population difference between the two states is subtle, generally, only one more nuclei in the 'spin up' level in one million nucleus bulk samples. The population difference between the two spin levels at an absolute temperature T can be defined by the energy difference of the Boltzmann distribution.

$$\frac{N_\beta}{N_\alpha} = e^{-\frac{\Delta E}{kT}} = e^{-\frac{\hbar\gamma B_0}{kT}} \quad \textbf{(4)}$$

Where, N_β and N_α represent the population in 'spin down' and 'spin up' state respectively, and k represents the Boltzmann constant.

Under general conditions, the value of hϒ will be much smaller than the value of kT. So the Boltzmann distribution equation can be simplified to the following-

$$\frac{N_\beta}{N_\alpha} = 1 - \frac{\hbar\gamma B_0}{kT} \quad \textbf{(5)}$$

When applying the Boltzmann distribution to the nuclear magnetization systems, it will be very useful to define a spin temperature term "T_s", which can simulate the general temperature term in the regular thermal equilibrium system.

$$\frac{N_\beta}{N_\alpha} = e^{\frac{-\Delta E}{kT_s}} = e^{-\frac{\hbar\gamma B_0}{kT_s}} \quad \textbf{(6)}$$

It is seen that this representation is very convenient to use the spin temperature T_s to describe the phenomenon of an NMR experiment. At the beginning of the experiment, the rf irradiation will find a population difference between the upper and lower levels. The population of the lower energy states will be higher than that of the higher energy state. The effect of the rf irradiation is that it makes more of the spin up (α) go higher energy level than the spin down (β) to go to lower energy level. After several transitions take place, N_α will decrease and N_β will increase so that the ratio in equation-4 will increase and approach unity. Through the spin temperature term in equation-6, we can imagine that there is an increase of spin temperature T_s in the spin system: a "warming up" of the nuclear magnetization spin system. We should notice that after the ratio in equation-4 or -6 approaches unity, any further applied radiofrequency irradiation will no longer have any impact on the spin system and produce no more net absorption. At that time, the spin system has reached saturation.

2.9.3 The effect of radiofrequency pulse[55a, 63a, 65]

To acquire an NMR spectrum, we must disturb the equilibrium state of spins. But, how can we tilt the net magnetization vector away from its equilibrium position? As the nuclear spin system in the sample is already present in a very strong superconducting magnet, it is not easy to rotate the net magnetization. Moreover, it is not possible to suddenly switch off the main static magnet and apply another small magnetic field along the x-axis to rotate the magnetization. One idea can solve this problem, which is to apply a very small magnetic field (generally denoted as B_1) along the x-axis but crucially – to make this field oscillate at or near Larmor frequency. If the oscillating field is *resonant* with the Larmor precession

frequency, it can make the magnetization move away from the z-axis even though the sample is already present in the B_0 field, which is many times greater in size than the oscillating field.

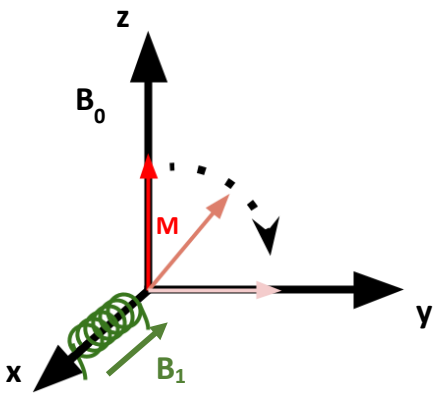

Figure 2.8. When a rf pulse (B_1) along the x-axis is applied, the net magnetization rotates in the y-z plane at a frequency $\omega_1 = \gamma B_1$.

So, a radio frequency pulse resonant with Larmor frequency can excite nuclear magnetization. When the nuclei are excited, they absorb energy and jump from lower levels to higher levels, and eventually they will relax back to lower levels and emit extra energy. The receiver (which is the same coil as pulse transmitter) detects the induced signal and converts it to signal seen in an NMR spectrum by applying Fourier transformation.

The B_1 oscillating field can be divided into two frequency components which rotate about B_0 field in opposite directions. We defined the two frequencies as $\pm\omega_{rf}$. When introduced a rotating frame of reference which rotates at frequency ω_{rf} around the B_0 laboratory frame, the effect of this B_1 field will be most easily seen. In this rotating frame of reference, the B_1 field appears static, which means its time dependence is removed.

When a sample containing NMR active nucleus is put in a static magnetic field (B_0), the nuclear spin vector M will precess around B_0 at a frequency ω_0 in the laboratory frame. Now, if an on-resonance radiofrequency pulse ($\omega_0 = \omega_{rf}$) is applied, the nuclear spins will appear stationary in the rotating frame. The only effective field left in the rotating frame will be the B_1 field while the B_0 field vanishes in this frame. The nuclear spins will precess (Figure 2.8) about the B_1 field at the following frequency:

$$\omega_1 = \Upsilon B_1 \qquad \textbf{(7)}$$

Here, ω_1 is known as the nutation frequency.

2.9.4 Free induction decay (FID)[55, 63a]

As long as the bulk magnetization lies along the z-axis, there is no signal. After the radiofrequency pulse is applied to tilt the net magnetization to the transverse plane and due to the presence of B_0 field, each and every spin will precess at Larmor frequency. If we have a coil wound about the laboratory x-axis, the precessing magnetization will induce the coil an oscillating current which we can detect. This is the NMR signal. As the signal decays without any influence and induces the coil, the signal is called *free induction decay* (Figure 2.9 (b)) or FID. The FID signal is a time-domain signal. The frequency-domain NMR spectrum is obtained by applying a mathematical tool, called Fourier Transformation.

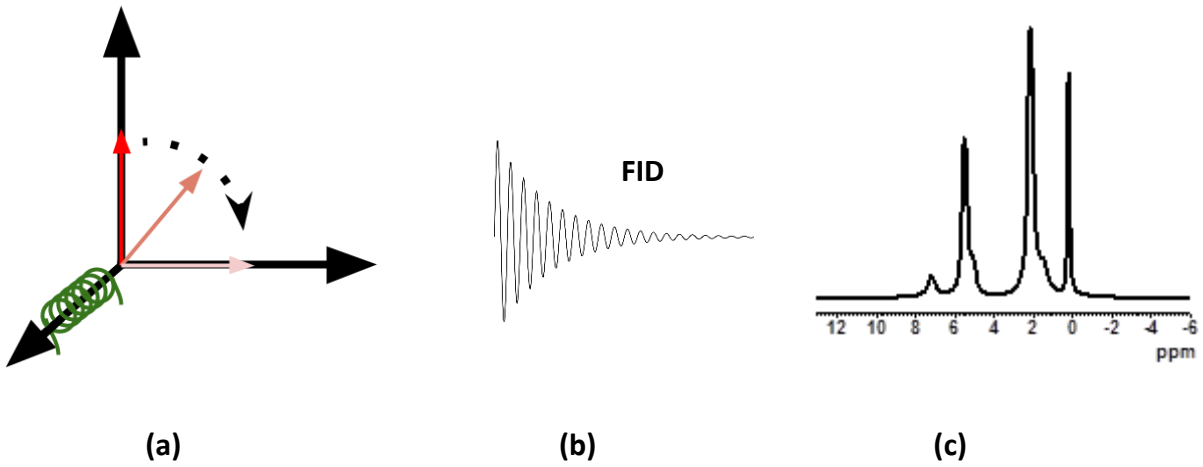

Figure 2.9. Schematic representation of, (a) the effect of the radiofrequency pulse, (b) the NMR free induction decay signal and (c) a ^{1}H NMR spectrum of a copolymer acquired in the solid state.

2.9.5 Chemical shift[55b, 65]

The Fourier transformed spectrum of NMR is a plot of intensity vs. frequency (as shown in Figure 2.9-(c)). The absorption line (or peak) at different frequency means that nucleus having different Larmor frequency for having different chemical shielding effect, and the integrated area of each peak tells about the population of that specific type of nucleus. However, NMR spectroscopist tends to use some rather unusual units, and so we need to know about these and how to convert from one to another. It was discussed previously in this chapter that the Larmor frequency depends on the applied static magnetic field and the frequencies at which NMR absorptions occurs scale linearly with the magnetic field strength. So, the frequency scale of the NMR spectra for the same substance, if acquired in different magnets, will be different. So, if the line from TMS (tetramethylsilane) protons comes out on one spectrometer at 400 MHz, doubling the magnetic field will result in it coming out at 800 MHz. If we wanted to quote the NMR frequency, it would be inconvenient to have to specify the exact magnetic field strength as well. To solve this problem, a 'chemical shift' scale relative to an agreed reference compound is introduced. For

example, in the case of proton NMR, the reference compound is TMS. If the frequency of the line we are interested in is ν (in Hz) and the frequency of the line from TMS is ν_{TMS} (also in Hz), the chemical shift of the line is computed as:

$$\delta = \frac{\nu - \nu_{TMS}}{\nu_{TMS}} \quad \textbf{(8)}$$

Typically, the chemical shift is rather small so it is common to multiply the value for δ by 10^6 and then quote its value in parts per million, or ppm. With this definition, the chemical shift of the reference compound is 0 ppm. And-

$$\delta_{ppm} = 10^6 \, x \, \frac{\nu - \nu_{TMS}}{\nu_{TMS}} \quad \textbf{(9)}$$

2.9.6 Pulse sequence[63a]

A simple 'one-pulse' experiment is sufficient to see an NMR spectrum. However, with a modern pulse spectrometer, we can do far more than simply obtain a spectrum. The spin system can be manipulated to force it to provide us with new useful information. A pulse sequence is a set of the pulses with appropriate delays, which is designed in such a way that gives specific information about a system. The pulse sequence can contain several pulses of different pulse lengths, phases and power levels with variable delay time between pulses. For example, an **'**inversion recovery' pulse sequence (shown in Figure 2.10) is used to determine the spin-lattice relaxation time of different types of nuclei. An 'inversion recovery' pulse sequence starts with a delay time, called the recycle delay, which allows all spin system

to come to the equilibrium position after the previous scan. After the recycle delay, a 180^{o} pulse is applied along the x-axis, which inverts the net magnetization to –z-axis. After a short delay, a second pulse, which is a 90^{o} pulse, is applied to acquire the spectra. During the second delay time, some of the spins come to its equilibrium state. By varying the value of the second delay, a number of spectra can be collected, and by analyzing those spectra, the spin-lattice relaxation time is calculated.

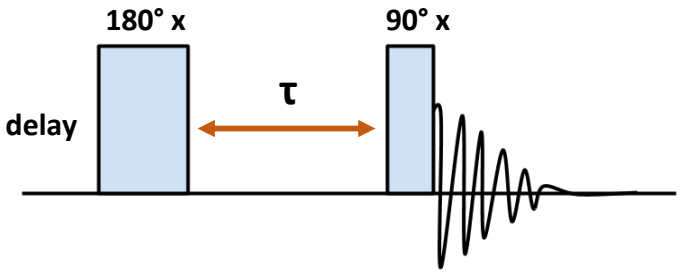

Figure 2.10. The inversion recovery pulse sequence diagram.

2.10 Essential Techniques for Solid-State NMR[4a, 55]

The resolution of the solid-state NMR spectra is typically not as good as that of the solutions. This arises in part because the averaging of the chemical shift anisotropy and the $^{1}H - ^{13}C$ dipolar interactions by magic-angle spinning and high-power decoupling is not as efficient as the averaging by chain motion in solution. The main two phenomena that contribute to the solid-state NMR linewidths are discussed:

2.10.1 Dipole-dipole interaction[4a, 55a]

Each NMR-active nucleus (spin ½) acts as a magnetic dipole which aligns with the B_0 in specific states. Since each nucleus, like a dipole, has a local field associated with it, the actual field each nucleus experiences is a sum of the external field (B_0) and contribution from all surrounding dipoles. The dipole-dipole interaction is highly dependent upon the angle between the direction of B_0 and the internuclear vector between the dipoles. In proton NMR spectrum, the very broad line width is obtained due to

homonuclear dipole-dipole interactions. In carbon NMR, in most organic substances, the carbon nucleus is surrounded by many protons, so the line width is broad because of heteronuclear ($^{1}H - {}^{13}C$) dipolar interactions. In solution NMR spectroscopy, due to the rapid isotropic molecular motion, the dipolar interaction is averaged, so, a narrow line is obtained. But in the case of solids, the molecular motion is restricted, which gives very broad lines.

2.10.2 Chemical shift anisotropy (CSA)[4a, 55a]

The second major contribution to solid-state NMR line width is the chemical shift anisotropy (CSA). Chemical shift anisotropy results from the interaction between magnetic fields of electrons in motion around a nucleus and the nuclear spin. The distribution of the electron around the nucleus depends upon the chemical bonding and are not uniform in all direction. So, an anisotropic condition arises which gives broad NMR linewidths.

Both dipole-dipole interaction and CSA is highly orientation dependent. In both cases, it was noted that molecular motion, especially random rotational and translation motion as experienced in the liquid state, resulted in the line narrowing by time-averaging. So, to obtain high-resolution spectra in the solid state, it is important to time-average the different interaction in solids.

2.10.3 Magic-angle spinning (MAS)[4a, 4b, 55a]

Magic angle spinning is used in solid-state NMR experiments to remove the chemical shift anisotropy and heteronuclear dipole-dipole interactions. At a very high magic angle spinning speed, MAS will also tend to remove the homonuclear dipolar interaction from solid-state NMR spectra. It is found that the magnitude of any of the above anisotropic interactions has a very specific angular dependence on- 1) the static field (CSA), 2) other nuclear spins (dipole-dipole interactions). Among other terms

describing the orientational dependence of these anisotropic interactions in each of the respective Hamiltonian operators is the term $(3cos^2\theta - 1)$. In each case, if the angle θ is chosen such that:

$$3cos^2\theta - 1 = 0 \quad \textbf{(10)}$$

all anisotropic contributions to the NMR spectrum will reduce to zero. This θ when equal to 54.7^o is called magic angle. Since all values of θ are possible in the non-crystalline or powdered solid, very few interactions naturally reduced to zero. However, when the sample is spun at a sufficient spinning speed at magic angle, the dipolar interaction and CSA will be reduced to zero.

Magic angle spinning can also be used for removing the effects of homonuclear dipole-dipole interaction if the MAS rate is high enough. When the MAS rate is very slow, meaning much less than the dipolar line-width, MAS will have very little effect on removing all the effects including homonuclear and heteronuclear dipole-dipole interaction and CSA. The broad line will still exist as the line in the absence of spinning. At intermediate MAS rates, around quarter to half of the dipolar line-width, spinning sidebands will appear. When the MAS rate is high enough, usually much faster that the dipolar line-width, all the three effects will be removed, making the lines narrow.

2.10.4 High power proton dipolar decoupling[55a, 66]

When observing a dilute spin, e.g. ^{13}C spins with ^{1}H or other abundant spins existing in the same nuclear magnetic spin system, broadening due to heteronuclear dipole-dipole interaction often causes additional problems to the already weak spectrum, since the ^{13}C only has about 1.1% abundance. The simplest means of removing the heteronuclear dipolar interactions is to decouple the interaction by applying a strong radio frequency pulse at the resonance frequency of the protons during acquisition of

the carbon signal. The decoupling rf pulse promotes rapid spin transitions or flips between spin states by the proton spins, thereby averaging the static dipolar interactions to zero. For most case, continuous wave (CW) decoupling is used. In the case of dipolar-coupled ^{1}H and ^{13}C spin pairs, where ^{13}C spin's signals are needed to be observed, the application of high power decoupling will consist of applying a continuous irradiation of very high power (100 – 1000 watts) at the frequency of the proton resonance during the acquisition of ^{13}C signals. In the CW decoupling, one very long single pulse is applied in a constant phase. This decoupling works nicely for most of the amorphous solids, but for crystalline macromolecules, it is found that more efficient decoupling is required. So, a variety of decoupling methods are developed, for example, composite pulse decoupling (CPD) with phase, frequency or amplitude modulation. One of the most common CPD sequences is 'two-pulse phase modulation' (TPPM) decoupling.[66] The TPPM decoupling sequence is composed of many (windowless) small pulses. The phase of the each alternating pulse changes from x-ϕ to x-ϕ. For effective decoupling with TPPM pulse sequence, high-speed MAS (at least 12 kHz) and high-power (proton v_1 at least 100 kHz) proton rf irradiation is required. Moreover, the appropriate pulse length and phase shift values for composite pulses are needed to be optimized each time before the experiments.

2.11 Special Features of NMR

2.11.1 Spin relaxation[55a, 67]

Relaxation is one of the fundamental aspects of magnetic resonance. At one level, relaxation has important consequences for the NMR experiment. The relaxation rates of single quantum transverse operators determine the linewidths of the resonances detected during the acquisition period of an NMR experiment. The relaxation rates of the longitudinal magnetization and off-diagonal coherences generated by the pulse sequence determine the length of the recycle delay needed between acquisitions. At second level, relaxation affects quantitative measurement and interpretation of NMR experimental

parameters, including chemical shifts and scalar coupling constants. And at third level, relaxation provides experimental information on the physical processes governing relaxation, including molecular motions and intra-molecular distances. In particular, cross-relaxation gives rise to the nuclear Overhauser effect (NOE) and makes possible the determination of three-dimensional molecular structure by NMR spectroscopy.

The equilibrium magnetization (M) (Figure 2.7) of the sample is aligned along the z-axis. The magnetization is a direct result of the difference in energy between the states. To alter the z component of the magnetization, M_z, we must change the energy of the spin system by perturbing the spins with the radio frequency pulse. After the rf pulse is applied to tilt the net magnetization to the xy plane, i.e. making the $M_z = 0$, the spin system again return to its equilibrium state with time by the phenomena is called relaxation. Two types of relaxation occur, spin-lattice relaxation and spin-spin relaxation.

The spin-spin relaxation[68] (also called transverse or T_2 relaxation) is the decay of phase coherence of the spins in the xy plane and used to measure the rate of relaxation in the xy plane. The transverse magnetization decays slowly because it is impossible to maintain exact synchrony between the precessing nuclear magnets. Since the microscopic magnetic fields fluctuate slightly, the precessing nuclear magnets gradually get out of phase with each other. This is called coherence dephasing. This relaxation does not involve energy exchange with the lattice, but it does transfer energy between spins, via a flip-flop type mechanism.

The spin-lattice relaxation[68] (also called longitudinal or T_1 relaxation) is a measure of the relaxation rate along the z-axis. After the rf pulse, the z component of net magnetization (M_z) starts growing exponentially and return to equilibrium with time. During this relaxation, the nuclear magnetization will lose its energy in the system to the surroundings (lattice) as heat. As the energy difference between the

higher and lower level spin states is very low, spontaneous relaxation cannot occur in NMR spectroscopy. If the probability per unit time for transition from the upper to lower energy state of an isolated magnetic dipole by spontaneous emission of a photon (of energy ΔE) is W, then probability is given by-

$$W = \frac{2\,\hbar\gamma^2\omega^3}{3c^3} \qquad \textbf{(11)}$$

Where, c is the speed of light. For a proton with a Larmor frequency of 500 MHz, W ≈ 10^{-21} s^{-1}; thus, spontaneous emission is a completely ineffective relaxation mechanism for nuclear magnetic resonance. NMR relaxation is, in fact, stimulated relaxation. The stimulation for relaxation comes from the molecular tumbling. Each NMR active nucleus can act as a small micro-magnet, and has its own magnetic field. When the molecule rotates or moves, due to changing the position and direction of those small magnetic dipoles, a fluctuating dipolar field is created. When the frequency of that fluctuating field is near Larmor frequency, the relaxation takes place most efficiently.

2.11.2 Nuclear Overhauser Effect (NOE)[68]

The nuclear Overhauser effect (NOE) is the change in intensity of one spin's signal due to magnetization transfer from another spin in a dipolar coupled spin system. The magnetization transfer occurs via dipole-dipole cross-relaxation. In normal relaxation process, magnetization transfer occurs via single-quantum transition. However, in the case of NOE, the magnetization transfer occur via zero or double quantum transition depending on the correlation time of the molecule or molecular segments. For example, we can consider an experiment where carbon signal will be acquired using high-power proton decoupling. During the proton decoupling period, the proton magnetization will be saturated or disturbed

from its equilibrium state. So, the system will try to regain the equilibrium state by relaxation process. This relaxation can occur via three pathways (as shown in Figure 2.11).

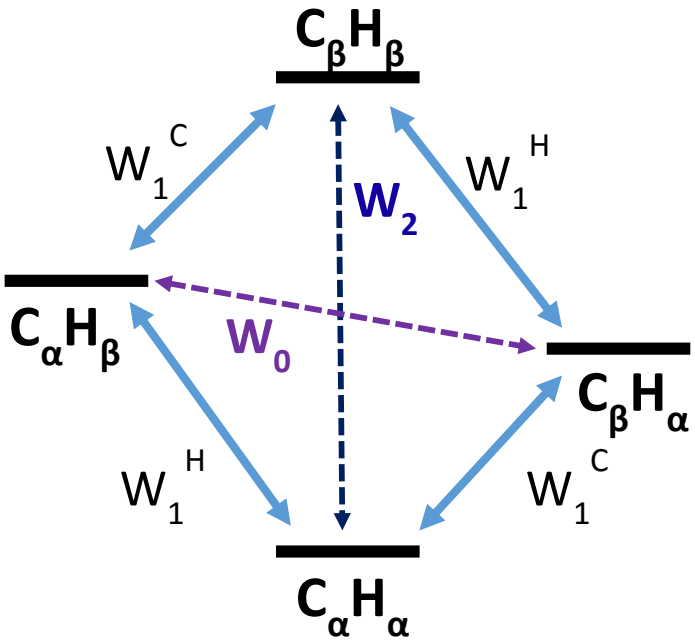

Figure 2.11. Energy diagram of various relaxation pathways.

Here, W_1, W_0, and W_2 are transition probabilities via single, zero and double quantum pathways. Relaxation through W_1 requires magnetic field fluctuations at a frequency in the order of the Larmor precession frequency, ν_{0H} Hz while W_2 requires field fluctuations around (ν_{0H} + ν_{0C}) Hz. Because the necessary field fluctuations are produced by molecular tumbling at a rate of (correlation time, τ_c)$^{-1}$, W_1 and W_2 are most efficient when $\nu_0\tau_c$ is near to unity. If only single quantum transition are active as relaxation pathways, no NOE will be observed. However, If W_0 or W_2 is the dominant relaxation pathways, the saturation of the proton nucleus will affect the carbon signal by decreasing or increasing the intensity respectively. The extent of NOE can be expressed by the following equation-

$$\eta_C(H) = \frac{W_2 - W_0}{W_0 + W_1^C + W_2} \times \frac{\Upsilon_H}{\Upsilon_C} \quad \textbf{(12)}$$

2.11.3 Cross-polarization (CP)[69]

In many NMR experiments, the transfer of energy between different sets of magnetic nuclei with different precession frequencies are required to enhance the signal. This energy transfer can be achieved via cross-polarization technique under the Hartmann-Hahn condition.[69] The transfer of energy from one kind of nuclei to another is possible if the two different nuclei have the same resonance frequency. The most common example of the cross polarization energy transfer is between ^{1}H and ^{13}C. As the carbon nucleus is of very low natural abundance, moreover the spin-lattice relaxation time for carbon is much higher than that of the proton, cross-polarization between proton and carbon is very useful NMR experiment for many systems.

Clearly, since the proton resonance frequency is a factor of four larger than that of ^{13}C, the transfer of energy between them is forbidden. This problem can be overcome by applying the Hartmann-Hahn condition. The first step in the Hartmann-Hahn process is to bring the proton nuclei to xy plane by a 90^{o}_{x} pulse. Next, each set of nuclei needs to be spin-locked to the y-axis by either a series of 180^{o}_{y} pulses or equivalent continuous irradiation at the appropriate frequencies (also called the contact pulse), then achieving the following state:

$$\gamma_C B_{1C} = \gamma_H B_{1H} \quad \textbf{(13)}$$

During the contact pulse, both sets of nuclei, within their respective rotating frames, precess with the same frequency about the y-axis, thereby providing an opportunity for exchange of energy via coupled spin flip-flop.

The cross-polarization (CP) experiment is very useful in solid-state NMR for many systems because it can acquire data relatively quickly (especially for those systems having very long T_1 relaxation time). However, this experiment is unable to provide quantitative information. In CP experiment, the energy is transferred from one nucleus to another by dipole-dipole interaction. So, the energy transfer efficiency depends on the molecular mobility. Moreover, depending on the density difference of abundant nuclei, CP efficiency can vary. So, CP experiment cannot be considered as a quantitative experiment.

2.12 Application of NMR Spectroscopy in Polymer Science[4a, 70]

NMR spectroscopy is the most versatile analytical techniques and being used to study many different types of systems, like small molecules in solution and solid, crystal structure, biological systems, bone, tissue and many more. This tool becomes extremely important in the study of macromolecules. Due to the complex nature of macromolecules, other analytical techniques failed to provide much information. However, NMR is capable of providing different types of information, like chemical structure, chain dynamics, intermolecular distance, chain packing, conformational state, stereo-regularity, crystal structure, etc. The first studies of polymers[71] were published only about a year after the first reports of the NMR phenomenon in the bulk matter by Bloch and Purcell in 1946. The early work dealt with nuclear relaxation and chain dynamics in the solid state. At some point of NMR development in the mid-1950s, when the study of small molecules had reached a fairly advanced state, it was thought that macromolecules could not give useful spectra even in solution because of their supposedly slow motion. There was also a feeling that their spectra would be too complex to interpret. However, due to the

invention of the many techniques in NMR, now, NMR is one the most useful analytical technique for macromolecules. The NMR spectroscopy is now so powerful that, it can provide chain specific information of highly complex polymers or copolymers. In this dissertation, two solid-state NMR methods are described which were developed to study the morphology of highly complex gradient copolymer system and semi-crystalline copolymer system. Both of those studies were done mostly depending NMR data.

CHAPTER 3

3 DEVELOPMENT OF THE SOLID-STATE NMR EXPERIMENTAL METHOD TO DETERMINE THE CRYSTAL-AMORPHOUS INTERFACE IN POLYETHYLENES

3.1 Introduction

The morphology of semi-crystalline polyethylene is complicated, and its physical and mechanical properties are a complex function of its morphology. A sound qualitative and quantitative understanding of the morphology of polyethylenes and its relation to physical and mechanical properties are crucial for designing a particular type of material with desirable properties. As polyethylene is one of the oldest polymers, and due to its excellent properties and usability, extensive research has been done to understand its morphology along with how the morphology affects its physical and mechanical properties. Previously, most of these studies were focused on crystalline and amorphous regions.[4] However, the interface between the crystalline and amorphous regions may also be important. As an example, Lai and Humbert's group recently showed that the crystalline-amorphous interface region has a significant effect on final physical and mechanical properties of polyethylene.[5] It is important to develop an experimental method which can quantitatively and reliably determine the composition of the different phases in polyethylene, especially the composition of the crystalline-amorphous interface.

Solid-state NMR (ssNMR) is recognized as one of the most powerful means for elucidating the structure and the dynamics of solid polymers, in addition to X-ray diffraction.[9, 72] However, for highly

complex amorphous or semi-crystalline polymers study, ssNMR is even better than X-ray diffraction, as the latter is mainly useful for ordered systems. Based on the correlation between the structure and chain properties, ssNMR can provide detailed information which will lead to the further development of material research in the future. In this contribution, a new solid-state ^{13}C ssNMR experimental method is presented for quantitative phase composition study of polyethylene, with particular emphasis on interfacial characterization.

Various experimental techniques have been used to investigate the solid-state morphology of polyethylene[6b, 11a], such as density measurement, thermal analysis (DSC, TGA),[73] microscopy (optical, SEM, TEM, AFM),[11] scattering measurements (WAXS, SAXS, small-angle neutron scattering),[9, 11a, 72, 74] spectroscopy (FT-IR, Raman, NMR).[3a, 4b, 6b, 6c, 7, 11a] The density measurement is the oldest, and most widely used method of determining the degree of crystallinity of polyethylene. However, it can give only a general idea about the sample based on two simple assumptions: that polyethylene is composed of two (crystalline and non-crystalline) phases and that the density of each phase is uniform within the sample and consistent from one sample to another.[6a] Differential scanning calorimetry (DSC) is another very popular analytical technique and widely used in industries to measure polyethylene crystallinity.[73b, 73c] X-ray diffraction provides information to answer the question of whether a polyethylene is crystalline or amorphous, oriented or unoriented, and to determine the size of the characteristic repeat distance.[8, 11a, 72, 75] Microscopy and scattering methods, while capable of providing information about crystallinity, are only useful for heavy atoms and sample preparation is difficult. Moreover, these techniques, although suitable for percent crystalline study, are unable to provide reliable information about the crystalline-amorphous interface. Recently, Savage et al. did an excellent study on the molecular conformation in the polyethylene interface using torsional-tapping AFM with super-sharp carbon-whisker tips.[12] Raman and

FT-IR spectroscopies[76] are capable of giving information about three morphological regions of polyethylene; however, the experimental and data analysis method is complicated.

In the last few decades, various NMR methods have been explored and developed for the investigation of polyethylene morphology, for example: ^{1}H wide-line NMR study, ^{1}H free-induction-decay analysis, relaxation study, spin-diffusion, cross polarization, etc.[13a-c, 13e, 46, 47b, 47d, 77] Among those, ^{1}H NMR is very attractive, as it can provide information about the crystalline and amorphous phases, as well as the interface, in a very short experimental time.[13e] Carbon NMR, although time-consuming, can provide additional information about the interface which cannot be obtained by ^{1}H NMR. As carbon NMR chemical shifts are chain-conformation sensitive in a high-resolution ssNMR spectrum, carbon NMR can differentiate between the trans and gauche conformers in polyethylene chains (which will be discussed later in detail).

In the current study, a solid-state ^{13}C NMR experimental method is presented which can quantitatively determine the distribution of polyethylene chains in different morphological regions. The developed method is a T_1 filter based, double acquisition, NMR pulse sequence which can simultaneously acquire quantitative data and T_1 filtered 'mobile-only' (signal only from mobile chain segments) data in alternating scans without complications from nuclear Overhauser effects. The purpose of using a double acquisition pulse sequence is to collect all the data required to calculate phase composition in a single experiment and to avoid the possibility of complications inherent to collecting data in two separate experiments. The details about the experimental method and calculation will be discussed in the rest of this chapter.

3.2 Method Development

3.2.1 Properties of PE chains

As discussed in detail in the previous chapter, polyethylene is a semi-crystalline polymer in which crystalline lamellae are embedded in the non-crystalline amorphous region. Between these two main phases, there is an interface which is composed of chains with properties different than that of the crystalline and amorphous phase. The crystalline region is composed of chains which are in a fully extended conformation; in other words, the chain in the crystalline region are in an all-trans conformation (Figure 3.1). The chains are packed in the crystal lattice arrangement, and the chain mobility is highly restricted. So, the crystalline chains can be termed as "rigid-all-trans" chains. On the other hand, in the amorphous region, PE chains are randomly oriented and loosely packed. Due to high entanglement between chains, the chains are randomly folded, which makes them have a mixture of trans and gauche conformations. The available free volume in the amorphous region allows the polymer chains to move very fast. It is well-known that the amorphous region is liquid like and the chains are in a very fast isotropic motion, maintaining an equilibrium trans-gauche density.[78] For these reasons, the amorphous chains can be termed as 'mobile trans-gauche' chains.

Besides these 'rigid-all-trans' and the 'mobile-trans-gauche' chains, there exist two more types of chains in PE bulk, which are believed to constitute the crystalline-amorphous interface.[4c, 47a, 47b] Due to adjacent re-entry, chains are folded by 180° which makes a tight loop of chain on the crystal surface. The mobility of these trans-gauche chains is restricted, and these tight loops are believed to constitute a part of the interface region and termed as 'constrained trans-gauche' chains. On the other hand, the part of these loose loops, cilia, and tie chains which are connected to the crystal surface are in an all-trans conformation in the interface region, but they are very mobile compared to the constrained amorphous chain. These chains are called 'mobile all-trans' chains.

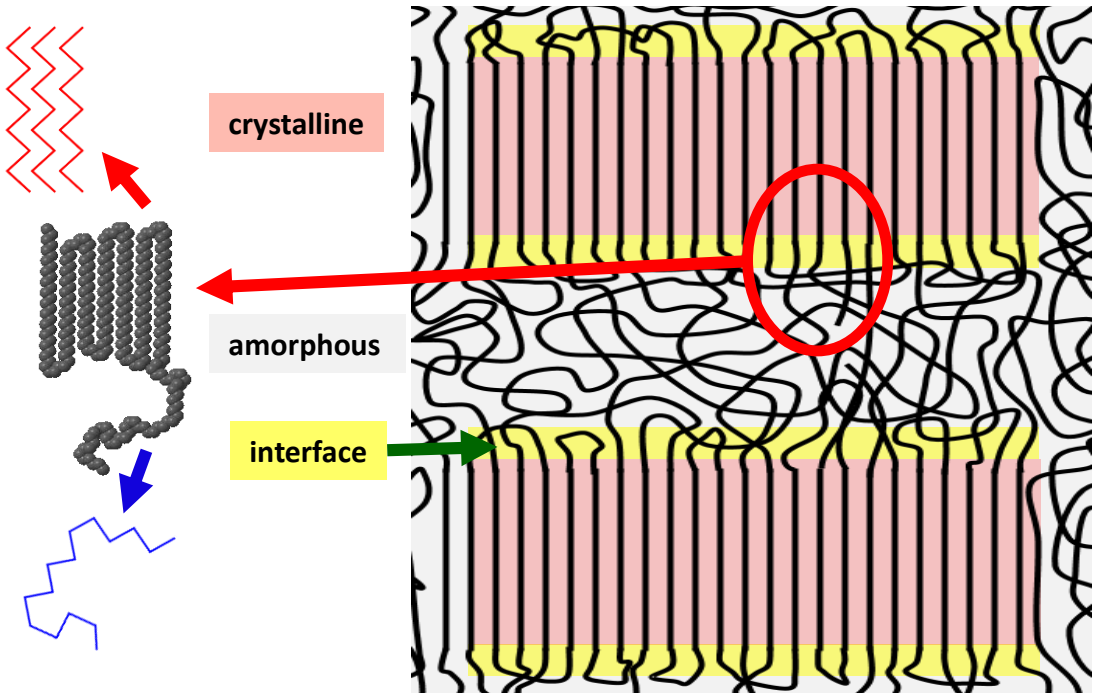

Figure 3.1. Schematic representation of the three-phase morphology model of polyethylene, showing the crystalline (pink), amorphous (gray) and the interface (yellow) regions. The cartoon on the left side represents a chain segment present both in the crystalline (all-trans conformation) and in the amorphous (mixed trans-gauche conformation) phase.

Polyethylene is the simplest polymer from a chemical perspective, with the whole PE chain composed mainly of methylene (-CH_2-) groups. As the molecular weight of the polymer becomes very high, or in other words, the chains are long, the fraction of the vinyl or other groups at chain ends is negligible compared to that of the methylene group. For this reason, in a carbon NMR spectrum, one should expect a single intense peak for methylene carbon, with a very small peak for chain-end carbons. However, that is not true for polyethylene. In a typical carbon NMR spectrum of polyethylene (as shown in Figure 3.2), a narrow, intense peak (at ca. 33 ppm) along with an up-field peak or shoulder (at ca. 31 ppm) are observed depending on the percent crystallinity.

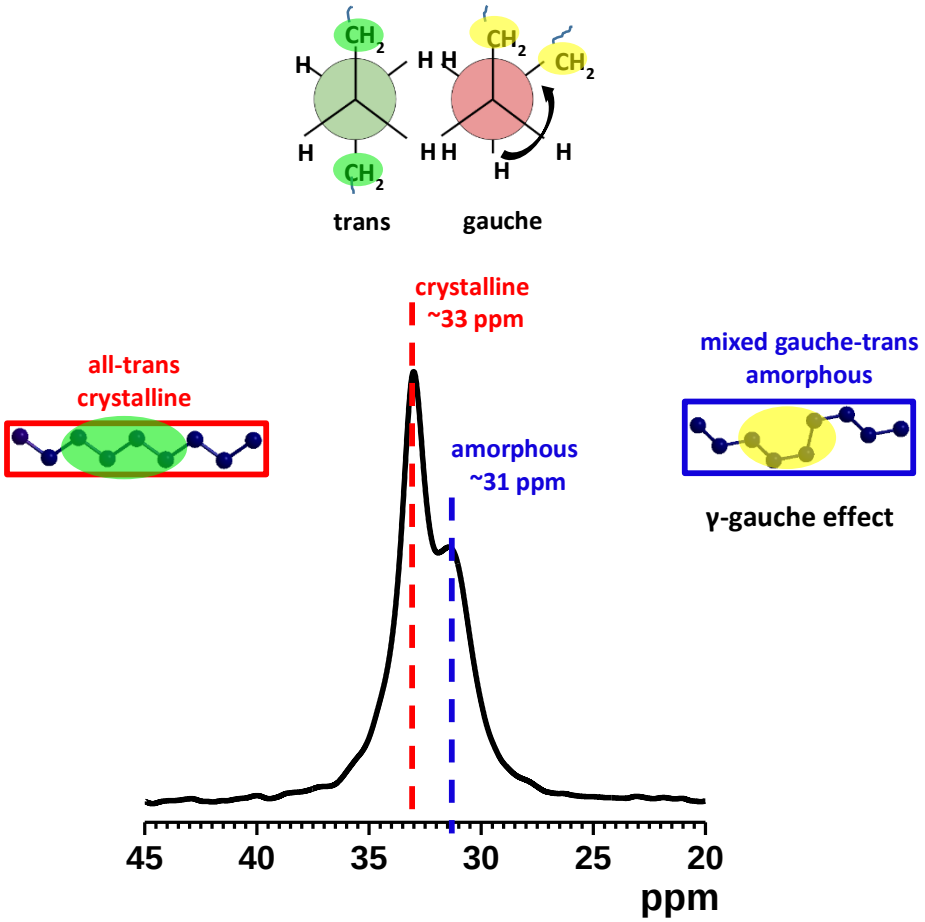

Figure 3.2. A typical ^{13}C NMR spectrum of polyethylene. The peak at ca. 33 ppm is for all-trans chains, and the shoulder at ca. 31 ppm is for trans-gauche chains. On the top, the Newman projection shows that two methylene groups come closer in the gauche conformer, which increases the electron density in that region causing an upfield shift.

Although the PE chains are composed of mainly methylene carbon and the whole chain is chemically identical, the presence of two different peaks in the carbon NMR spectrum shows that the electron density of all carbons are not the same. Due to the presence of gauche conformation in the chain, the two methylene groups in the gamma position come closer, which increases the electron density in that region, thus increasing the chemical shielding. This phenomenon is called the gamma-gauche effect.[79] As the crystalline regions are composed of all-trans chains, and the amorphous regions are composed of a mixture of trans and gauche chain, the peak at ca. 31 ppm is assigned to the amorphous region and the downfield peak at ca. 33 ppm is assigned to the crystalline regions.

The crystalline regions are composed of all-trans chains; however, different peaks for the crystalline region can be observed, depending on the presence of different types of crystalline structures. The most stable crystalline structure in polyethylene is the orthorhombic state. However, metastable crystalline structures, like monoclinic or hexagonal structures, can be produced depending on the processing condition of polyethylene. In the monoclinic crystal structure, the chain density is slightly lower than that of orthorhombic structure, so another crystal peak (or shoulder) slightly downfield to the orthorhombic peak (at ca. 34.4 ppm) might appear for some PEs.

Unlike the crystalline peak which is nearly fixed at 33 ppm, the amorphous peak position changes depending on the gauche conformer densities. Moreover, the chain packing in the amorphous phase is not the same for all regions and affects the position of the amorphous peak. Due to the wide distribution of density of the gauche conformer and chain packing, the amorphous peak is considerably broader than that of the crystalline peak.[80] In a high-resolution quantitative ^{13}C NMR spectrum acquired in the solid state, two, or three (if monoclinic crystal phase is present), peaks are easily seen, and the % crystallinity can be determined by deconvoluting those peaks by the appropriate method. However, the presence of "constrained amorphous" or "mobile all-trans" peaks are not obvious in the total spectrum. To get a clear idea about those two interfacial components, additional information is needed.

3.2.3 Chain dynamics and ^{13}C spin-lattice relaxation time, T_{1C}

As discussed in the previous chapter (Chapter 2), the spin system, disturbed by a radiofrequency pulse to attain the NMR signal, eventually comes back to the Boltzmann equilibrium state by the spin-lattice relaxation process, that follows the equation mentioned below:

$$Mz\,(t) = Mz_{eq}\,(1 - e^{-t/T_1}) \qquad \textbf{(14)}$$

Where, T_1 is the spin-lattice relaxation time constant.

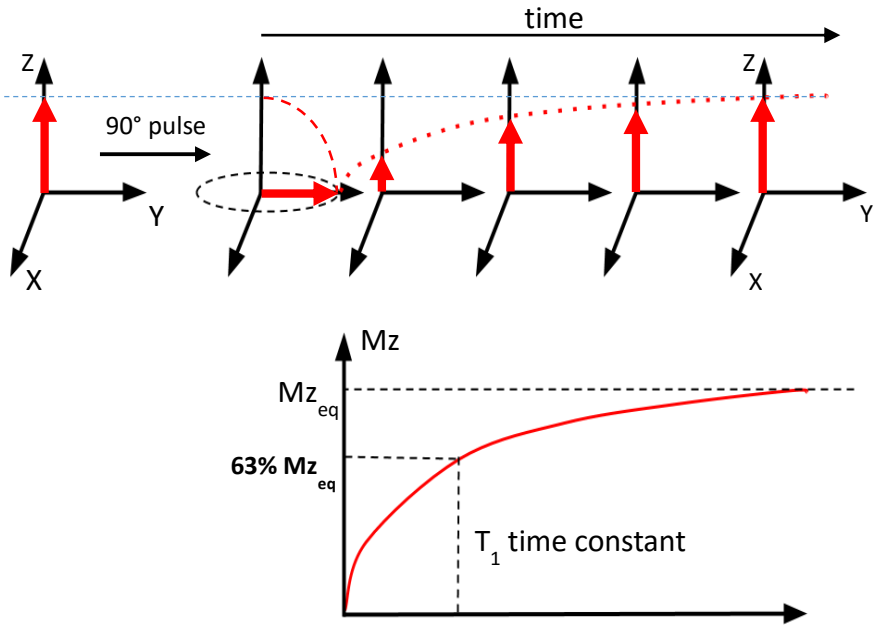

Figure 3.3. Recovery of magnetization to equilibrium state by spin-lattice relaxation process.

Figure 3.3 and equation 14 show that within one T_1 time, 63% of magnetization relaxes back to its equilibrium state, and for complete relaxation, one needs to wait at least five times the T_1 relaxation time constant. Since the energy difference between the "spin-up" and "spin-down" state is very low, this relaxation process is not spontaneous, rather a stimulation is required for efficient relaxation. So, what is the source of the stimulation? Each ^{1}H and ^{13}C present in the polymer molecules have their individual magnetic dipolar field. The dipolar interaction depends on the distance and the angle of interactions. As the molecules are in continuous motion (translational and rotational), the molecular tumbling causes

fluctuation in the dipolar field. This fluctuating dipolar field is the source of stimulation for relaxation. When the frequency of this fluctuating dipolar field is near the resonance frequency, or the Larmor frequency of the nucleus, the relaxation process is most efficient.[81]

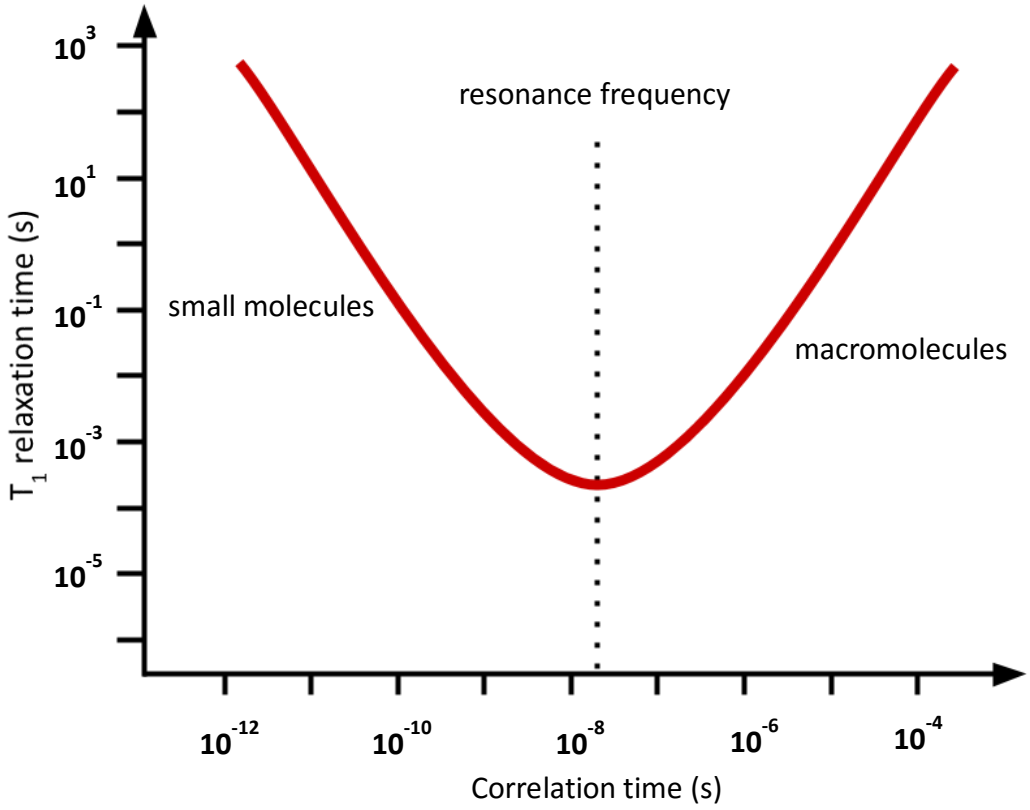

Figure 3.4. The plot shows the relation between the correlation time and the T_1 relaxation time for a given Larmor frequency.[81]

The polyethylene chains in the solid state are not static, rather the chain segments in polymer bulk are constantly rotating and moving. However, the speed of the chain motion is not the same for all phases. This motional speed is defined by a term, called the correlation time (τ_c). The correlation time can be defined as the average time a polymer segment takes to rotate through one radian. In the amorphous region, because of loose chain packing and available free volume, the chains can move relatively freely. So, in the amorphous regions, the rotational frequency of polymer chains is high. On the other hand, the

chains in the crystalline region are packed, and the mobility of chains is restricted. So, the chain motion is slow compared to that of the amorphous chains. In Figure 3.4, the carbon spin-lattice relaxation time is minimum when the correlation time of the chain segments is around 10^{-8} seconds in a 300 MHz magnet. If the correlation time is higher or lower than this value (in a 300 MHz magnet), the relaxation time increases.

In the polyethylene bulk, the amorphous chain segment's rotational frequencies are near to the Larmor frequency, and so the relaxation is highly efficient for the amorphous mobile chains. On the other hand, the chain segments in the crystalline region, having restricted mobility, rotate slowly, thus the relaxation process is slow. The ^{13}C spin-lattice relaxation of the crystalline and the amorphous regions in semi-crystalline polyethylene usually differ by two or three orders of magnitude.[82]

3.3 Method Development Scheme

In this contribution, the aim was to develop an NMR experimental method to obtain quantitative information about the phase composition of solid polyethylene. Historically, many complex NMR pulse sequences have been used to obtain specific information about different systems. Those complex pulse sequences are good for research purposes, but not widely accepted in industries for routine characterization. The aim was to develop a method which is (1) simple to use and understand, and (2) capable of providing reliable and quantitative information. The method was developed based on two very simple properties of polyethylene chains:

1) Chain conformation, and
2) Chain dynamics

The experimental scheme is shown in Figure 3.5. According to this scheme, we need three spectra to calculate the phase composition quantitatively, (1) a quantitative NMR spectrum which contains signals from the whole sample (both rigid and mobile regions), (2) a 'mobile-only' spectrum which contains signals only from the mobile chain segments, and (3) a 'rigid-only' spectrum that contains signals only from the rigid chain segments. The 'mobile-only' spectrum provides information about the amorphous phase and the 'mobile all-trans' chains. On the other hand, the 'rigid-only' spectrum contains signals from the crystalline phase and the 'constrained amorphous' phase. In the 'mobile-only' spectrum, the signal from the mobile all-trans chains is clearly visible, and easily distinguishable from the rigid-all trans chain signal. This is not possible with only the 'total' spectrum. The same is true for the constrained amorphous chain signal which is present in the 'rigid-only' spectrum. Using these three spectra, the phase composition can be calculated reliably. In the later sections, the acquisition of these three spectra from a single experiment will be discussed.

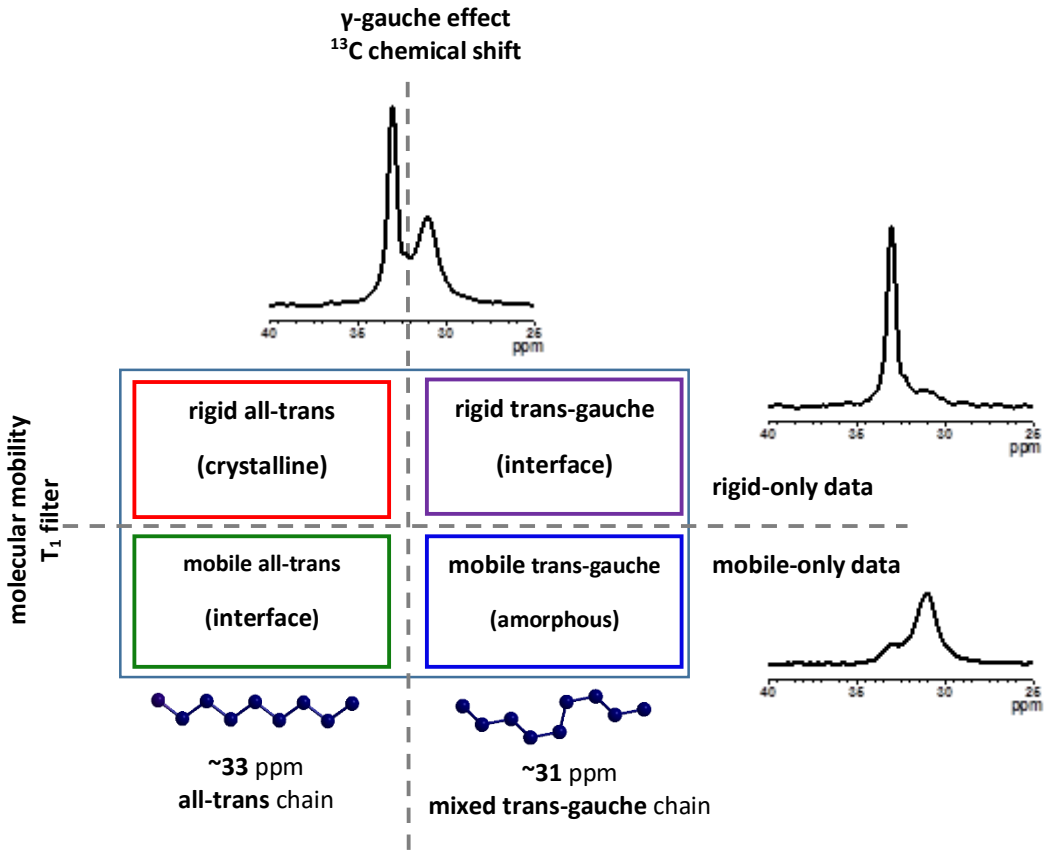

Figure 3.5. Scheme of the experimental method. The signal from the all-trans and trans-gauche chains are separated due to the Gamma-gauche effect. By applying T_1-filter, the signal from the mobile and rigid chains can be separated. Thus, all the information for phase composition can be obtained from a single experimental acquisition.

3.3.1 T_1 filter to acquire 'mobile-only' spectrum

The large difference between the T_1 relaxation times of the mobile and the rigid phases in polyethylene allows us to develop an experimental method to acquire signals only from the 'mobile' chain segments by filtering the rest of the signals coming from the rigid chain segments. The NMR experiments (pulse sequence) start with a recycle delay time (τ_1 in Figure 3.6), the purpose of which is to allow the spin system to relax back to the equilibrium state after the radiofrequency pulse is turned off. It is discussed above that after each acquisition the spin system needs some time to relax, and to allow all the spins to relax one need to wait at least $5T_1$ after each acquisition. If not enough time is allowed between each scan, then some slowly relaxing spins will be saturated and won't be seen on the next scan.

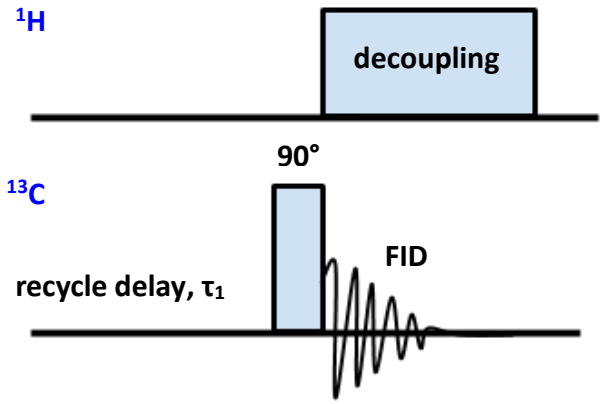

Figure 3.6. A single-pulse ^{13}C NMR pulse sequence with high-power proton decoupling.

It is found in the literature that the T_1 relaxation time for the crystalline region varies from 50 – 500 seconds (depending on the percent crystallinity), and for the amorphous region, the T_1 relaxation time is in the millisecond range.[47b, 83] So, in a single-pulse experiment, if a short delay time is set, which is long enough for mobile spins to relax, but too short for spins in the rigid region, the signal from the rigid region will be saturated in subsequent scans. This is how we can detect the signal only from mobile chains, which we call the 'mobile-only' spectrum.

In this reported method, one second was chosen as the delay time for the T1 filter. The spins that relaxed within one second were located within the mobile region. All other spins were assigned to the rigid regions. For the polyethylene mobile-only spectrum, the use of a 1 second T_1 filter is also found in the literature.[47b, 83] To check the validity of this selection, a saturation recovery experiment (Figure 3.7) was done to determine how the spectral line-shape changes with increasing delay time. In Figure 3.7, at a very short delay time (10 milliseconds to 1-second), the signal in the all-trans region is mostly filtered out. The sharp crystalline signal starts to appear if the delay time is more than one second. So, the use of one second for the T_1 filter is reasonable. On the other hand, the total spectrum can only be obtained when the delay time is more than the five times the maximum T_1 relaxation time for the system. It was determined that a 2000 second delay time was enough for the samples tested.

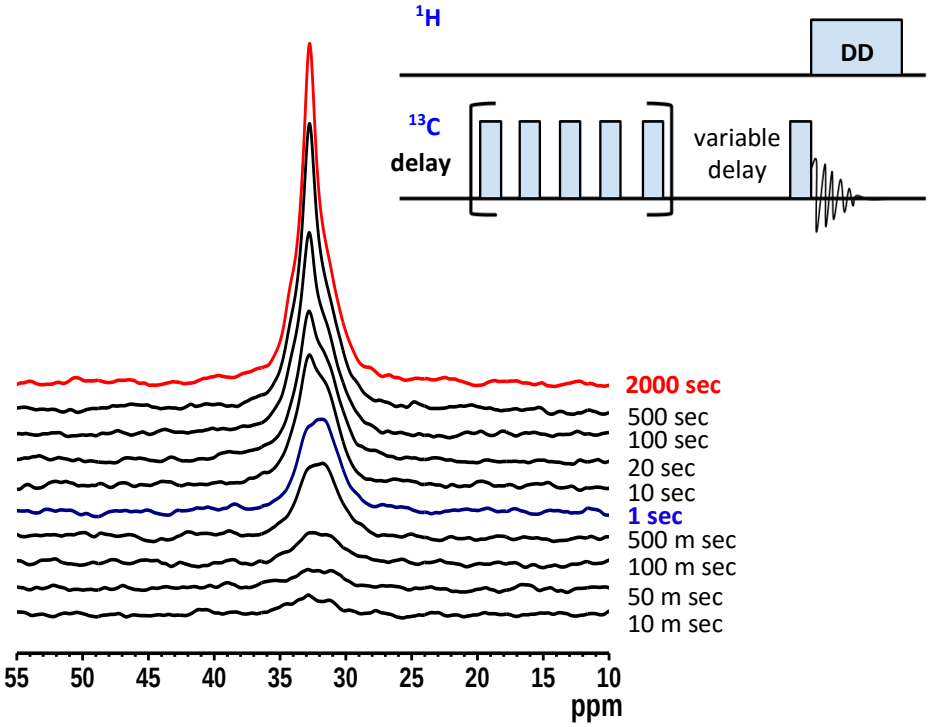

Figure 3.7. The results of the saturation recovery experiment on the sample L289. The sharp crystalline signal appears when the relaxation delay is more than 1 second. The pulse sequence of the saturation recovery experiment is presented on the top.

3.3.2 The 'rigid-only' data

The 'mobile-only' data can easily be obtained by applying a T_1 filter with appropriate delay time. However, acquiring a *quantitative* 'rigid-only' spectrum by an NMR experiment is not simple. One method is to use a cross-polarization (CP) experiment with short contact time. In the cross-polarization experiment, the polarization transfer from ^{1}H to ^{13}C is most efficient in the rigid chains. During the CP contact pulse, the transfer occurs only in the rigid chains at the beginning due to the higher polarization transfer efficiency in the rigid region. But in the mobile regions, the transfer is less efficient at the beginning of the contact pulse. So, with a short contact pulse, sufficient enough to allow the transfer of the rigid signals, but not the mobile signals, a "rigid-only" spectrum can be acquired. However, the cross-polarization technique is not quantitative. Moreover, the 'rigid-only' spectrum obtained by a CP method

cannot be compared with the 'mobile-only' spectrum obtained by a direct polarization method. As the aim is to get quantitative information about the phase composition, the CP method was not used to acquire the "rigid-only" spectrum.

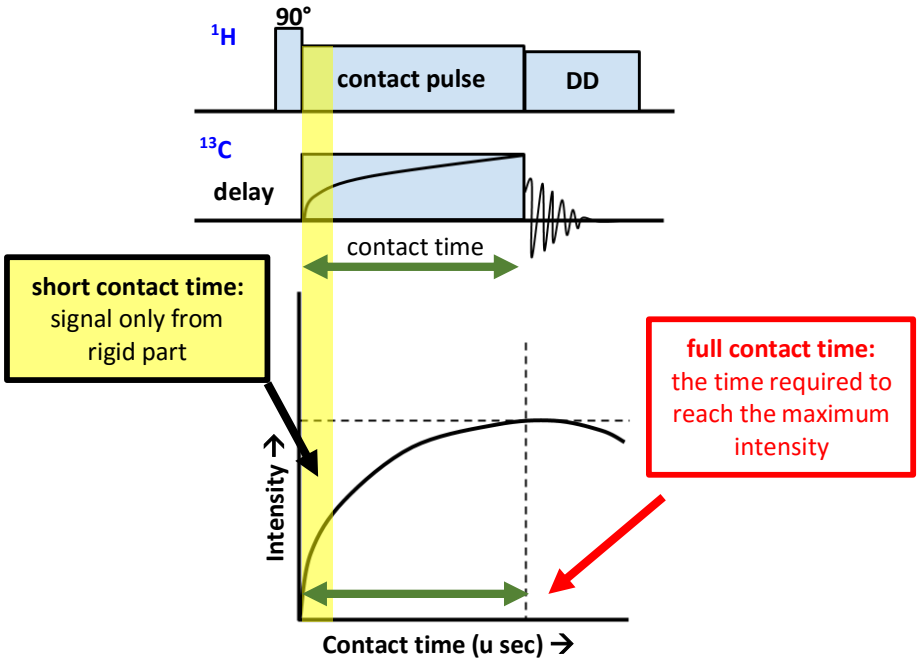

Figure 3.8. The schematic diagram is showing how short-contact CP experiment can acquire 'rigid-only' spectrum. At the beginning of the contact pulse, polarization transfer occurs mostly in the rigid chains, so short contact CP will acquire a rigid-only carbon spectrum.

Considering that the 'total' spectrum (quantitative spectrum obtained with a 2000 second recycle delay) and the 'mobile-only' spectrum are acquired in exactly the same experimental conditions and for the same amount of sample, these two spectra are directly comparable. The 'rigid-only' spectrum can thus easily be obtained by simply subtracting the 'mobile-only' signal from the 'total' spectrum. So, two single-pulse NMR experiments (with and without T_1-filter) in the same experimental conditions are sufficient to calculate the phase composition of PE.

3.3.3 EASY: a double-acquisition background suppression pulse sequence

Although two simple single-pulse experiments (with and without T_1-filter) (Figure 3.6) in the same conditions are sufficient for collecting all the data of phase composition, the aim was to develop a single experiment that will provide fully quantitative data. The recycle delay for the quantitative experiment is long (2000 seconds), and the magnetic conditions might slightly change during this extended period, making the data questionable for quantitative comparison. So, a double-acquisition experiment was developed, which can acquire both the 'total' and the 'mobile-only' spectra in alternate acquisitions, making the method more reliable and quantitative.

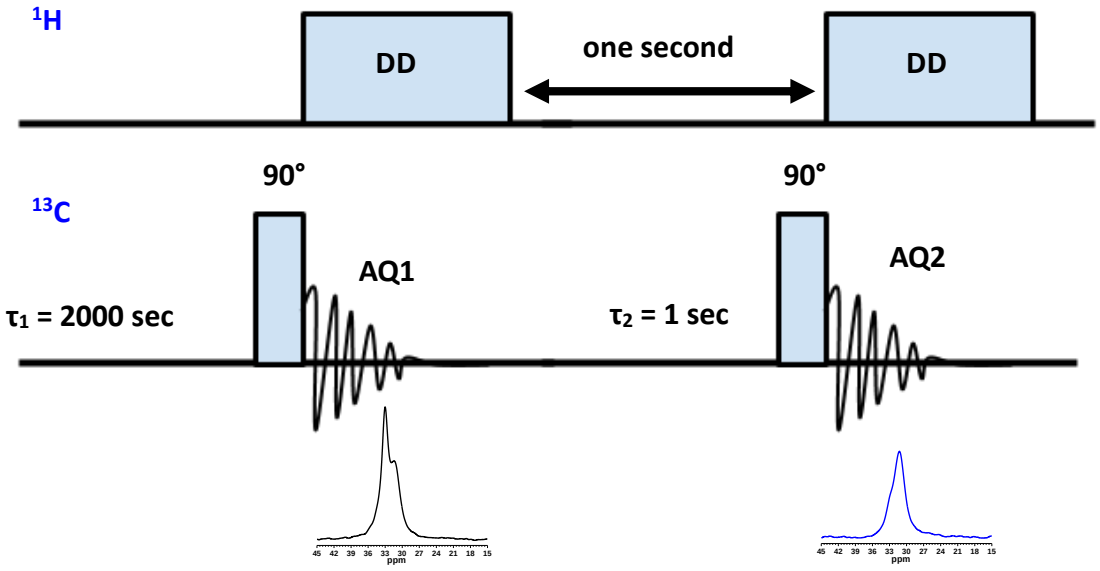

Figure 3.9. The double-acquisition pulse sequence, EASY.[84] The first acquisition with 2000 sec recycle delay will acquire the 'total' spectrum, and the second acquisition with 1 second recycle delay acts as the T_1-filter.

Recently, Jaeger and Hemmann reported a double-acquisition background suppression pulse sequence, called EASY (Elimination of Artifacts in NMR Spectroscopy).[84] The EASY pulse sequence (Figure 3.9) is a simple combination of two single-pulse carbon experiments that we recognized could be used to acquire the 'total' and the 'mobile-only' data by setting appropriate delay times for the two acquisitions.

The EASY pulse program was used with τ_1 = 2000 seconds and τ_2 = 1 second to acquire the 'total' and the 'mobile-only' spectra in the first and the second acquisition, respectively. All the experimental conditions, except the recycle delay, were the same for the first and the second acquisition. However, when we compared the 'total' and the 'mobile-only' spectra, we found an unexpected result (Figure 3.10). We found that the signal intensity for the mixed trans-gauche chain in the 'mobile-only' spectrum was higher than that of the 'total' spectrum, which is completely impossible. So, we found the 'original' EASY pulse sequence was not suitable for the quantitative determination of the phase composition of solid PE.

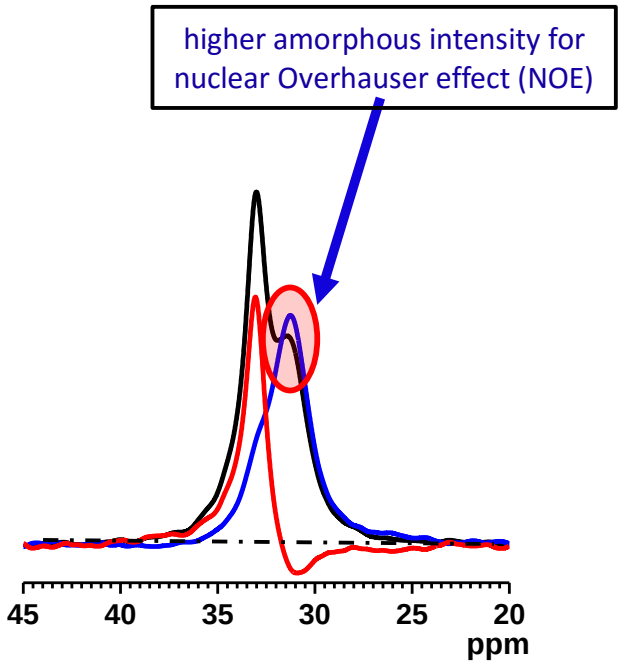

Figure 3.10. The results of the original EASY experiment. The signal for the trans-gauche chains in the 'mobile-only' spectrum (blue line) is found to be higher than that of the 'total' spectrum (black line) due to the nuclear Overhauser effect. The red line represents the difference spectrum obtained by subtracting the 'mobile-only' spectrum from the 'total spectrum'.

3.3.4 Modified-EASY pulse-sequence

To understand the source of the enhanced signal, we ran several control experiments with the same (and different) delay time for the first and the second acquisitions. We found that when the τ_1 and τ_2 values (Figure 3.9) are sufficiently long (more than 5 seconds), the spectral line-shape from both acquisitions are reasonable. However, for τ_1 or τ_2 = 1 second (or less than 5 seconds), the signal was enhanced enhancement in the mobile region. By several control experiments, we realized that the enhanced signal is due to the nuclear Overhauser effect (NOE) in the mobile region of PE. During the high-power decoupling in the first acquisition, the proton spin system becomes saturated and will relax back to the equilibrium state after the decoupling pulse is turned off. However, the T_1 relaxation time for the proton in the mobile chain is around 1 second which needs at least 5 seconds for the complete relaxation process. If not enough time is allowed, the carbon signal in the mobile chain can be enhanced by cross-relaxation by the double-quantum transition between the excited proton and carbon. The signal enhancement due to NOE can be seen by the Solomon equation,

$$\frac{d\,(C_z - C_z^0)}{dt} = -\rho_C\,(C_z - C_z^0) - \sigma_{CH}(H_z - H_z^0) \qquad \textbf{(15)}$$

Where C_Z and H_Z are the net magnetization of the carbon and proton nucleus along the z-axis respectively, C_Z^0 and H_Z^0 are the net magnetizations of carbon and proton *in the equilibrium state* respectively, ρ_C is the self-relaxation rate, and σ_{CH} is the cross-relaxation rate. So, to avoid the signal enhancement in the carbon spectra, we need to stop the cross-relaxation which can be done by making the term $\sigma_{CH}\,(H_Z - H_Z^0)$ (in the equation -15) equal to zero. As we don't have control on the cross-relaxation rate, we must deal with the $(H_Z - H_Z^0)$ part of the equation, and this term can be eliminated by increasing the time (τ_2) between the two acquisitions, in order to allow all the proton spins to relax back to equilibrium after the

first acquisition. But if we just increase the τ_2, a portion of the signal from the rigid chains will also be collected in the second acquisition. To solve this problem, we had to modify the pulse program. The modified-EASY pulse sequence is shown in Figure 3.11.

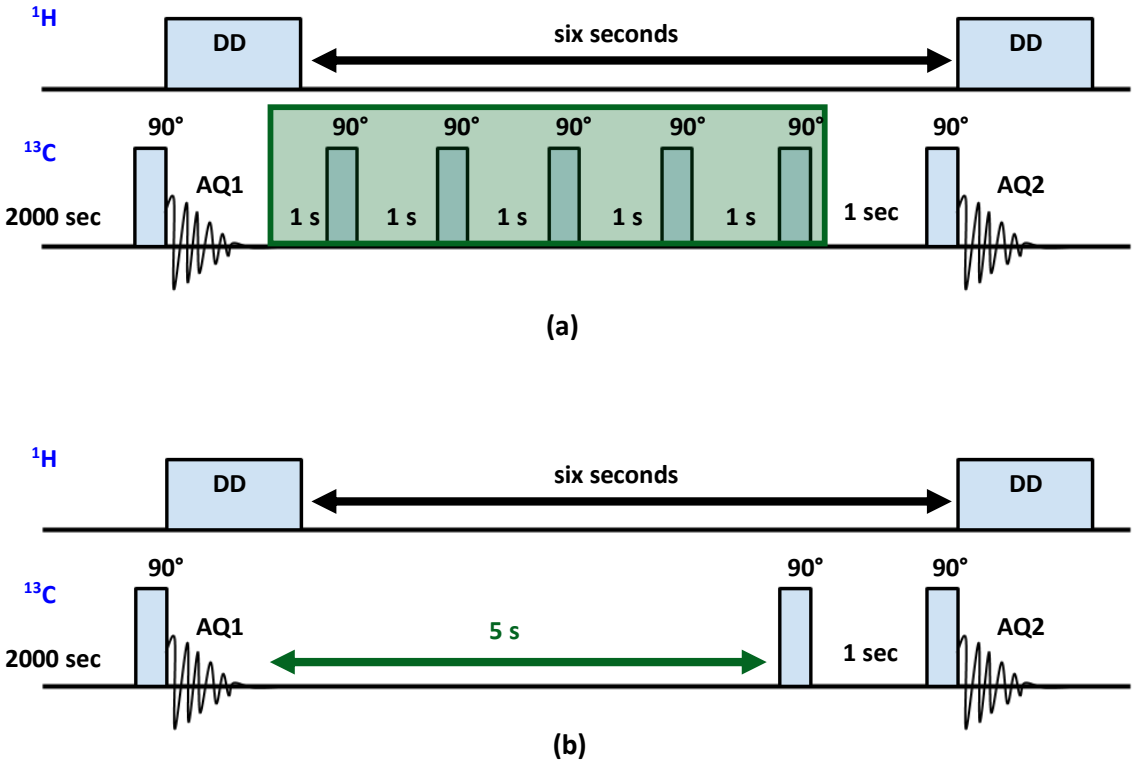

Figure 3.11. Two versions of modified-EASY pulse sequences are shown, a) version 1: five 90° spoiler pulses are inserted between the two acquisition pulses to increase the delay between the two acquisitions and to saturate the signal from the rigid chains.[85] b) version 2: only one spoiler pulse is sufficient to suppress the signal enhancement if the total time between the two acquisitions is more than 5 seconds.

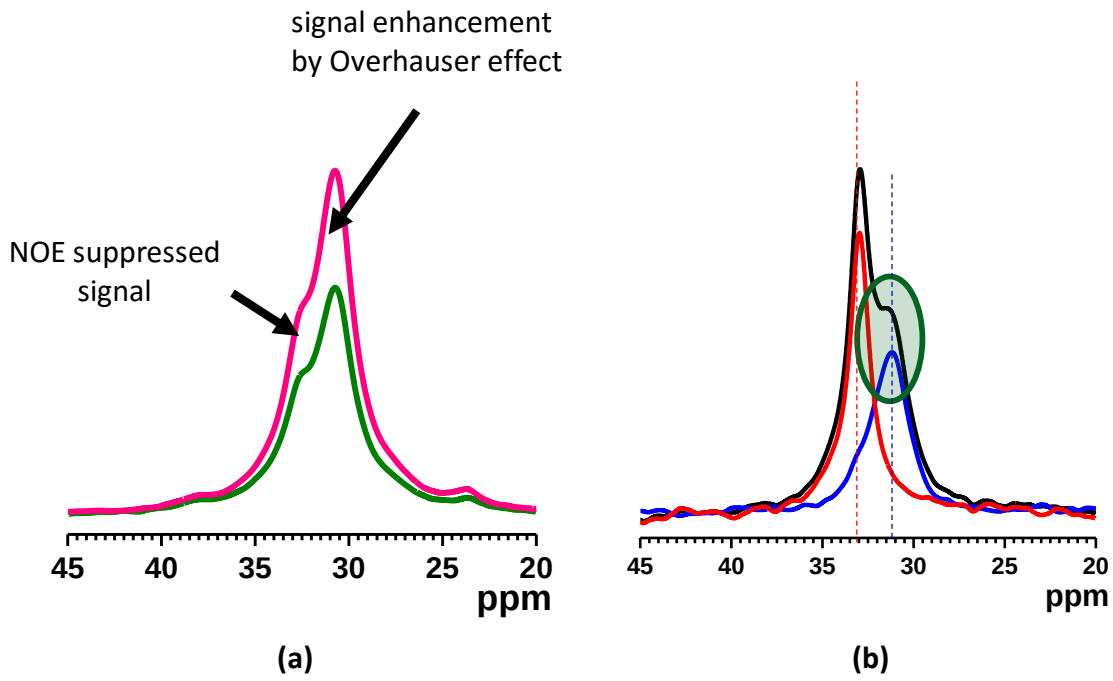

Figure 3.12. (a) Compares the 'mobile-only' spectra acquired by the EASY (pink line) and the modified-EASY (green line) pulse sequence which shows that the Overhauser effect is eliminated in the case of the modified-EASY pulse sequence, (b) an improved result obtained by the modified-EASY pulse sequence, no signal enhancement is seen in the 'mobile-only' spectrum.

To stop the signal enhancement (by NOE), we inserted a few spoiler pulses with appropriate delays (modified-EASY version 1, Figure 3.11-(a)) between the two acquisition pulses. These pulses have two purposes, (1) to increase the time-distance between the two acquisitions, and (2) to keep the rigid-signal saturated so that we get 'mobile-only' spectrum in the second acquisition. However, although we used a train of 5 spoiler pulses at the beginning, later we found that, only one spoiler pulse is sufficient as long as the total delay between the two acquisition pulses is more than 5 seconds and the delay between the spoiler pulse and the second acquisition pulse is 1 second (modified-EASY version 2, Figure 3.11-b)). We found that both the version (1 and 2) of modified-EASY produced the same results.

3.3.5 Improved results with the modified-EASY pulse sequence

The modified-EASY pulse program was tested for the polyethylene sample with a short delay time. Figure 3.12(a) compares the mobile-only spectra of a PE sample, the pink-lined spectrum was collected without an NOE suppression spoiler pulse, and the green lined spectrum was obtained with a spoiler pulse, the result is evident from Figure 3.12(a). When the 'total' and the 'mobile-only' spectra were acquired using the modified-EASY pulse program, a reasonable result was found as shown in the Figure 3.12(b).

In Figure 3.12(b), the black line represents the 'total' spectrum, the blue line represents the 'mobile-only' spectrum, and the red line is the difference spectrum or the 'rigid-only' spectrum. It is clearly seen in Figure 3.12(b) that the trans-gauche chain intensity in the 'mobile-only' spectrum is lower than that of the 'total' spectrum. In the same chemical shift region in the 'rigid-only' spectrum, the presence of signal proves the existence of 'constrained amorphous' chains. The presence of the mobile all-trans chain is confirmed by the presence of the signal at ca. 33 ppm in the 'mobile-only' spectrum.

3.4 Spectral Deconvolution and Data Calculation

The data obtained from the modified-EASY experiment were analyzed to calculate the phase composition of the solid polyethylene. The rigid-only data was obtained by subtracting the 'mobile-only' signal from the 'total' spectrum using the NMR control software (XwinNMR or Topspin). The 'mobile-only' spectrum contains two signals, at ca. 31 ppm for the mobile trans-gauche chains which constitutes the amorphous region and at ca. 33 ppm for the mobile all-trans chains which are believed to form a part of the interface. The 'rigid-only' spectrum also contain two signal populations. The signal at ca. 31 ppm is for the constrained amorphous chain, which constitutes the crystal-amorphous interface along with the mobile all-trans chains, and the orthorhombic crystalline signal was seen at ca. 33 ppm. For some samples, we saw a signal for the monoclinic crystalline phase at ca. 34.4 ppm in the rigid-only spectrum. As

mentioned earlier, the chain density of the monoclinic crystal is lower than that of the orthorhombic crystal, so the monoclinic crystalline peak appears slightly downfield to that of the orthorhombic peak.

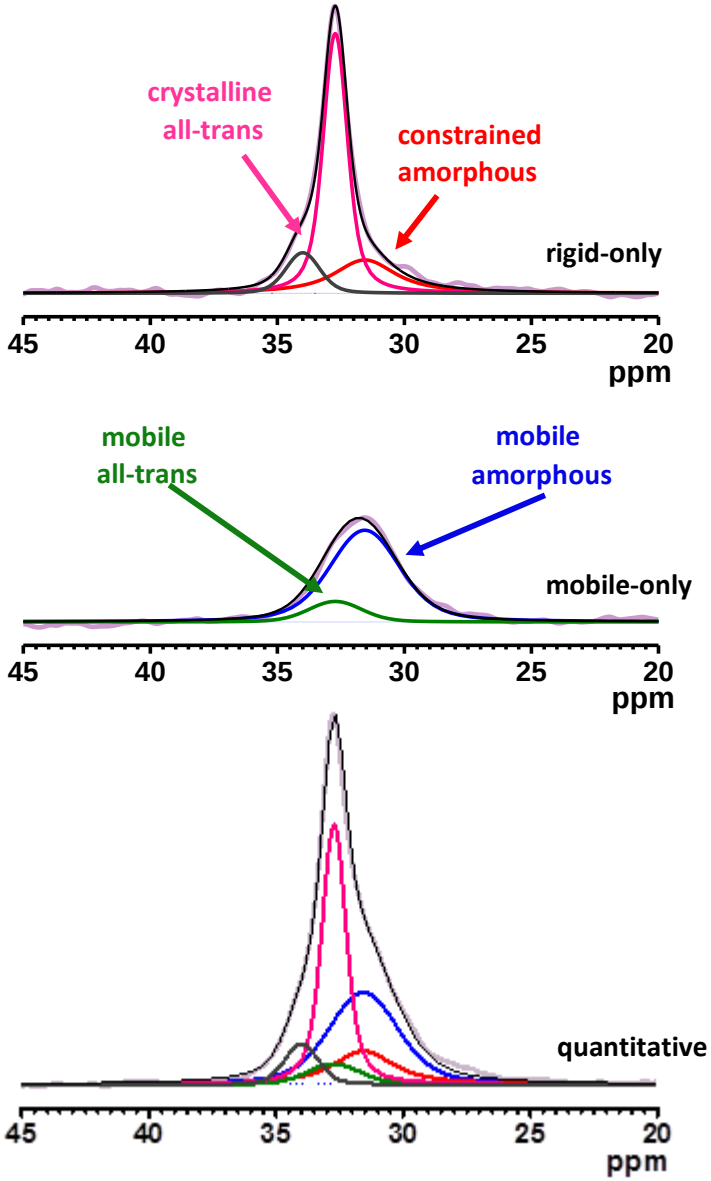

Figure 3.13. Deconvolution of the 'rigid-only' (top) and the 'mobile-only' (middle) spectra to calculate the phase composition. The fitting parameters for each component (obtained in the 'rigid-only' and the 'mobile-only' deconvolutions) were used without any modification to reconstruct the total spectral line-shape (bottom).

The phase composition data or the fraction of each chain type was determined by spectral deconvolutions using OriginPro 9 software (Figure 3.13). The 'mobile-only' spectrum was deconvoluted using two Voigt functions, a convolution of Gaussian and Lorentzian functions. The integrated area under the component at ca. 31 ppm and ca. 33 ppm were assigned to the mobile-amorphous and the mobile all-trans chains, respectively. As the chemical shift value for the trans-gauche chains varies sample to sample, depending on the equilibrium trans-gauche density and the chain packing, the peak position of the trans-gauche chains was determined from the 'mobile-only' spectrum by the manual peak picking method. The 'rigid-only' spectrum was deconvoluted using two (or three, if the monoclinic crystalline signal is present) Voigt functions- one at ca. 31 ppm is assigned to the constrained amorphous chains and the other at ca. 33 ppm is assigned to the orthorhombic crystal state (or rigid all-trans chains). The Gaussian to Lorentzian ratio for the mobile components were found to be less than one, and for the rigid components were greater than one. Here a point should be noted that the 'total' spectrum was not fitted by the method mentioned above, rather all the fitting parameters obtained from the 'mobile-only' and the 'rigid-only' spectral deconvolutions were just copied to reconstruct the 'total' spectrum line-shape.

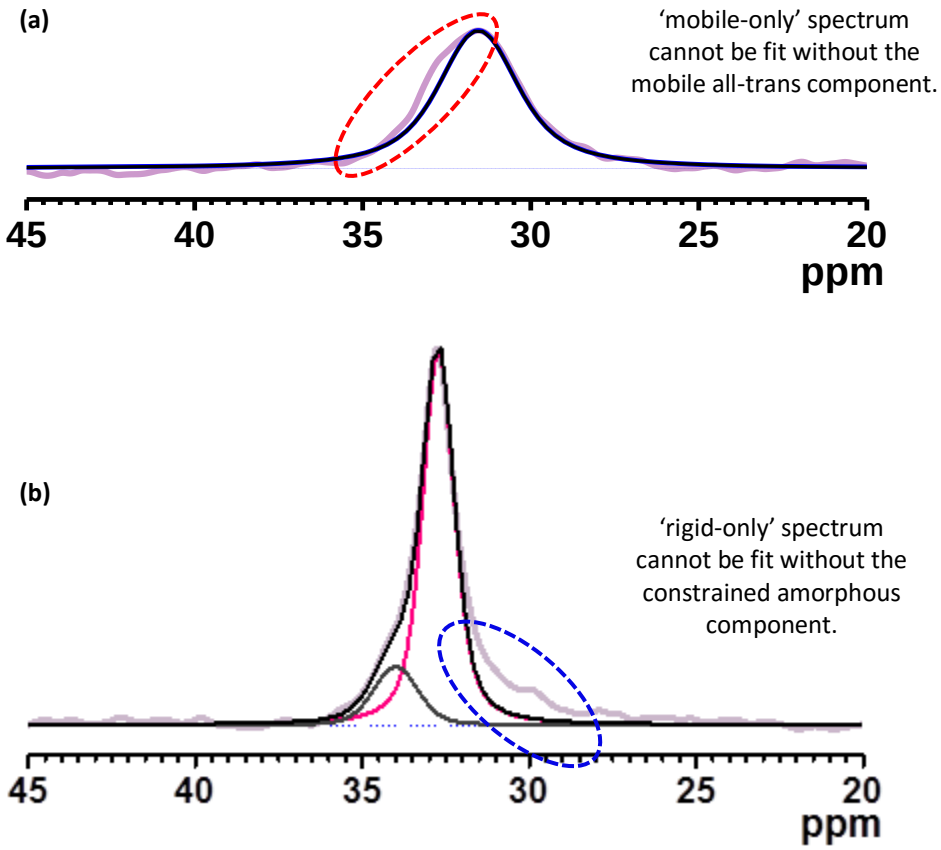

Figure 3.14. Showing that the mobile all-trans and the rigid trans-gauche components are necessary for the spectral line-shape fitting. (a) The 'mobile-only' spectrum cannot be fit without the mobile all-trans component, and (b) without the constrained amorphous component at ca. 31 ppm, the rigid-only spectrum cannot be fit.

The four (or five) components used for the spectral deconvolution have physical meanings and are required to properly fit the spectra. As is seen in Figure 3.14(a), an attempt to fit the 'mobile-only' spectrum with only one component at ca. 31 ppm does not work. It confirms the obvious presence of all-trans chains which are very mobile, and their mobility is comparable to that of the amorphous chains. Similarly, the 'rigid-only' spectrum was attempted to be fit without the constrained amorphous component, and a similar result was obtained for most of the samples (Figure 3.14(b)). The integrated

areas for each fitting component were used to calculate the phase composition. For the total crystalline calculation, the integrated areas of the orthorhombic and the monoclinic crystalline regions were added. The total interface fraction was calculated by adding the mobile all-trans and the constrained amorphous intensity. A sample calculation is shown in equation 16.

$$\%\ total\ crystalline = \frac{(A^{orth.\ crystal} + A^{mon.\ crystal})}{A^{total}} \times 100 \quad \textbf{(16)}$$

Here, $A^{orth.\ crystal}$, $A^{mon.\ crystal}$ and A^{total} represent the integrated area of the orthorhombic crystalline region, the monoclinic crystalline region and the total integrated area.

3.5 Conclusion

In this chapter, a solid-state NMR experimental method is presented that was developed for the polyethylene phase composition study. The method is very simple and easy to optimize. As the pulse sequence is capable of acquiring both the 'total' and the 'mobile-only' spectra in alternate scans, the data required for polyethylene phase composition calculation is obtained in a single experimental acquisition, and the results are fully quantitative and reliable. Although the experiment was designed for polyethylene samples, this pulse program can also be used for other heterogeneous systems having a large difference in T_1 relaxation times.

CHAPTER 4

4 THE INFLUENCE OF CHAIN LENGTH AND CHAIN ARCHITECTURE ON THE CRYSTALLINE/AMORPHOUS INTERFACE IN SOLID POLYETHYLENE*

4.1 Introduction

Polyolefins have been the dominant materials class on the plastic market. A major component of the polyolefin market is polyethylene (PE), and it is the most widely used thermoplastic in the world, being fashioned into products ranging from clear food wrap and plastic bags to laundry detergent bottles and automobile fuel tanks.[86] PE is a semi-crystalline polymer which structure and morphology have received much attention in the polymer scientist community for the last few decades. One reason is its very simple chemical structure that can serve as a model for polymers. Although PE is one of the simplest polymers in the chemical perspective, its morphology, physical and mechanical properties can vary widely depending on the manufacturing procedure and post-synthetic processing. With recent advances in the catalyst technology, polyethylene can be synthesized with different chain architectures (linear or with short/long chain branches) and the average molecular weight, and the chain length & topology can be controlled precisely.[19, 87] For example, properties and morphology of linear low-density polyethylene's (LLDPE's) synthesized using two different catalysts, Ziegler-Natta or single-site metallocene catalysts, can be

* *The content of this chapter has been published in Macromolecules, 2015, 48, 3040-3048.*

significantly different.[88] From a phenomenological point of view, a semi-crystalline polyethylene can be considered to be crystallites embedded in a non-crystalline (amorphous) matrix. Plenty of research have already been done on understanding PE morphology, and new findings are being reported regularly, as the existence of the intermediate phase having properties in between the crystalline and amorphous phase.[89] Such an old and simple polymer is still attractive in the polymer research field. Much of the renewed interest in PE stems from growing evidence that the interfacial region, or interphase, between the crystalline and amorphous phases, is an important factor in controlling the final properties.

In this work, the role of chain length versus chain architecture on the nature and composition of the crystalline/amorphous interface for a series of solid PE reactor fluffs was systematically studied. The various routes of polyethylene production are outside the scope of this work. The interested readers are encouraged to check these references.[6a, 19, 87c] Being a very old polymer with complex morphology, polyethylene morphology, and physical properties has been theoretically and experimentally studied in both the melt and solid state by many academic and industrial researcher for decades.[90] Many different techniques like, differential scanning calorimetry (DSC), scanning electron microscopy (SEM), X-ray diffractometry (XRD), Raman or infrared spectroscopy have been employed to study the morphology of PE for the last few decades.[6a, 91] The DSC measurement being one of the most popular methods for polyethylene study for its experimental simplicity, and it can provide an idea about the fraction of crystalline and non-crystalline phase based on the thermal analysis. Other spectroscopy and microscopy techniques do the similar job, i.e. give a rough idea about the crystallinity, and none of those provide chain specific information about the crystalline/amorphous interface. However, nuclear magnetic resonance (NMR) spectroscopy has proven to be a useful tool for understanding the solid-state structure of polyethylene, including linear PE, linear low-density PE copolymers, high-density PE, and ultrahigh-molecular-weight PE (UHMWPE). Methods ranging from static ^{1}H wide-line methods to relaxation analysis

to polarization-transfer ^{13}C site-resolved experiments have been used extensively for the past 30 years to discern the basic phase structure of PE.[47c, 92] Almost all aspects of the relationships between chain dynamics and relaxation/polarization transfer properties, chain conformation and crystal structure versus chemical shift, quantitative detection of components in one and two dimensions, spin-diffusion, and weaker spin-coupling, as well as connections between NMR responses and mechanical or physical properties, have been explored extensively for PE's.[93] Yao and co-workers recently nicely demonstrates how representative modern solids NMR methodologies can be applied to study phase behavior in UHMWPE.[77b]

It is now generally accepted from previous research using different methods (calorimetry, microscopy, scattering, diffraction and other spectroscopy) and NMR spectroscopy that PE morphology has four distinct components: (i) a primarily orthorhombic crystalline phase with chains in all-trans conformation, (ii) non-crystalline amorphous regions with chains containing a large equilibrium gauche conformer content and which undergo rapid reorientation, (iii) chains in all-trans conformations that exhibit increased mobility relative to the crystalline all-trans chains, and (iv) chains with equilibrium gauche conformer content whose mobility is reduced relative to the amorphous region chains. The crystalline/amorphous interface is believed to be composed of the rigid trans-gauche and the mobile all-trans chains. Additional chain types and phases, such as monoclinic crystalline phases or highly mobile detrital chain fragments, can be generated in drawn fibers.[78, 94] Due to the advancement of the catalyst and manufacturing technology, and availability of different comonomers, it is now possible to control the copolymerization process to design specific chain architecture. It is important to understand the link between the chain length, architecture, and the post-synthetic processing with the phase composition, as this knowledge can help us to design new types of polyethylene of desired properties for specific

purposes. For this reason, a straightforward and reliable method needs to be developed to systematically and quantitatively determine the phase composition of solid PE.

^{1}H NMR methods are attractive because it is fast, and in static experiments three out of four components can be resolved by analyzing the free induction decay signal or by relaxation experiments. Moreover, proton NMR can determine the domain size of crystalline or amorphous phase by well-established spin-diffusion experiments.[4b] Inexpensive bench-top NMR systems can provide access to experiments of this type.[78] ^{13}C NMR methods, while more time-consuming, provide additional information not accessible in the ^{1}H experiments through chemical shift resolution of chain conformations, thereby increasing the resolution and specificity for the four distinct chain types and their domains[95] and also revealing dynamic processes involving chain interconversion between those conformations.[4b, 95-96] While not discussed at length here, the chain-diffusion process described by Schmidt-Rohr and Spiess is assumed to be operative in linear PE.[96a]

The systematic analysis of the interfacial characteristics of PE as a function of chain length and the number and type of branches, i.e., linear versus short-chain branched versus long-chain branched, is required in order to fully understand the role that the interface plays in final properties and how the interface is defined by synthesis and processing conditions. In this contribution, a ^{13}C MAS (magic angle spinning) NMR experiment (discussed in detail in Chapter III) was used to quantitatively reveal the amounts of the mobile all-trans chains and the constrained amorphous chains that comprise the interfacial region in PE's as a function of chain length and chain topology. Separating contributions from increasing molecular weight and increasingly complex chain architecture were a specific motivating factor in this work, as was the need to acquire the necessary experimental data revealing all four phase components in a single experimental acquisition that can be completed in a reasonable amount of time for typical polyethylenes.

As discussed in the previous chapter in details, a version of the EASY (Elimination of Artifacts in NMR Spectroscopy) background suppression experiment,[84] which is a double-acquisition pulse sequence, was modified to suppress Overhauser effects such that quantitative sub-spectra were collected on alternate scans and which when taken together quantify all four phase elements. While the EASY experiment was introduced as a robust background suppression method for solid state NMR, results described here indicate that it has much broader potential to clarify important questions in solid systems, even when background signals are not an issue. Most importantly, the experiment resolves the two components that constitute the interfacial regions. The amounts of the mobile all-trans chains and the constrained amorphous chains in the interface are shown to increase with increasing molecular weight for the liner PE's. The fate of the interfacial components can be followed for PE's with specific introduction of short, long, or long with short chain branches, and results reported here indicate that interface in the latter is truly unique compared to linear polymers with the same molecular weight. The spirit of this project is represented by systematically varying chain structures depicted in Figure 4.1.

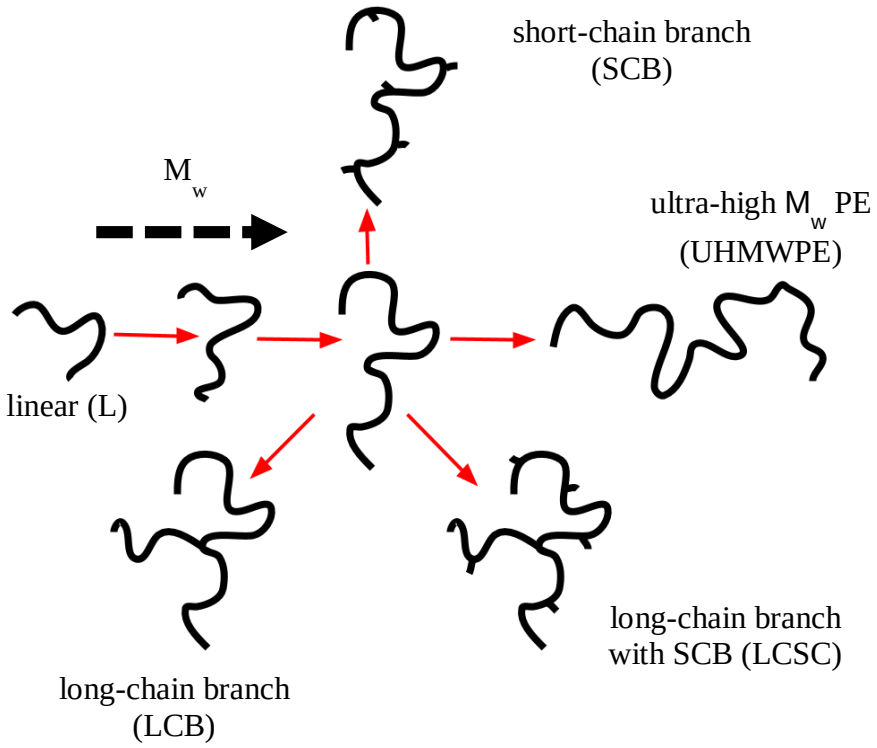

Figure 4.1. Schematic representation of PE chain structures considered in this study,[83] ranging from low molecular weight linear to high molecular weight linear, and also including chains with short branches from alkene comonomer incorporation, long-chain branches, and polymers with both long and short branches.

4.2 Experimental Section

In this study we have investigated fifteen well characterized PE samples of different molecular weight and chain architecture (Figure 4.1), ranging from linear, chain with short chain branches (SCB), chain with long chain branches (LCB) & long chain branches containing short chain branches (LCSC), supplied by Chevron Phillips Chemical Co., Bartlesville, OK. Thirteen of the fifteen PE's are as synthesized reactor fluff; those with additional thermal treatments are identified throughout the text. Expect the one commercial grade UHMWPE sample (U-1466 in Table 4 – 1; obtained from Ticona as GUR4120) prepared via Ziegler-Natta synthesis, all polymers were made using single site metallocene catalysis. Some solvent

fractionated materials were also used. Peak temperatures and heat flows were found using a linear integration along the baseline of the peaks. Percent crystallinity was found by taking the heat flow of the initial scan peaks and dividing that by 293 J/g (i.e., heat flow for 100% crystalline PE). The characteristics of the samples are listed in Table 4 – 1.

Sample molecular weight and distribution values were measured using a PL220 high- temperature GPC/SEC system (Polymer Laboratories, UK, now an Agilent company) equipped with three HMW-6E columns (Waters Corp., Milford, MA) for polymer separation and an IR4 detector (Polymer ChAR, Spain). Molecular weight determinations were made using Cirrus software (Polymer Labs) and the integral calibration method. A broad MWD HDPE Marlex™ BHB5003 resin (Chevron Phillips Chemical) was used as the broad MW standard. Chromatographic conditions are set as the following: column oven temperature: 145 °C; flow rate: 1.0 mL/min; injection volume: 0.4 mL; polymer concentration: nominally at 2.0-2.5 mg/mL but lower for high M_W polymers, depending on samples. In addition to conventional molecular weight measurements, molecular weight and distribution measurements were also made on selected samples using a PL220 GPC/SEC unit coupled to multi-angle laser light scattering detector (Wyatt) via a heated transfer line as previously described.[97] Short chain branching content in the samples was measured using C^{13} NMR as described by Randall,[98] whereas long chain branching content was obtained from the SEC-MALS method described above.

Table 4—1. Description of polyethylene samples used in this investigation. Note that L = linear; U = UHMWPE; SCB = short chain branch; LCB = long chain branch; LCSC = long chain branch with SCB. All samples are reactor fluff precipitate, with the exception of L294 and U1466. For the polymers with short chain branches, the type of comonomer used to generate the branch is denoted by b **= butene,** h **= hexane, and** o **= octene.**

Sample	M_w (kg/mole)	M_n (kg/mole)	PDI	SCB/1000 TC	LCB/10,000 TC
L-45	45	7	6.4	0	0
L-165	165	57	3.5	0	0
L-184	184	74	2.5	0	0
L-241	241	68	3.5	0	0
L-289	289	63	4.6	0	0
L-294[#]	294	109	2.7	0	0
L-400	400	95	4.2	0	0
U-1466	1466 2012*	261 412*	3.9 4.9*	0	0
SCB-43-h	43	7	6.1	7	0
SCB-146-b	146	127	1.15	12	0
SCB-148-o	148	128	1.15	12	0
SCB-184-o	184	129	1.44	12	0
LCB-161	161 235*	40 56*	4.0 4.2*	0	0.34
LCSC-284-h	284 417*	184 314*	1.5 1.33*	11.9	0.13
LCSC-627-h	627 1155*	458 1025*	1.4 1.13*	11.6	0.10

[#] This linear PE was examined following a compression molding step.
*Obtained via SEC-MALS

^{13}C magic-angle spinning (MAS) NMR experiments were acquired using a Bruker DSX Avance 300 MHz instrument on a 4-mm MAS triple-resonance probe equipped with a boron nitride stator. All data reported herein were collected at room temperature with MAS speeds between 5-6 kHz, and with ^{1}H decoupling during the acquisition time at radio-frequency field strengths ranging from 70-100 kHz. Direct polarization was used to generate carbon signals with typical 90^{o} pulse widths of 3.4 μs, and 32 scans were typically collected. To avoid inherent uncertainties about quantitative detection of spins in different phases, cross-polarization was not used in any of the experiments reported here. Unless specifically labeled as single-pulse experiments, all data reported herein were collected using a modified version of the recently reported EASY experiment,[84] which was proposed earlier this year by Jaeger and Hemmann

as a convenient method to eliminate troublesome background signals in solid state NMR. Background signals are not an issue for collecting PE spectra on most commercial solids NMR probes, as the PE signals are confined to the narrow 30-35 ppm range of the spectrum. As described in detail in the previous chapter (Chapter III), the EASY experiment is a double-acquisition pulse sequence which is designed based on relaxation time difference. This sequence is applicable to heterogeneous systems having a reasonably large difference in spin-lattice relaxation time (T_1) between different phases. It is well known in the literature that the spin-lattice relaxation time of the mobile amorphous chain is very short, on the order of few tenths of a second, and for the rigid crystalline chain the T_1 value varies from 50-500 seconds.[47c, 89, 95] So, T_1 filter is a good method for acquiring NMR spectrum containing signal only from mobile chains, 'mobile-only' spectrum. While the total spectrum (containing signal from all chains) can only be obtained when sufficient time (five times the largest T_1 relaxation time) is allowed between every scan. As 'EASY' is a double acquisition pulse sequence, both the 'total' spectrum and the 'mobile only' spectrum can be acquired in an alternate scan by allowing appropriate delay time before each acquisition, and this will minimize complications inherent to collecting two separate experiments. The 'rigid-only' spectrum can be obtained by subtracting the 'mobile-only' signals from the 'total' spectrum. The 'mobile-only' spectrum contains signal from the mobile amorphous and the mobile all-trans chain while the 'rigid-only' spectrum provides information about the rigid all-trans (crystalline) and the constrained amorphous chains. The signal corresponding for each physical regions can be obtained by using spectral line-shape fitting software, thus, phase composition results can be obtained by appropriate calculation. In the original EASY experiment, there is insufficient time to allow all ^{1}H magnetization in highly mobile phases to return to equilibrium following the first decoupling period, which causes nuclear Overhauser enhancement in the 'mobile-only' spectrum. To avoid this signal enhancement, the original EASY pulse program was modified by inserting a series of ^{13}C 90° saturation or "spoiler" pulses between the first and second acquisition, as shown in Figure 4.2. Although five "spoiler'' pulses with 1-second delay were used to collect data of some

samples, it was found later that only one spoiler pulse (τ_2 seconds before the second acquisition pulse) is sufficient as long as the total time between the two acquisition is enough for all the proton magnetization comes to equilibrium. The beauty of this new method is, all the data required to calculate phase composition is collected in a single experimental acquisition within a reasonable amount of time.

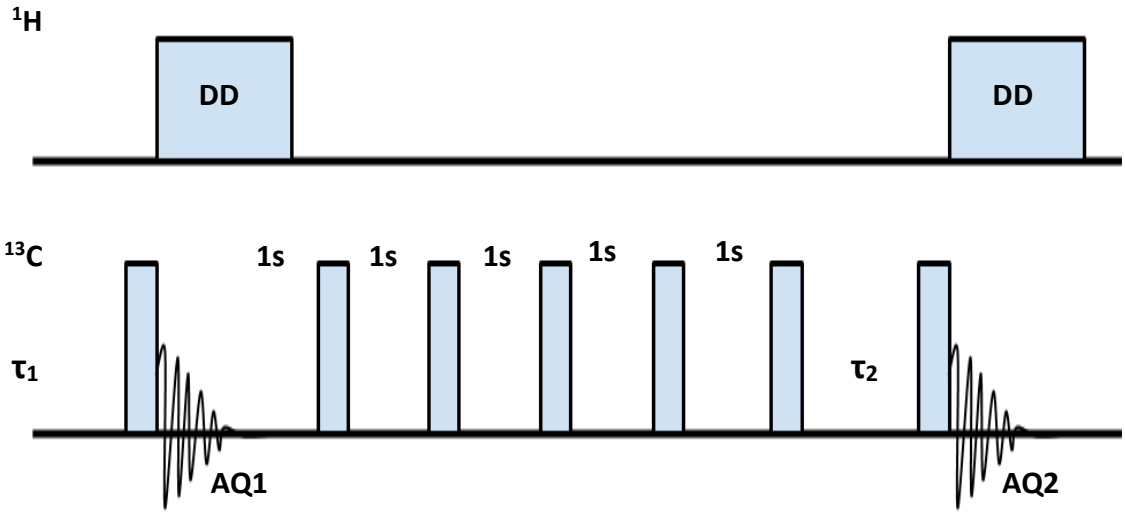

Figure 4.2. Pulse sequence diagram for the modified-EASY experiments,[83] in which ^{13}C saturation pulses have been inserted between the first and second acquisition to eliminate transient Overhauser effects and ensure carbon magnetization that has undergone only 1 s of spin-lattice relaxation is accurately sampled. While five saturation pulses were used for most of the data reported here, one is sufficient. All ^{13}C pulses shown are 90° pulses. The total sequence as written is repeated n times for signal averaging, with n = 32 for the data reported herein, τ_1 = 2000 s, τ_2 = 1 s.

4.3 Results and Discussion

Linear PE samples with a wide range of M_W, spanning from 45K-400K, were examined using a combination of simple one-pulse and the modified EASY experiment to show the molecular weight dependence of interfacial morphology. Figure 4.3 shows the quantitative single-pulse spectra, acquired using a 2000-s recycle delay, of three of the linear PE's listed in Table 4 – 1. As has been observed many

times in the literature, two major peaks are observed depending on the percent crystallinity, with the ca. 33 ppm peak often assigned to the crystalline fraction and the ca. 31 ppm peak assigned to the amorphous fraction. However, this is an incomplete designation; the downfield peak arises from chains in an all-trans conformation and the up field peak from chains with an increased equilibrium concentration of mixed trans-gauche conformations.[80, 99] Whether or not all-trans chains appear only in the rigid crystalline region cannot be discerned from a simple experiment like that shown in Figure 4.3. Clearly, the fraction of chains with increased gauche conformer content increases with increasing PE molecular weight, and while one might be tempted to simply deconvolute the total line-shape using two components to assign percent crystallinity, this has been shown to be an incomplete representation of PE systems.[77b, 89]

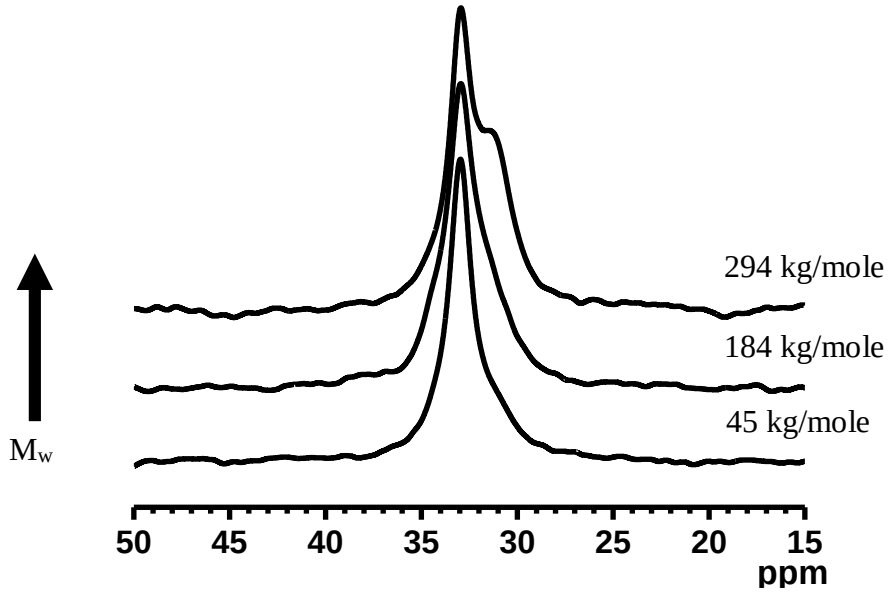

Figure 4.3. Quantitative single-pulse ^{13}C MAS spectra acquired with a 2000 s recycle delay and high power ^{1}H decoupling (CW) for a subset of the linear PE series listed in Table 4 – 1.[83]

The 'mobile only' spectra were obtained by applying T_1 filter which reveals that heterogeneity exists even in simple linear PE's. Figure 4.4 compares short (1-sec) and long (2000-sec) recycle delay

spectra of two different linear PE's. Single pulse ^{13}C MAS NMR was used to acquire these spectra in separate experiments. It is clear from the Figure 4.4 that the short-delay spectra contain signal mainly from amorphous chains. Although unexpected, the short-delay spectra also contain obvious downfield signal components from all-trans chains, indicating that all-trans chains exist whose chain mobility is similar to the amorphous mobile chains.

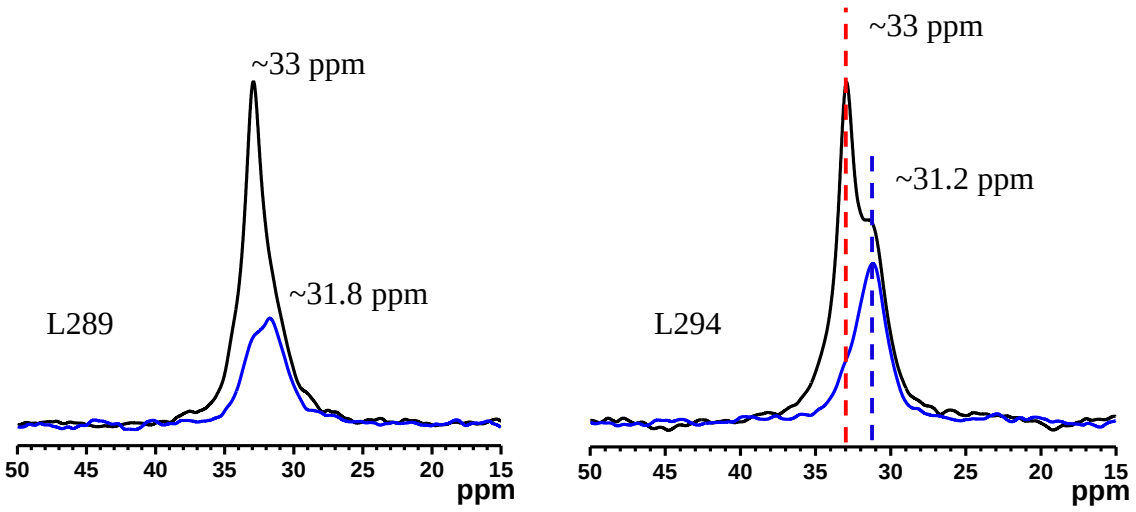

Figure 4.4. Quantitative single-pulse ^{13}C MAS spectra acquired with a 2000 s recycle delay (black) and, in separate experiments, a 1 s recycle blue) for two linear PE's at similar M_w.[83] Both spectral traces for each sample differ between the two polymers, even though the molecular weight is similar (289 K vs. 294 K). However, the thermal history for the two is different; the sample on the right was rapidly cooled from the melt by forming a compression-molded plaque while the sample on the left is the reactor fluff.

Although the molecular weight values of these two linear PE's (shown in Figure 4.4) are almost identical, the line-shape of the long and short delay experiments are quite different which tells us that different thermal histories have a considerable effect on PE morphology. The sample labeled as L294 has different thermal history compared to the other sample, L289. The former was quenched or cooled quickly by forming a pressed plaque from the melt while the latter was the as-prepared reactor fluff, which never

sees any thermal treatment. Note that the crystalline (all-trans chains) peak chemical shift serves as an internal reference, as it is constant for each sample spectrum. However, the ca. 0.5 ppm difference between the chemical shifts of the amorphous trans-gauche signal (31.8 vs. 31.2 ppm) in the 1-s recycle spectra is real, and reproducible in multiple experiments. The differences in the amorphous component chemical shifts cannot be reliably discerned in a simple quantitative single-pulse spectrum, like those shown in the top trace of Figure 4.4 for L289, as too much uncertainty exists in assigning or fitting such a weak shoulder on the main peak. This result indicates that the rapidly-cooled L294 PE either has an amorphous phase characterized by chains with a higher equilibrium gauche fraction than in the L289 PE, as the amorphous peak is more resolved in the L294 case or experiences differences in chain packing that can contribute to changes in the chemical shift.[80, 99] In addition, the possibility that intermediate conformational angles in regions of strain cannot be discounted. Acquiring ^{13}C NMR spectra at long and short recycle delays is not new. However, the power of the T_1 selection is illustrated here for similar M_w samples with different thermal histories, and perhaps more importantly, clarified for the reader as acquisition of long- and short-recycle spectra in a single experiment forms the basis of the modified-EASY experiment that will be described below to elucidate chain length and architecture contributions to interfacial behavior.

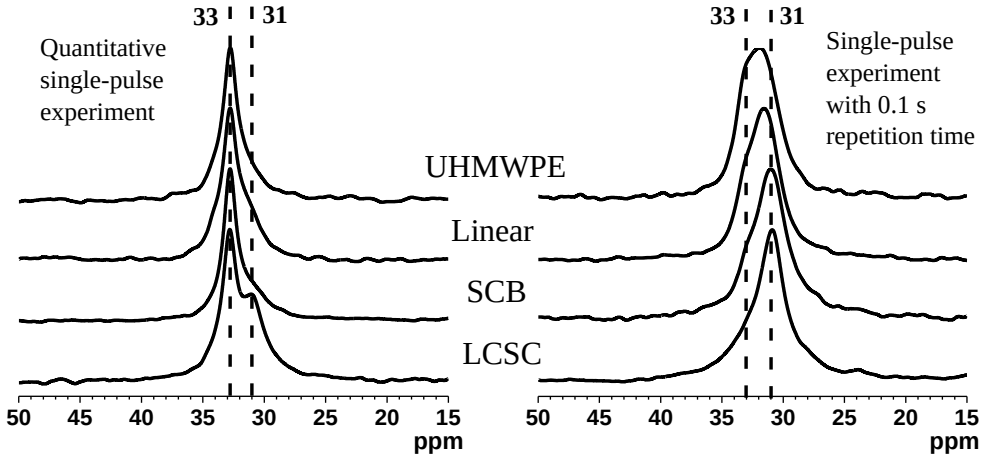

Figure 4.5. Quantitative single-pulse spectra (left column) and spectra acquired with 0.1 s recycle delay (right column) for four different PE chain types.[83] Specifically, from top to bottom, the samples are listed in Table 4 – 1 as U1466, L184, SCB43, and LCSC284. The limiting chemical shifts of 31 and 33 ppm are observed in all spectra.

To confirm the presence of the highly mobile all-trans chain which mobility and chain dynamics is similar to conformationally dynamic amorphous chains, a more stringent T_1 filter was applied, and the result is shown in Figure 4.5. The left column of Figure 4.5 compares single pulse quantitative ^{13}C spectra of a wide range of PE chain types, including linear, SCB, LCB, and UHMWPE. The right column compares 0.1 s delay single spectra of the same set of samples. Note that the delay used here is an order of magnitude shorter than some of the data shown in Figure 4.4, and all of the spectra in the right column of Figure 4.5 contain clear all-trans signal contribution near 33 ppm. This observation indicates that there are all-trans chain segments undergoing fast anisotropic reorientation on a timescale similar to that of the most mobile trans-gauche chain conformers in the amorphous region. The line-shape for the UHMWPE and linear PE samples are markedly different in the 0.1 s recycle spectra when compared to the corresponding SCB and LCB/SCB spectra. The apparent chemical shift of the amorphous trans-gauche signal varies from 31.8 to 31.1 ppm in the 0.1 s recycle spectra for the different PE types in Figure 4.5. This result indicates one of two situations: (1) the average gauche fraction of the mobile amorphous chains

is lower for the UHMWPE and linear PE relative to the other two chain topologies, or (2) mobile all trans chains are undergoing fast exchange with trans-gauche chains in the UHMWPE, and to a lesser extent in linear PE, but are not doing so for the SCB and LCB/SCB polymers. Given that clear all-trans chain signals are still discernable at 33 ppm in the UHMWPE and linear PE 0.1 s recycle spectra, the former explanation is most reasonable, and is consistent with the trans-gauche conformer shifts discussed above in Figure 4.4 for spectra obtained with a 1-s recycle delay for two linear PE's of the same molecular weight, but different thermal processing sequences. Recall in Figure 4.4, a 31.2 ppm shift was observed for trans-gauche chains in the linear PE rapidly cooled from the melt, while a 31.8 ppm shift was observed for the reactor product. We can conclude from both Figure 4.4 and Figure 4.5 that the fast recycle time experiments reveal differences either in the average gauche-fraction of chains in the nominally amorphous, but strictly speaking, trans-gauche regions of the PE, or possibly, differences in chain packing in the amorphous regions as described above. Such differences are detectable for PE's at the same molecular weight but different thermal histories, as well as for different PE chain architectures.

Individually, the quantitative data or the T_1 filtered 'mobile-only' data, when acquired in separate experiments, are insufficient to quantitatively measure all four phase components. However, when acquired together using the modified-EASY pulse sequence in a single experiment, the amounts of phases with all-trans crystalline, mobile all-trans, constrained trans-gauche, and mobile trans-gauche chains can be quantified. Here, the interface/interphase is defined as the combination of the mobile all-trans and constrained amorphous chains. Figure 4.6 (linear PE) and Figure 4.7 (SCB PE) show examples of the results from this approach, in which the total spectrum from quantitative 2000-sec recycle acquired in the first scan (top), the 1-sec T_1-filtered acquisition selecting for mobile components in the second scan (middle), and their difference revealing signals from the crystalline all-trans and constrained amorphous phases (bottom). It is worth mentioning here that the choice of a 1-second delay time for the second portion of

the EASY experiment is somewhat arbitrary, but does reflect a reasonable starting point for ^{13}C T_1 discrimination in semi-crystalline polymers based on historical data.[47c, 89, 95] Moreover, the spectral lineshapes of saturation recovery experiment (shown in the previous chapter) for different recovery times indicate that the choice of '1 s' delay for acquiring 'mobile-only' spectrum is quite reasonable. One might expect a distribution or gradient in polymer chain relaxation behavior as the interfacial region between crystalline and amorphous domains is traversed, as suggested by the 0.1 s recovery data shown in Figure 4.5. In future work, we will attempt to probe this by exploring a two-dimensional (2D) version of the EASY experiment, in which the τ_2 value shown in Figure 4.2 is incremented. While a 2D NOE-compensated EASY would be an extremely long experimental acquisition, and difficult to practically implement for a large sample set like used in this study, it could potentially provide insight into dynamic gradients across the interface in suitably selected materials. Such an experiment would be improved relative to simple variable delay experiments that are typically done to measure ^{13}C T_1's since amorphous line-shapes are artificially enhanced at short recovery times due to transient Overhauser effects arising from cross-relaxation in the most mobile amorphous segments.

The acquired spectra from modified-EASY experiments were deconvoluted using OriginPro 9 software to extract phase composition data (the details about the spectral deconvolution and data calculation is discussed in chapter III). Voigt functions were used for all the line shape components to fit each sub-spectrum (shown in Figure 4.6 and Figure 4.7). The "mobile-only" spectrum (middle trace in Figure 4.6 and Figure 4.7) was fitted first using two fitting components which are physically assignable to regions of PE. The fitting components centered at 33 ppm and 31.6 ppm are for the all-trans (mobile all-trans) and the trans-gauche (amorphous) chain segments, respectively. The "rigid-only" spectrum (top trace in Figure 4.6 and Figure 4.7) was deconvoluted in the similar fashion. The all-trans component at 33 ppm is assigned to the crystalline all-trans chains and the trans-gauche component at ca. 31.6 ppm is

assigned to the constrained amorphous chains. In the "rigid-only" spectra, for some samples, a third component was seen at ca. 34 ppm which is for the presence of small amount of monoclinic crystalline phase. The "total-spectrum" that was acquired in the first acquisition of the modified-EASY pulse sequence was not deconvoluted; instead, all the fitting parameters obtained from the fitting of the "mobile-only" and the "rigid-only" sub-spectra were directly copied to fit the "total-spectrum", which gives a perfect fit. The phase composition data (shown in Table 4 – 2) were calculated from the area of each component.

Table 4—2. The phase composition and the interface content in PE's extracted from the modified-EASY experiment. The total amorphous content, while not listed, follows from the reported total crystalline percentage. Total crystalline percentages do not include the mobile all-trans contribution. The reported ranges in each data point correspond to one standard deviation arising from deconvoluting each set of EASY sub-spectra three times.

Sample	M_w (kg/mole)	total crystalline	mobile all-trans	constrained amorphous
L-45	45	74.6 ± 0.4	3.9 ± 0.1	1.4 ± 0.5
L-165	165	59.6 ± 0.8	3.7 ± 0.1	3.4 ± 0.2
L-184	184	51.7 ± 0.3	5.3 ± 0.1	3.9 ± 0.3
L-241	241	56.9 ± 0.7	5.2 ± 1.4	4.4 ± 0.6
L-289	289	50.6 ± 1.6	5.3 ± 0.3	7.8 ± 0.9
L-294	294	49.6 ± 2.0	5.4 ± 0.2	6.9 ± 0.7
L-400	400	50.5 ± 0.8	8.1 ± 0.5	6.4 ± 0.6
U-1466	1466	54.1 ± 0.5	7.6 ± 0.2	5.8 ± 0.3
SCB-43-h	43	63.8 ± 0.2	5.3 ± 0.9	6.4 ± 0.2
SCB-146-b	146	40.0 ± 0.5	8.2 ± 0.5	3.8 ± 0.2
SCB-148-o	148	44.6 ± 0.6	11.6 ± 0.9	1.9 ± 0.6
SCB-184-o	184	41.6 ± 0.3	9.0 ± 0.7	5.4 ± 0.1
LCB-161	161	48.3 ± 0.8	5.7 ± 0.1	6.0 ± 0.6
LCSC-284	284	35.9 ± 0.5	12.4 ± 0.1	7.5 ± 0.4
LCSC-627	627	41.3 ± 0.5	13.3 ± 0.3	7.1 ± 0.3

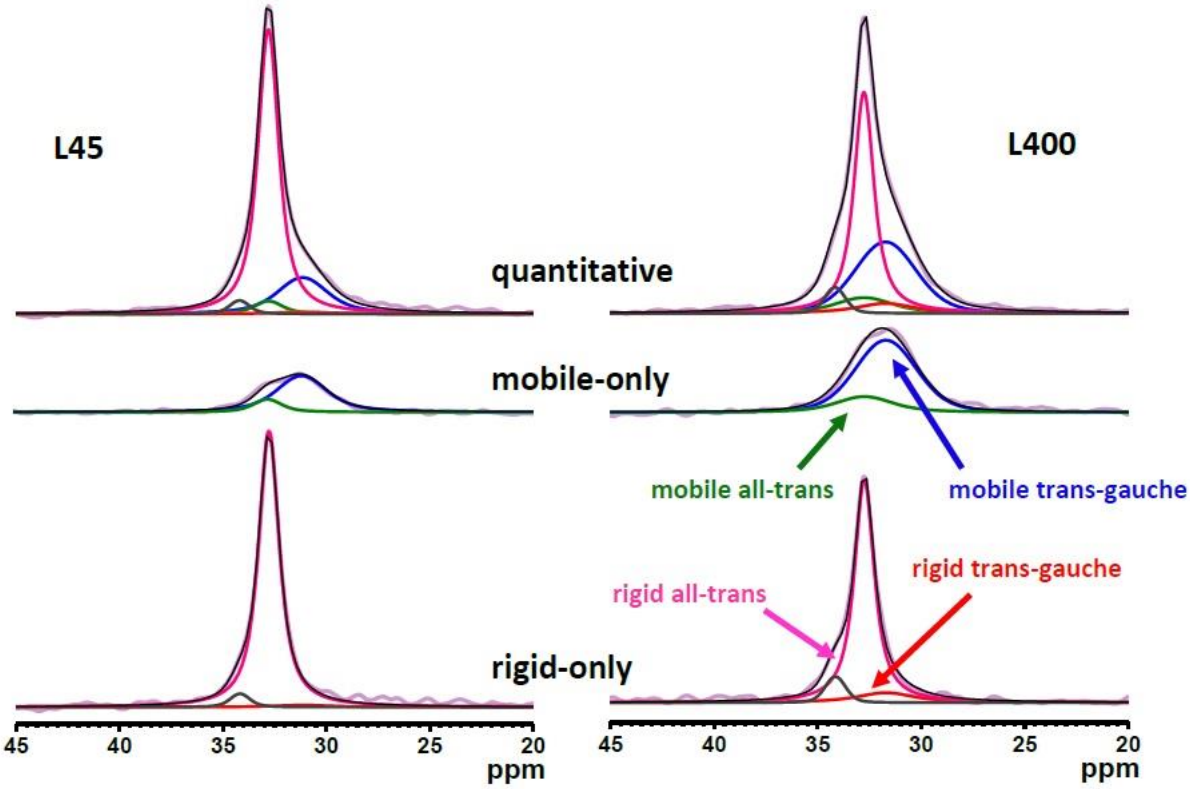

Figure 4.6. Spectral results from the modified-EASY experiment,[83] demonstrating fitting of quantitative 2000 s EASY spectra (top row) based on extraction of individual components from short delay mobile-only spectra (middle row), and the rigid-only difference spectra (bottom row) of samples L-45 (left column) and L-400 (right column). For clarity, the individual components are identified only on the L-400 PE, but the same assignments apply to all other PE's. In all spectra, the most intense red line component at 32.9 is the signal from crystalline chains, while the blue trace at 31.7 ppm is from chains in the mobile amorphous phase. The smaller red trace and the green trace represent the intensity from the interface, i.e., constrained amorphous 31.7 ppm and all-trans mobile chains at 32.9 ppm, respectively. The small black trace at 34 ppm is from a monoclinic crystalline component, which appears in many, but not all, samples. Individual components are extracted from the mobile only and rigid-only sub-spectra and then used without modification to fit the quantitative spectrum in the top row. Note the excellent agreement of the fit.

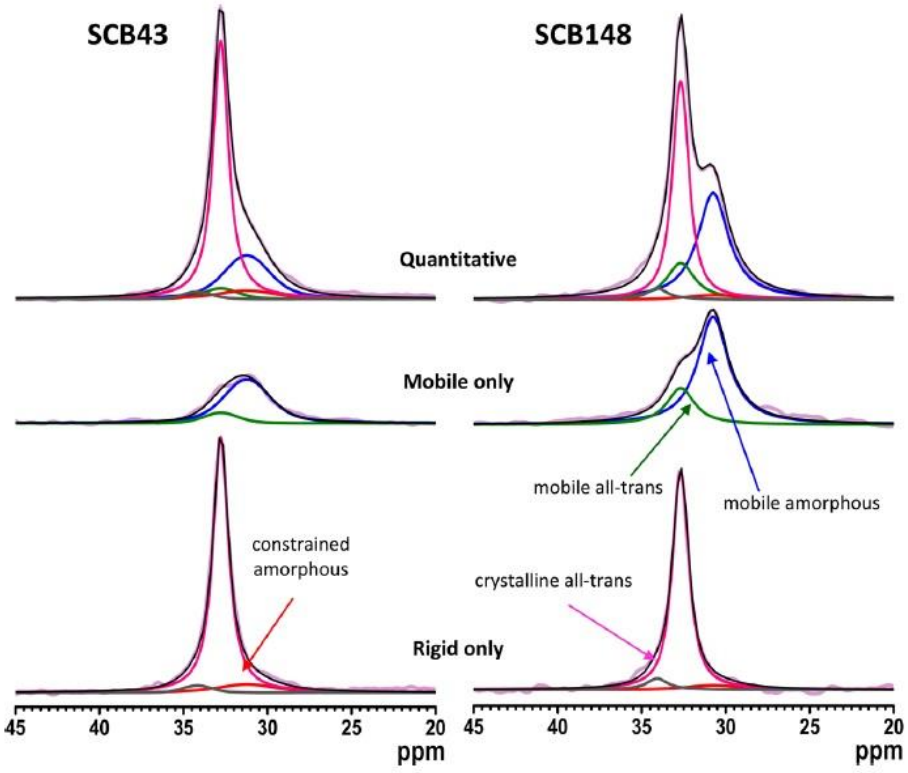

Figure 4.7. Spectral results from the modified-EASY experiment,[83] using the same component analysis procedure described in the text and the Figure 4.6 caption. Shown in this example are the quantitative 2000 s EASY spectrum (top row), short delay mobile-only spectrum (middle row), and the rigid-only difference spectrum (bottom row) for short-chained branched PE SCB-43 (left column) and SCB-148 (right column). The individual components are labeled as in Figure 4.6.

The total crystalline fraction reported in Table 4 – 2 is the sum of orthorhombic and monoclinic crystalline fractions and is in general agreement with (fast heat) DSC crystallinity results as shown by the graph in Figure 4.8; the largest deviation between the two methods is ca. 10%. Note that the NMR percent crystallinity is assigned here as the relative fraction of total intensity derived *only* from the rigid all-trans line shape. The interface intensity of sample L-400 (Figure 4.6, right column) was found to be significantly higher than that of sample L-45 (left column). Using the approach described above and exemplified in Figure 4.6 and Figure 4.7, the amount of each of the four components (or five in the cases where a

monoclinic crystalline fraction was detected) were determined for the PE's in Table 4 – 1. The results are summarized in Table 4 – 2 and depicted graphically for the mobile all-trans and constrained amorphous fractions versus M_w in Figure 4.9. The total interface fraction (mobile all-trans + constrained amorphous) exhibits a nearly linear relationship with M_w for the linear PE's but exhibits significant deviation from that relationship once short-chain branching is introduced for the same M_w, as shown in both Figure 4.9 and Figure 4.10. Figure 4.9(a) and Table 4 – 2 show that most of this increase arise from the increased mobile all-trans fraction of the SCB relative to their corresponding molecular weight linear analogs. Moreover, the UHMWPE synthesized using Ziegler—Natta catalysis (U1466), and the LCSC samples are clearly outliers relative to the base linear M_w dependence. We note with interest that the two LCB polymers with SCB's (LCSC) have by a wide margin the largest interfacial content. The single "pure" LCB data point, denoted by the "**+**" in Figure 4.10 at a M_w = 161K, has an interfacial content that lies between the general trend exhibited by the linear and short-chain branched PE's, as might be expected given its very low 0.34 branches/10000 total carbons. However, the extra detail afforded by Figure 4.9 (a) & (b) shows that this LCB has a higher constrained amorphous content than the corresponding linear or SCB PE per unit molecular weight.

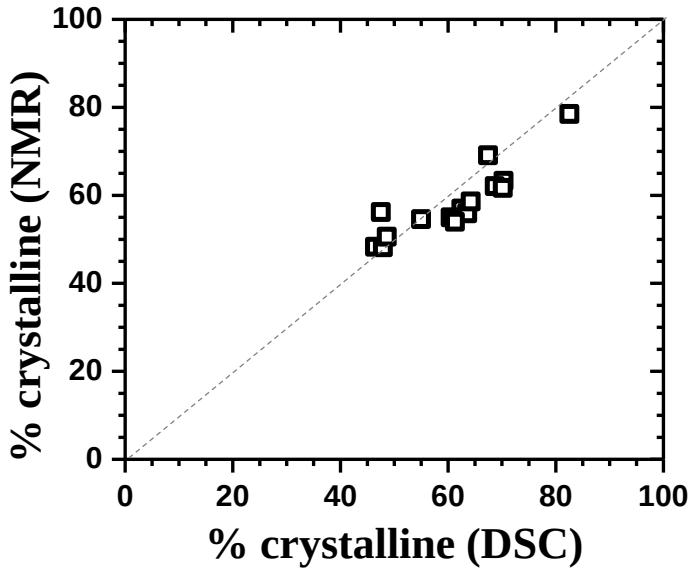

Figure 4.8. Comparison of percent crystallinity obtained from NMR and DSC. The enthalpy of fusion from the first heat was used to calculate the DSC crystallinity, and thermal histories were kept as constant as possible. The NMR data only includes the rigid all-trans components as assigned to the crystalline phase; the mobile all-trans is not included in the total crystallinity.

To clarify, potential confusion could arise between the "constrained amorphous" term, as used here to denote that fraction of amorphous polymer that does not survive the ^{13}C T_1 filter used in the EASY experiments, and other constrained or rigid amorphous phases previously discussed by others.[78, 100] Other discussions of novel uses of T_{1C} filters have also appeared, targeting identification of intermediate phases.[47d] Proton dipolar couplings have been used as the discriminatory parameter in ^{1}H spin-spin relaxation, spin-diffusion, and multiple-quantum echo methods, all of which rely on chain dynamics in the $10^4 - 10^5$ s^{-1} spectral density regime, uniquely different than the effective spin – lattice spectra densities (~ 10^8 s^{-1}) required for the ^{13}C T_1 relaxation filter used here. It is likely that the T_{1C} selection in a stronger filter regarding the subset of the population it selects relative to the proton methods cited above.

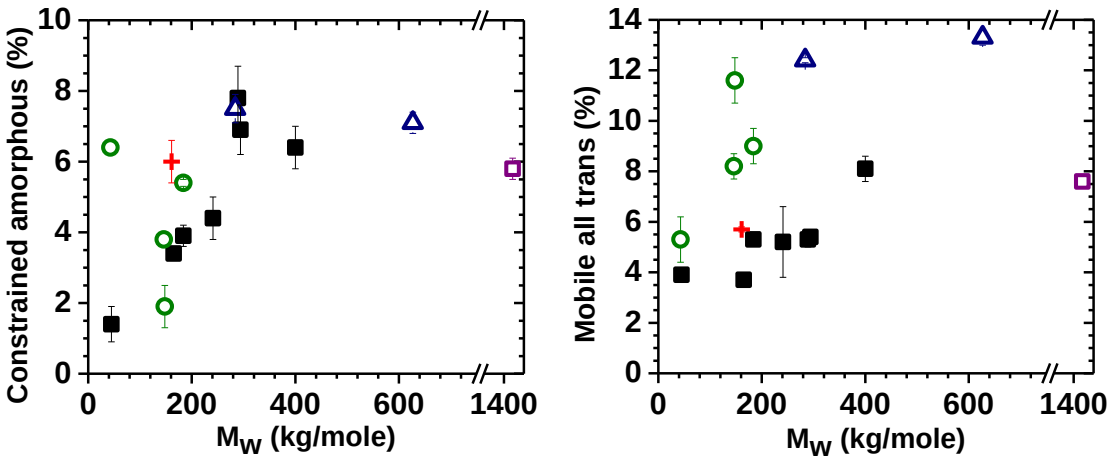

Figure 4.9. Graphical summary of data from modified-EASY experiments demonstrating how interfacial morphology varies with PE chain length and chain architecture: (a) mobile all-trans chain fraction; (b) constrained amorphous chain fraction (■, = linear PE; ○, = SCB; +, = LCB; Δ, = LCSC and □, UHMWPE).

As discussed in the Experimental Section and Introduction, the materials used here were essentially all reactor fluffs. Obviously, thermal history, polymerization temperatures, reactor pressure, and other variables can contribute to perturbations in final sample morphology. All of these variables were controlled in facilities capable of making commercial-grade polymers within narrow specification ranges, and we believe that the method introduced in this contribution is capable of accurately representing the total contribution of structural variables certainly can contribute to changes within a polymer class, but Figure 4.10 suggests that a major factor in shifting polymer chain types to new interfacial contents is the presence of branches and the kind of branches.

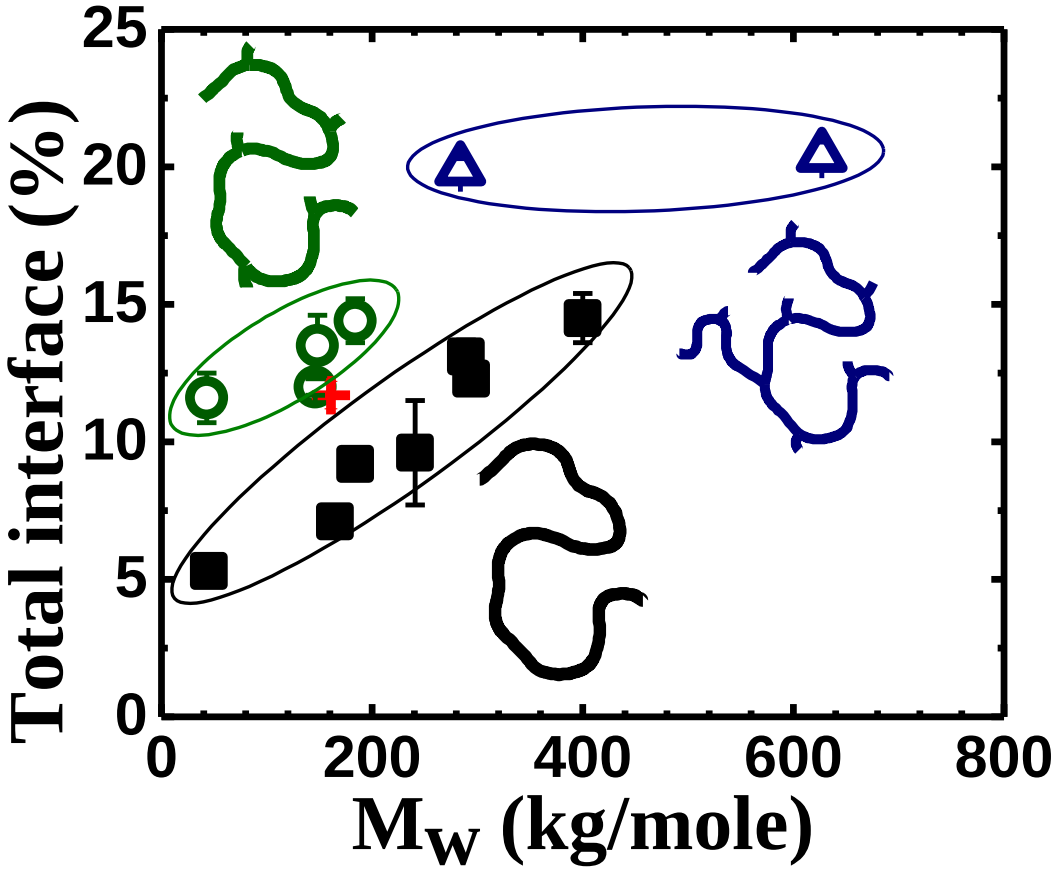

Figure 4.10. Results from modified-EASY experiments demonstrating molecular-weight dependencies of the total interfacial content[83] (mobile all-trans plus constrained amorphous) for different PE chain topologies (■, = linear PE; ○, = SCB; +, = LCB; Δ, = LCSC and □, UHMWPE). Note the unique grouping according to PE chain architecture.

4.4 Conclusions

The morphology of PE interfacial region of a wide variety of polyethylene samples was studied in the solid state by using a very simple NMR experiment. The double acquisition modified-EASY pulse sequence was found to be successful to reliably quantify the individual phase percentage in a single experimental acquisition. The chain length and chain architecture dependence of PE morphology was revealed using that simple experimental method. The individual components of the interfacial region were

found to increase with the increased molecular weight and increased chain architecture complexity. Morphological heterogeneity arising from different thermal histories was also detected and shown for similar M_w polyethylenes.

CHAPTER 5

5 EFFECT OF THERMAL HISTORIES ON THE MORPHOLOGY OF LINEAR POLYETHYLENES

5.1 Introduction

In the previous chapter, the result of a wide variety of as-synthesized polyethylene samples (PE reactor fluff) was presented to show the effect of chain length and topology on the morphology of polyethylenes. The reactor fluffs are as-synthesized polyethylene, collected from the reactor after synthesis, and without any thermal treatment. However, no practical product can be made without thermal processing. For any type of molding to make products, the polymer needs to be melted first, and then cooled from the melted state to the solid state. During this thermal treatment, the polymer morphology is affected. For this reason, studying polyethylene morphology as a function of thermal history is important. In this chapter, the morphological data of a set of linear samples, which underwent different thermal processing, will be presented. The data will be compared with the untreated sample data, to understand the effect of thermal history on polyethylene morphology. Studying the thermally processed samples is more logical, which will represent the morphology and properties of the end-use polymer. However, for a clear understanding of the morphology and to compare the effect of thermal processing, one must study the as-synthesized samples as a control to provide an idea of how morphology changes as a function of different thermal histories.

5.2 Experimental

A subset of linear samples (except L69 and L134) listed in (Table 4 - 1, Chapter 4) were picked for this study. The linear samples of different molecular weight were prepared using the previously mentioned method. In this part of the work, two sets of the sample having the same average molecular weight but different thermal histories were studied. The reactor fluff samples of the same reaction batch were divided into three portions. One part was used for morphology study by the solid-state NMR and DSC without any thermal treatment, and the data was presented in the previous chapter (Chapter 4). The other two portions were thermally treated to prepare the pressed plaque. Carver Auto Series NE Automatic ASTM Hydraulic Press with programmable heating and cooling (Wabash, IN) was used to make the thermally treated plaques from the reactor fluff samples. The sample fluffs were placed in a 5 X 7 X 0.08-inch aluminum molds and then placed between two 0.25 inch aluminum plates (top and bottom) with the Kapton films placed between the mold and aluminum plates. The samples were melted by heating for 5 minutes at 190 °C at 1000 lbs force contact pressure, followed by another 5 minutes heating at 60,000 lbs force pressure. To make the fast-cooled samples, cold water was used and cooled from 190 ^{o}C to 98 ^{o}C in 2.25 min (cooling rate = 42^{o}/min), then slowly cooled to room temperature. The slow-cooled samples were melted in the same way as for the fast-cooled samples, then cooled down to room temperature at a rate of 0.5^{o}/min (according to ASTM F1473). The pressed plaques were then cut into 10 cm pieces and cooled in dry ice for 30 minutes; then the samples were placed in a Retesch Model ZM-1 cryogenic Mill to make powder.

Here, the important point is, the reactor fluffs, quenched (fast-cooled), and the annealed (slow-cooled) samples were synthesized in the same batch of the reactor, but thermally treated in different ways after the synthesis. Thus, the average molecular weight and M_w distribution are the same. In this study, we characterized six fast-cooled samples and five slow-cooled samples which are listed in Table 5

– 1. In Table 5 -1, the sample names represents their topology, molecular weight, as well as, their thermal processing condition. The initial 'L' means it is a linear sample, the number followed by the letter represents its weight average molecular weight (M_w), and the last two letters are to represent their thermal history (rf- reactor fluffs which didn't undergo any thermal processing, fc- fast cooled or quenched sample, and sc- slow cooled or annealed samples.

Table 5—1. List of the linear polyethylenes that were studied in this part of the work. The sample names ending with 'rf', 'sc' and 'fc' represent that the samples are reactor fluff (no thermal treatment), slow-cooled, and fast-cooled, respectively. The fluffs were heated to 190 °C, then cooled to room temperature at a cooling rate mentioned in the table.

sample	M_w (kg/mole)	cooling rate (°/min)
L69rf	69	-
L69sc	69	0.5
L69fc	69	42
L134rf	134	-
L134sc	134	0.5
L134fc	134	42
L165rf	165	-
L165sc	165	0.5
L165fc	165	42
L241rf	241	-
L241sc	241	0.5
L241fc	241	42
L289rf	289	-
L289sc	289	0.5
L289fc	289	42
L400rf	400	-
L400sc	400	0.5
L400fc	400	42

The NMR data were acquired using the modified-EASY (version 2) pulse sequence (Figure 5.1) that was described in the previous chapter. The only changes in the experiment are the proton decoupling method and the magic-angle spinning (MAS) speed that was used. The data presented in the previous chapter (Chapter 4) were collected using the continuous wave (CW) decoupling method. However, the

data presented in this chapter were acquired using a composite pulse decoupling sequence as we realized that the composite pulse decoupling (cpd) method can provide more resolved spectra. All the data were collected in the Bruker DSX Avance 300 MHz instrument on a 4-mm MAS triple-resonance probe equipped with a boron nitride stator. The typical duration of 90° pulse was ca. 3.4 µs and the acquisition time was 30 ms. The two-pulse phase modulation (TPPM) decoupling sequence was used. For effective TPPM decoupling, the sample needs to be spun at a high MAS speed. Therefore, the sample was spun at 12 kHz (the maximum stable MAS speed in the 4-mm probe in our lab) instead of the 5 kHz that was used for the fluff samples. The TPPM conditions were optimized and checked for each of the samples to get the best decoupling efficiency. Typically, for all the samples, the proton nutation frequency was at least 100 kHz for decoupling, the phase angle (ϕ) of CPD pulse was ca. 15° and CPD pulse length was ca. 5.5 µs.

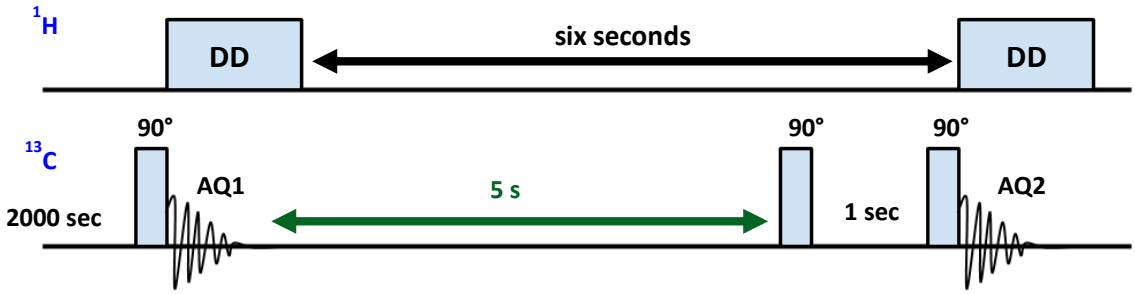

Figure 5.1. Modified-EASY (version 2) pulse sequence.

5.3 Results and Discussion

The effect of different thermal treatments as well as the molecular weight contribution on the morphology of linear polyethylene was assessed by analyzing three sets of linear PE samples of different thermal histories. The molecular weight ranges for the samples were 70 – 400 kg/mole. The modified-EASY (version 2) pulse sequence was used to acquire the data. Figure 5.2 compares quantitative ^{13}C spectra of three linear samples of same average molecular weight, which were synthesized in the same batch. However, their thermal histories are different. L241rf is the as prepared reactor fluffs, the L241sc is the slow-cooled sample which was prepared by melting the L241rf first, and then cooling at a rate of

0.5°/min to room temperature, and the L241fc sample was prepared from the same fluff sample, but the cooling rate was ca. 42°/min.

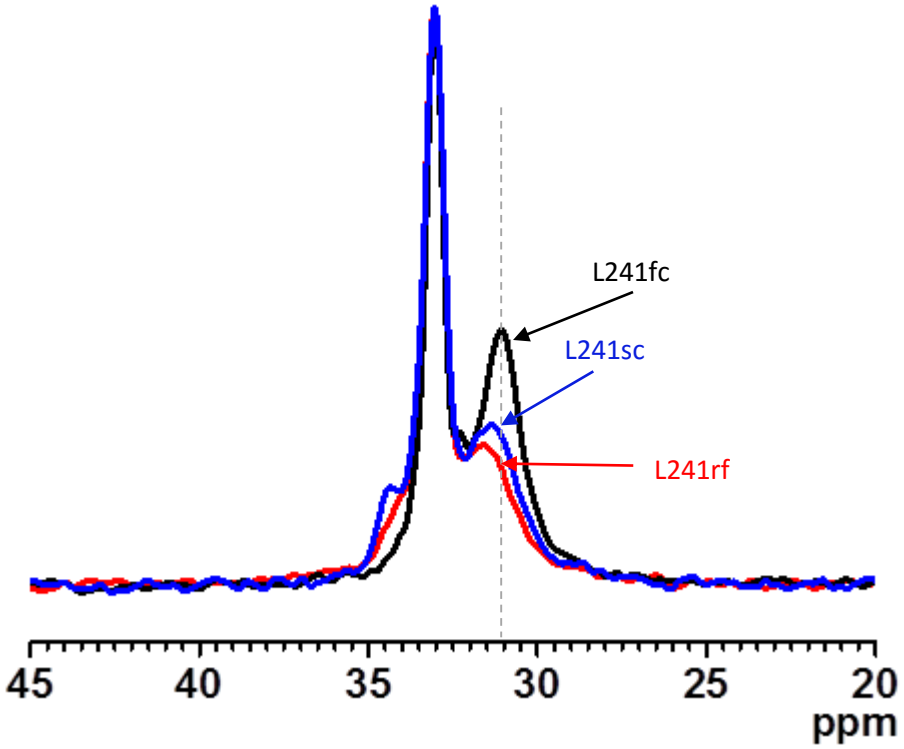

Figure 5.2. ^{13}C quantitative spectra (normalized by the all-trans peak height) of sample L241rf (red), L241sc (blue), and L241fc (black) show a significant difference in the spectral line-shape at the trans-gauche region due to different thermal histories of same M_w samples.

The red, blue and the black lines in Figure 5.2 represent the (normalized by the all-trans peak height) quantitative ^{13}C spectra of L241rf, L241sc, and L241fc, respectively. The all-trans peaks at 33.04 ppm for all three samples were normalized to unity to compare the spectral line shape. As we see in Figure 5.2, both of the thermally treated samples have a higher equilibrium gauche conformer content than the untreated sample. Moreover, the highest difference in chemical shift between the all-trans and the trans-gauche peak for the fast-cooled sample proves that it has the highest equilibrium gauche conformer density.[79] When melted, the polymer chains gain enough energy to move relatively freely, and the chain movement in the melted state is much higher than that in the solid state. In the melted state, the

equilibrium gauche density in the polymer chains increases due to disorganization of chains after melting all of the crystalline domain. If the sample is cooled very quickly, the chains don't have enough time for complete crystallization. For that reason, the fast-cooled sample has higher trans-gauche chains, or higher amorphous fraction.

The slow-cooled sample is expected to have the lowest amorphous content, but Figure 5.2 indicates that it has a slightly higher amorphous content than the untreated sample. If we focus on the monoclinic crystalline region of the spectra, the slow-cooled sample has a higher percent of monoclinic crystalline content than that of the untreated sample. As discussed in the previous chapter, the monoclinic crystalline state is a metastable state of polyethylene which can be formed during the thermal treatment. During the calculation, the monoclinic and orthorhombic crystalline fraction were added together to find the total crystalline content. So, it is found that the percent amorphous of the untreated and the slow-cooled samples are nearly the same but lower than that of the fast-cooled sample. The similar trends were also seen for percent crystalline data.

The monoclinic crystalline fraction was found to be the lowest in the fast-cooled sample (L241fc) which deviated from the expected results. As this sample was cooled at a very fast rate, we would expect more metastable monoclinic crystalline state than that of the other two. The reason behind the lower monoclinic crystal content in the fast-cooled sample is, most likely, during the melting process, the previously monoclinic crystalline chains in the untreated samples become disordered and could not recrystallize during the very fast cooling process, and become a part of amorphous and interface regions.

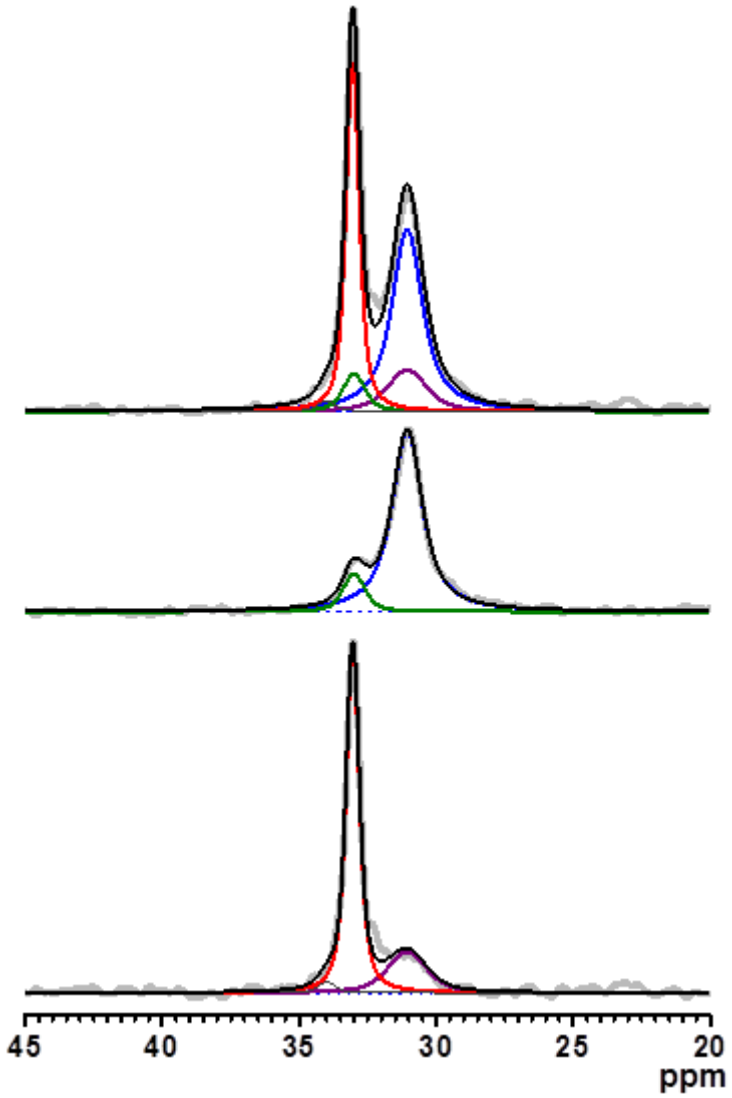

Figure 5.3. Deconvolution of the 'rigid-only' (bottom) and the 'mobile-only' (middle) spectra of sample L400fc. In the 'rigid-only' spectrum, the purple line (at ca. 31 ppm) and the red line (at ca. 33ppm) represent the constrained amorphous and crystalline all-trans chain component respectively. In the 'mobile-only' spectrum, the blue line (at ca. 31 ppm) and the green line (at ca. 33 ppm) represent the mobile amorphous and mobile all-trans components respectively. The 'total' spectrum (shown on top) was not deconvoluted, rather the fitting parameters obtained from the fitting of the two sub-spectra were directly used (without any modification) to reconstruct the 'total' spectrum line-shape.

Spectra acquired by the modified-EASY (version 2) experiment were deconvoluted by OriginPro 9 software to calculate the phase composition. As discussed in the previous chapter, the 'mobile-only' and the 'rigid-only' spectra were deconvoluted first, and then the fitting parameter for those deconvolutions was used to reconstruct the 'total' spectrum and compared to the experimental result. The phase composition results from the deconvolution process are listed in Table 5 - 2.

Table 5—2. The phase composition results obtained from the spectral deconvolutions are listed:

sample	M_w (kg/mole)	total crystalline (%)	total amorphous (%)	mobile all-trans (%)	constrained amorphous (%)	total interface (%)
L69rf	69	-	-	-	-	-
L69sc	69	61.70 ± 0.6	24.93 ± 1.1	11.05 ± 0.7	2.31 ± 0.5	13.37 ± 0.6
L69fc	69	62.86 ± 0.2	25.76 ± 0.6	7.69 ± 0.3	3.79 ± 0.3	11.48 ± 0.5
L165rf	165	59.60 ± 0.8	36.7 ± 0.8	3.7 ± 0.1	3.4 ± 0.2	7.1 ± 0.1
L165sc	165	47.37 ± 0.4	41.04 ± 1.1	7.01 ± 0.4	4.58 ± 0.3	11.59 ± 0.7
L165fc	165	46.88 ± 0.4	37.76 ± 0.1	9.29 ± 0.2	6.08 ± 0.2	15.37 ± 0.4
L241rf	241	56.9 ± 0.7	37.9 ± 0.7	5.2 ± 1.4	4.4 ± 0.6	9.6 ± 1.9
L241sc	241	54.05 ± 0.3	32.46 ± 0.7	8.45 ± 0.1	5.04 ± 0.5	13.49 ± 0.4
L241fc	241	40.57 ± 0.2	42.46 ± 0.3	6.06 ± 0.3	10.9 ± 0.2	16.97 ± 0.2
L289rf	289	50.6 ± 1.6	44.1 ± 1.9	5.3 ± 0.3	7.8 ± 0.9	13.1 ± 0.6
L289sc	289	50.29 ± 0.7	34.89 ± 0.3	8.94 ± 0.8	5.88 ± 0.2	14.81 ± 0.9
L289fc	289	37.58 ± 0.5	42.72 ± 0.1	6.63 ± 0.1	13.07 ± 0.6	19.7 ± 0.6
L400rf	400	50.5 ± 0.4	41.4 ± 0.4	8.1 ± 0.5	6.4 ± 0.6	14.5 ± 0.9
L400sc	400	48.16 ± 0.7	36.76 ± 0.6	12.66 ± 0.3	2.42 ± 1.0	15.08 ± 1.1
L400fc	400	36.83 ± 1.1	45.65 ± 0.7	6.25 ± 0.2	11.27 ± 0.6	17.52 ± 0.4

The phase composition data were graphically summarized in Figure 5.4. The total crystalline content was found to decrease with increased M_w for all sets of samples (Figure 5.4(a)). The percent crystalline contents for the fast cooled samples are lower than that of the untreated samples, which is logical. As the samples were cooled very quickly from the melted state, less amount of the chain could crystallize during the cooling period. The percent amorphous (Figure 5.4(b)) for the slow-cooled samples

show similar results for the untreated samples. For the amorphous content similar results were seen; the fast-cooled samples have a higher amorphous content than that of the other two.

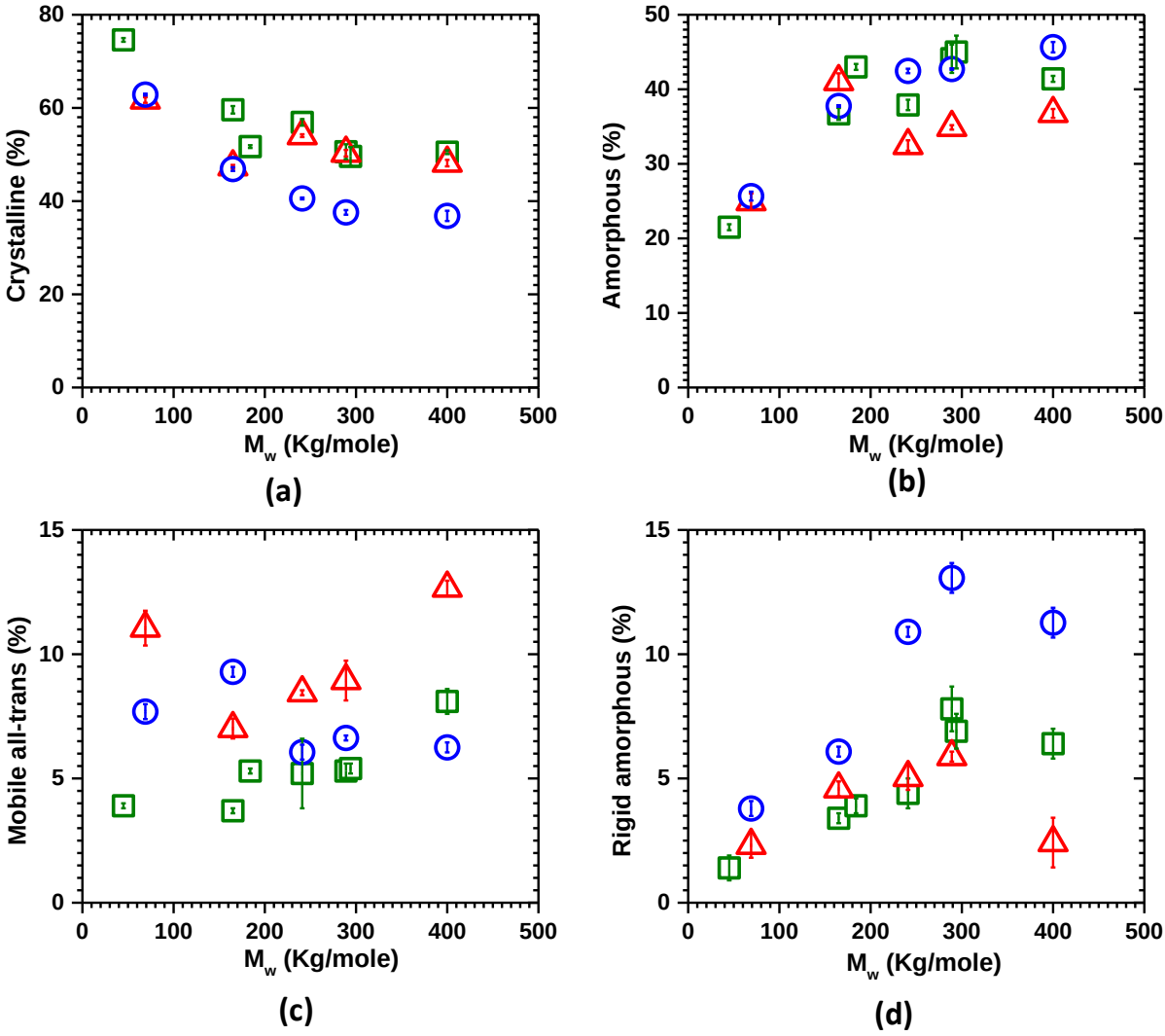

Figure 5.4. The graphical representation of molecular weight and thermal history effect on the individual morphological components of linear polyethylenes. (fluff - □, annealed - Δ, and quenched - o)

The mobile all-trans chain fraction increases with the increase of the molecular weight for slow-cooled samples (Figure 5.4(c)). For the fast-cooled samples, the mobile all-trans content isn't significantly affected by the molecular weight change. The rigid amorphous (or rigid trans-gauche) (Figure 5.4(d) fraction linearly increases with the molecular mass of all sets of samples.

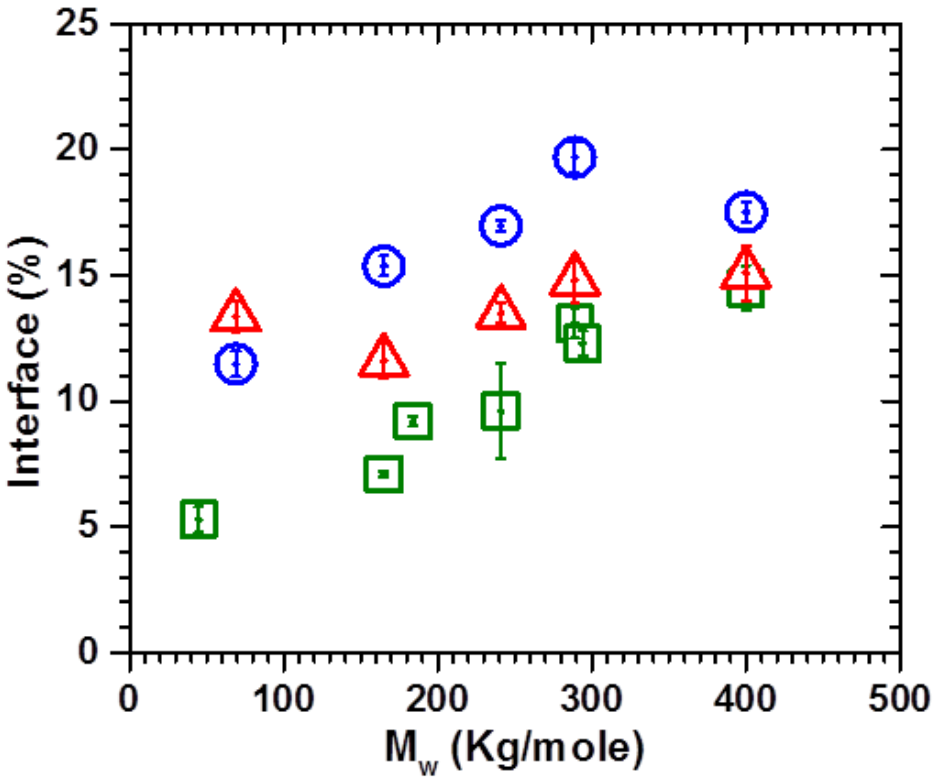

Figure 5.5. The M_w and the thermal history effect on the total interface content of the PE samples listed in Table 5 – 1. The interface content was found to increase linearly with M_w for all of the thermal histories. (fluff - □, annealed - Δ, and quenched - o)

The total interface content was calculated by adding the mobile all-trans and rigid trans-gauche chain signals. The total interface content (Figure 5.5) has a fairly linear relationship with the molecular weight of all sets of samples of different thermal histories. The highest total interface was seen in the fast-cooled samples. The reason behind this is, probably, during the fast cooling process the randomly organized chains start to crystallize, however, as the crystallization time is limited, all crystallizable chain

cannot organize themselves in the crystal lattice within that short time. A portion of chains that would crystallize if enough time was provided, but could not crystallize and form a thicker rigid amorphous phase. From Figure 5.4 and 5.5 it can be assumed that the interface content is mainly controlled by the rigid amorphous content.

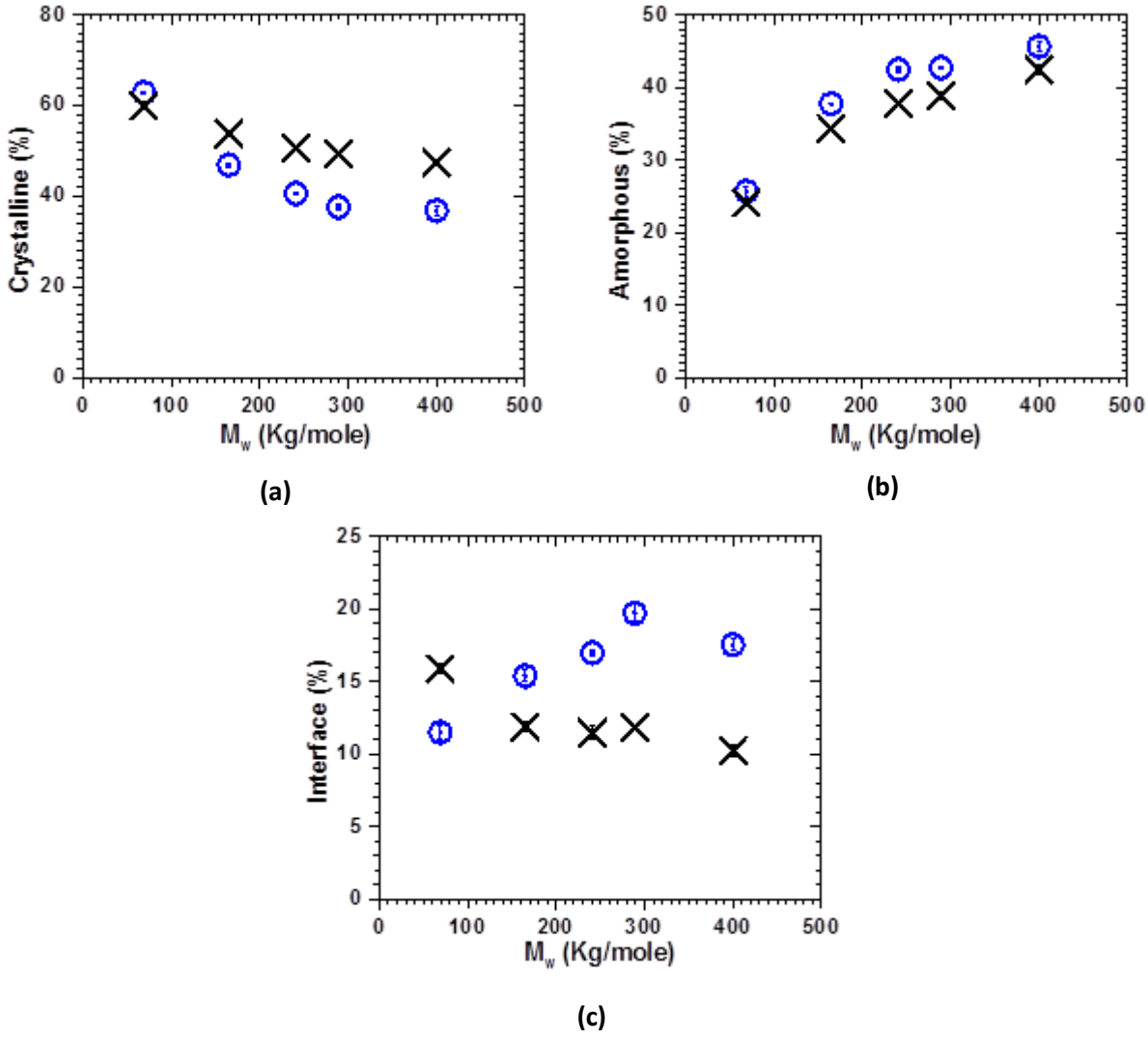

Figure 5.6. Plots comparing the data for the fast-cooled samples obtained in different time which shows the change in phase composition due to physical aging. The blue circle (O) represents the data that were acquired just after the samples were received, and the data shown by the black cross (X) was acquired six months after the first data acquisition.

The interface content of both of the fast-cooled and the untreated samples are equally responsive to the increased molecular weight. For the slow-cooled samples, however, the total interface content was found to be less affected by the change of chain length.

The modified EASY experiment was also found to be useful to study the physical aging of polyethylene. To check the effect of physical aging, two sets of data were acquired for the fast-cooled samples. The first set of data was acquired just after receiving the sample in June 2015. Then, the samples were kept at room temperature for six months in a plastic bag. The second set of data were acquired in December 2015. It was found that secondary crystallization occurred in the fast-cooled samples. Figure 5.6(a) shows that for all the samples the crystalline content increases. However, the change in the amorphous content is not so obvious (Figure 5.6 (b)) as for the crystalline content. The interface content was found to decrease due to the physical aging process (Figure 5.6(c)). By comparing Figure 5.6 (a), (b) and (c), it can be concluded that, a fraction of the rigid amorphous phase converted to the crystalline phase during the secondary crystallization process.

5.4 Conclusions

In this contribution, linear polyethylene samples were examined to show the effect of thermal history on the polyethylene phase composition, especially, how the interface content is affected by the different thermal processing. The modified-EASY (version 2) pulse sequence with TPPM decoupling reveals that for all sets of samples, the crystalline-amorphous interface of polyethylene has a linear relationship with the molecular weight for all of the thermal histories. It was found from this study that, the fast-cooled samples have higher interface content than that of the fluffs and the slow-cooled polyethylenes. Moreover, the slow-cooled samples were found to be less responsive to the molecular weight change.

In the future, we will characterize more samples with different chain architectures and thermal histories. A set of short chain branched polyethylenes, with different branch contents, branch lengths, as well as different thermal histories, will be studied using the developed method. This will give a better understanding of the structure morphology relationship of the polyethylene copolymers.

CHAPTER 6

6 RIGID-PHASE AND SOFT-PHASE HETEROGENEITY IN GRADIENT COPOLYMERS REVEALED BY MAGIC-ANGLE SPINNING ^{1}H NMR[†]

6.1 Introduction

There has been an increasing need for polymeric materials engineered at the micro-scale for use in highly specialized applications. Polymeric materials that incorporate two or more types of monomers are of particular interest because unique macroscopic properties may result depending on microscopic properties such as composition, the degree of polymerization and arrangement. Alteration of any of these properties can potentially yield materials with significantly different physical properties. Advancement of synthetic techniques permits more control over monomer sequence distribution during the copolymerization of two or more monomers which can create a vast array of new materials. One key example is the recent development of 'gradient copolymer' which are particular types of copolymers in which the chemical composition varies gradually along the length of the polymer backbone.[101] A schematic diagram comparing block, the random and gradient copolymer is shown in Figure 6.1. While recent advances in controlled living polymerization techniques have led to many new gradient copolymers (linear, parabolic, hyperbolic, etc.), direct experimental evidence about how gradient copolymers organize

Figure 6.1. Schematic representation of the block, random and gradient copolymer chains.

[†] *The content of this section has been published in Macromolecules, 2014, 47, 2625-2631.*

block copolymer

random copolymer

gradient copolymer

or order, the temperature dependence of that ordering, and the relationship between morphology and chain architecture is hard to assess, especially for solid systems. What is clear from the investigations published to date is that gradient copolymers are complex, heterogeneous systems characterized by distributions in glass transitions, chain dynamics, and relaxation times that can reflect the type of gradient that predominately exists in the polymer chains.[102]

Both theoretical and experimental studies suggest that the properties of neat gradient copolymers are intermediate to their random and diblock copolymer counterparts.[103] Unlike block copolymers, interfaces of gradient copolymers are often "blurred" and poorly defined. In solution, their micellar properties are also different than typical block copolymers.[103-104] Designing new material, i.e. gradient copolymer with desired properties, requires precise knowledge of how the synthesis condition affect the microstructure, and the relation of microstructure with the morphology and the final properties of the material. To understand the morphological heterogeneity in the gradient copolymer, it is important to develop robust experimental strategies which can tell us about the different phases including the interface.

One key objective of copolymerization is to develop a new material with desired properties. For this reason, the monomers with different properties are selected in such a way that the final properties of the copolymer lie in between. Like many well-known copolymer systems, gradient copolymers often contain monomers that in pure form would generate polymers with large glass transition temperature (T_g) differences. Such differences are attractive for end-use materials, since strength and flexibility are optimized over very wide temperature ranges, and this is one reason why the styrene−butadiene gradient systems are so attractive. Therefore, one could generally expect that a quantitative measure of the fraction of rigid versus soft chains in the overall gradient copolymer morphology would constitute a relevant parameter, given its direct relationship to high versus low-T_g character. In principle, bulk rigid versus soft fractions in heterogeneous copolymers can be determined via traditional static ^{1}H NMR echo methods based on fits of the free induction decays or echoes, as has effectively been employed by the Saalwachter group and extended to cases involving relatively inexpensive low-field or bench-top NMR systems.[105] Some technical issues make it difficult to exactly determine the total signal intensity at the initial condition, due to very fast dipolar relaxation during the receiver recovery period, but ways to minimize this problem are known and discussed in the literature involving different solid echo and dipolar refocusing pulse sequences.[105b, 106] The presence of such small absolute, but consistent, errors in the total initial signal amplitude does not preclude the use of these methods for meaningful polymer structure/property investigations.

Component-specific responses of mixed polymeric systems are often difficult or impossible to discern by static solid-state nuclear magnetic resonance spectroscopy. Stated differently, the chemical component contribution to the soft or hard phase cannot easily be identified in a mixed polymer system by static methods. Such complications are compounded in gradient copolymer systems, compared to simple block polymers, as differential monomer incorporation leads to unique and complex gradient

shapes at the comonomer interfaces, and most likely, these complex interfaces influence the final morphology.

In this contribution, experimental strategies using magic-angle-spinning (MAS) solid-state NMR spectroscopy are applied to understand the complex morphology of styrene—butadiene (PS-PB) gradient copolymers synthesized under different conditions. The developed method is simple and can identify and quantify the amount of rigid and mobile phases in PS-PB gradient copolymers. An approach based on comparisons between fast and slow MAS ^{1}H experiments were investigated as a first step toward determination of component-specific behaviors in rigid and mobile segments of the gradient copolymers. In addition, a spin-counting strategy was introduced, adapted from a previous contribution of our group related to catalyst characterizations,[107] that easily quantifies the amount of the low-T_g, or "soft", butadiene component that is incorporated into the rigid domains of gradient copolymers. It was demonstrated that the fast MAS and spin-counting NMR methods can detect, in an experimentally straightforward approach, differential properties of the copolymers that are modified by varying the gradient copolymer synthesis conditions. The key advantage of the spin-counting approach is the ability to compare measured signal intensities for each polymer component to the theoretical intensities based on known compositions. This work follows and builds upon previous work by the Saalwachter group, which described in detail how magnetic resonance methods at low and high field could be used to address differential behavior in copolymers and to detect "hardening" and "softening" of different phases.[105] Other experimental approaches that exploit NMR's unique advantages for detecting differential mobility in complex polymer systems are available and typically rely on relaxation (primarily T_2 or $T_{1\rho}$) or specific magnetic interactions (e.g., dipolar, chemical shift anisotropy) to determine structure−property relationships.

6.2 Experimental Section

6.2.1 Samples

In this study, a number of samples of different chain structure and composition are analyzed including PS-PB gradient copolymers of different relative PS/PB composition and different gradient types, PS-PB block copolymers, and pure polybutadiene and polystyrene homopolymers (for control experiments). Only a few of those will be discussed in this chapter which is shown in Table 6 – 1. All block copolymers were prepared by batch living anionic polymerization in cyclohexane similar to the method described by Leibler and co-workers.[108] The first block is a pure polybutadiene block, followed by copolymerization of equal weights of styrene and butadiene and then finished with additional styrene to increase the molecular weights of styrene blocks. The discrete block copolymer would skip the copolymerization step with an adjustment in butadiene and styrene at first and the last block to maintain similar molecular weight. The gradient copolymer denoted as PS-grad-PB was prepared in the absence of any polar modifiers while the PS-grad-PB_THF sample was prepared with the addition of tetrahydrofuran (THF) at a molar ratio of THF/Li = 2.6 before alkyllithium was added. The pure PS was a low melt flow index, commercial general purpose polystyrene by free radical bulk polymerization. In contrast, the pure polybutadiene copolymer was a commercial medium vinyl high molecular weight polybutadiene by anionic polymerization. The composition of the samples is determined by high-resolution ^{1}H solution NMR, which revealed that the composition of the PS−PB block copolymer was 51:49 wt:wt % styrene:butadiene. Solution NMR revealed that the two gradient copolymers described above contained 49−51 wt % butadiene, essentially identical to the PS−PB block copolymer. Two additional gradient copolymers, prepared in the same manner as the PS-grad-PB_THF, had additional styrene added to the end block to provide samples with modified content but with the same gradient structure. These two materials are denoted as grad_THFb and grad_THFc in Table 6 – 1 and 6 – 2.

6.2.2 NMR

Solid-state MAS and fast-MAS NMR measurements were collected on a Bruker DSX-300 spectrometer operating at a magnetic field strength of 7.05 T, using a 2.0 mm double resonance magic-angle spinning probe provided by Revolution NMR in Fort Collins, CO. Measurements were recorded using a windowless eight-count composite 90° pulse sequence for background suppression (Figure 6.2a),[109] with a typical pulse width of 2.1 μs, a receiver dead time of 3−4 μs, and a 10 s repetition delay time (longer than $5T_{1H}$ for either PS or PB). ^{1}H spin-counting[107] measurements were acquired at 5 kHz, using a Bruker 4.0 mm MAS probe on the same spectrometer. Spectra were obtained using a single 90° pulse (Figure 6.2b) with a 3.5 μs pulse width and a 10 s repetition delay time.

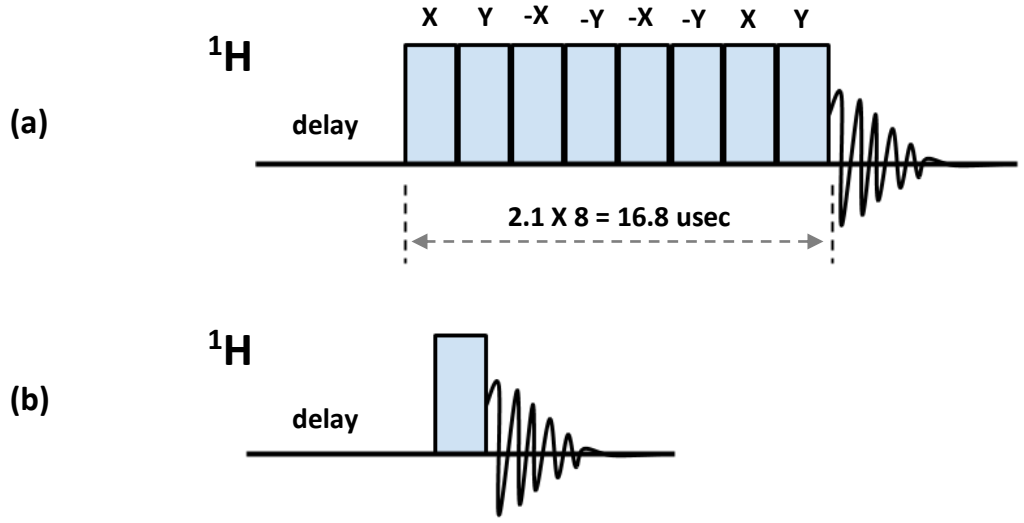

Figure 6.2. Schematic representation of the NMR pulse sequences used in this study. (a) ^{1}H NMR pulse sequence containing a windowless composite of eight 90° pulses with controlled phase cycling to eliminate the unwanted background,[109] (b) Simple one-pulse ^{1}H NMR pulse sequence with only one 90° pulse.

In spin-counting ^{1}H NMR method, polydimethylsiloxane (PDMS) was used as internal standard. The details of the spin counting method were described previously by our group.[107] Approximately 2 mg

of PDMS was added to rotors containing known masses of the polymer. As communicated in that report, Teflon spacers were used to limit the sample region to the middle ca. 20% volume element of the rotor to ensure maximum radio frequency homogeneity, thereby resulting in uniform excitation and determination of the intensity per ^{1}H using the PDMS internal standard. The effective sample region in the rotor was a cylinder of 4 mm in diameter and ca. 4 mm in length. Control experiments, in which a known amount of hexamethylbenzene (HMB) and a known amount of PDMS were added to the rotor, yielded 101 ± 4% of the expected theoretical HMB intensity. Using the spin-counting experimental method, the % rigid PB (or missing PB signal in mobile phase) can be calculated by knowing the mass of PDMS and the copolymer used, the composition of the copolymer and by comparing the ^{1}H integrated area of PDMS and the copolymers. The detailed calculation of spin-counting experiment is discussed later in this chapter.

6.2.3 Spectral deconvolution and calculations

The acquired ^{1}H spectra were deconvoluted to get individual component's integrated area using OriginPro 9 software. To fit the total spectra, a set of Voigt line-shape were used for each physical components (Figure 6.6 and Figure 6.7). The Lorentzian/Gaussian ratio of the narrow peak for mobile components was > 1, and the broad peak (hump) for the rigid components were < 1. Although the data were acquired using a composite of eight 90° pulse sequence[109] to suppress the background, we could still see background which intensity is negligible compared to the actual peak intensity but due to having very wide line-width the total integrated area of the background signal has a considerable effect on the total intensity. The background signal line-shape for empty rotor was found to be same for both 5 kHz and 32 kHz MAS acquisition, which tells that the background is coming from the stator of the probe. To eliminate the background, we have, at first, fit the background signal line-shape and then for each deconvolution, the fitting parameter of the background line-shape was used along with the other components to fit the

spectra, but its integrated area was not counted during the calculation. More details about the spectral deconvolution and data analysis are discussed later in this chapter.

6.3 Results and Discussion

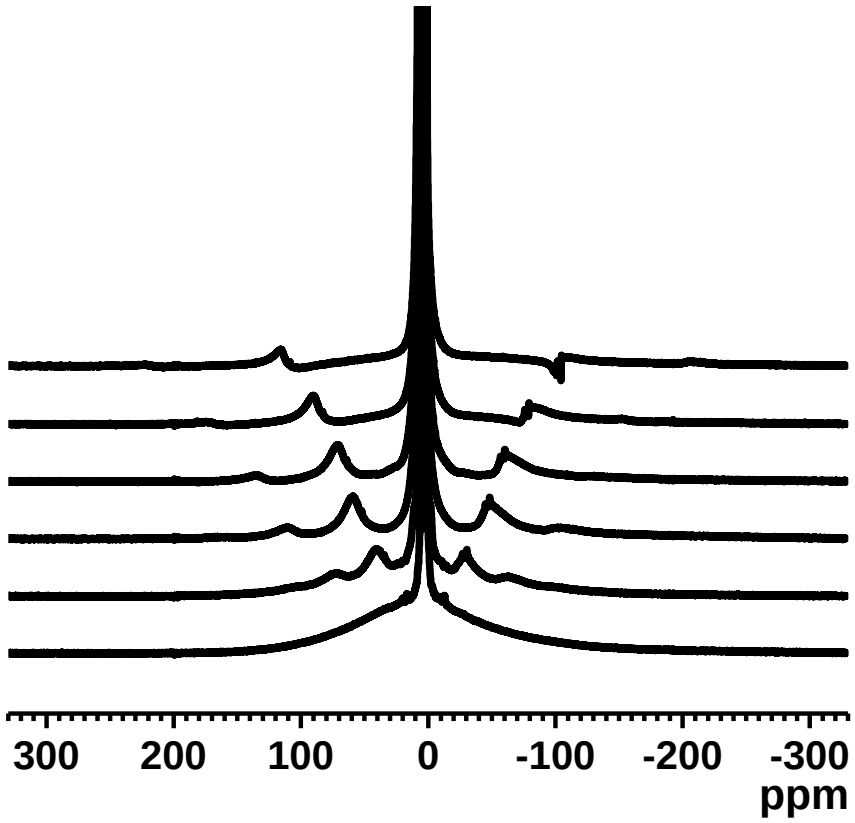

Figure 6.3. ^{1}H MAS NMR spectra of PS-PB block copolymer obtained at different spinning speed (bottom to top: 5 kHz, 10 kHz, 15 kHz, 20 kHz, 25 kHz, and 32 kHz).

^{1}H MAS NMR spectra for a 51:49 wt:wt % styrene−butadiene (PS−PB) block copolymer at different MAS speed (Figure 6.3) show that, with the increase in spinning speed from 5 kHz to 32 kHz, the very wide rigid PS signal breaks into several spinning side bands, depending on the spinning speed, and at 32 kHz the rigid PS wide peak is almost totally absent. Figure 6.4 compares the same spectra only for 5 and 32 kHz spinning speeds, where the signal for rigid PS at 5 kHz spinning speed is clearly shown above the

dotted line. As is expected for a styrene−butadiene copolymer in the solid state, two types of signals are observed at 5 kHz MAS, a narrow set of signals near 0 ppm and an extremely broad ca. 200 ppm (60 kHz) signal (above the dotted line in Figure 6.4) extending across the majority of the spectral window. This broad signal arises from rigid polystyrene segments whose motional correlation times are too slow to average homonuclear ^{1}H dipolar couplings. As the spinning speed is increased to 32 kHz, the broad component is essentially eliminated, resolving into the aromatic and aliphatic PS peaks. Spectra acquired

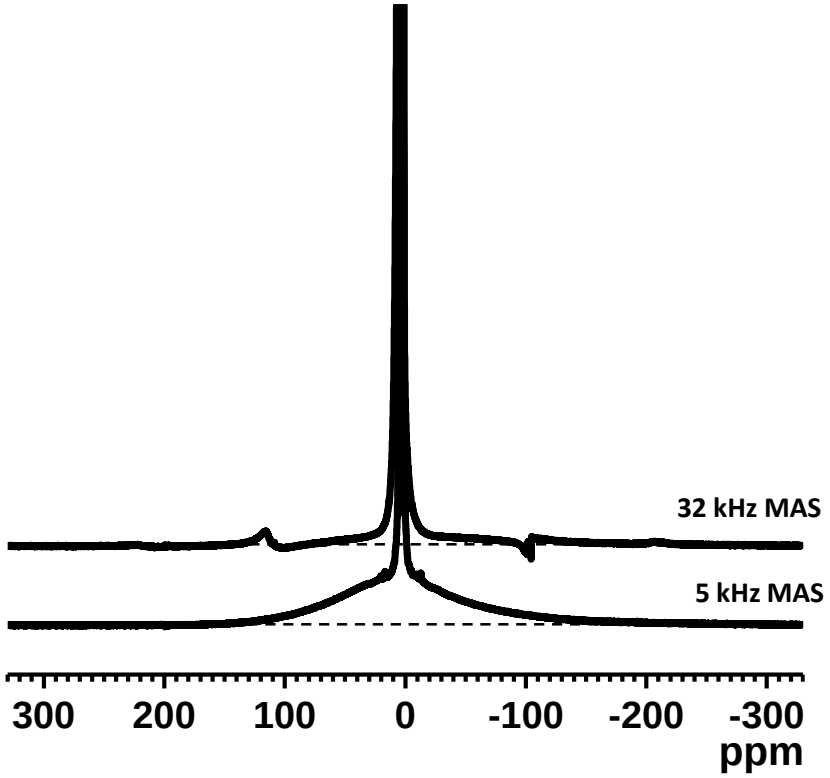

Figure 6.4 Slow and fast ^{1}H MAS NMR spectra for a PS-PB block copolymer obtained at spinning speeds of 5 and 32 kHz, respectively. The top part of the spectra are truncated to show the rigid PS component properly.

at 32 kHz should, within the known constraints of signal loss due to receiver dead time, reflect the total signal arising from all polymer segments. In addition, errors in total signal intensity that may arise from the fitting of broad components due to small errors in the baseline selection are removed at 32 kHz.

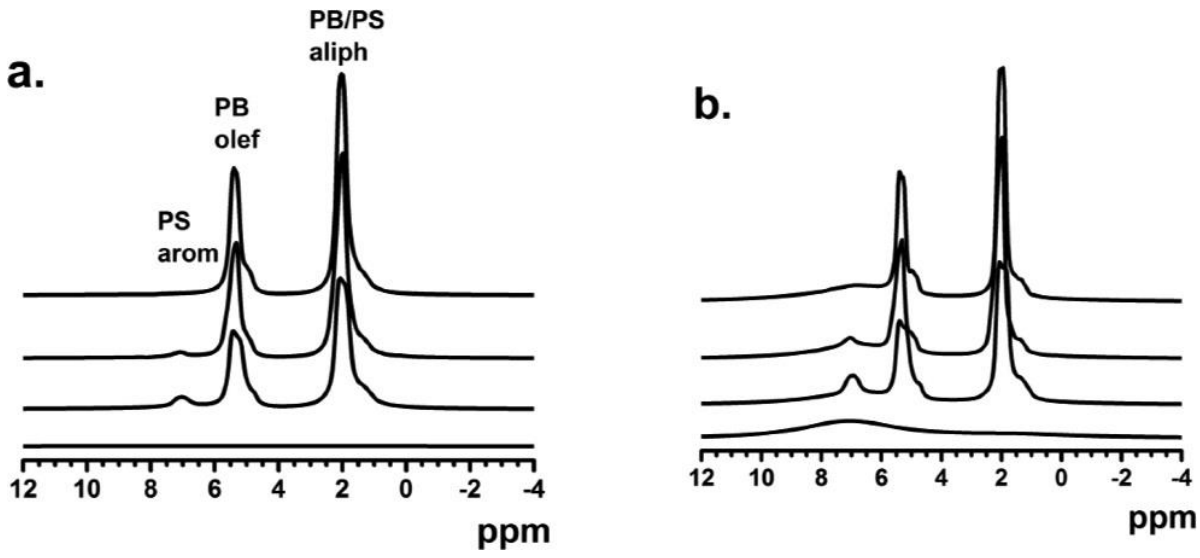

Figure 6.5. Isotropic regions of ^{1}H MAS NMR spectra at different MAS speeds.[110] From bottom to top: ^{1}H MAS NMR spectra of pure PS, PS-grad-PB_THF, PS-grad-PB (no THF), and the PS-PB block copolymer at (a) 5 kHz and (b) 32 kHz. All spectra were acquired at room temperature.

All the spectra were analyzed using a simple two-component rigid and mobile (hard and soft) model. Mobile components are defined as narrow signals whose line widths at half-maximum are less than 2 ppm in spectra obtained at 5 kHz MAS. Expansion of the isotropic region is shown in Figure 6.5 (a) and (b) for the two gradient copolymers denoted as PS-grad-PB_THF and PS-grad-PB and the same PS−PB block copolymer previously shown in Figure 6.4. Although all copolymer samples are essentially identical near 50:50 wt:wt % styrene:butadiene composition, variations in the individual peaks in the room temperature spectra of Figure 6.5 reflect differences in the chain dynamics of the individual components. For reference, the spectrum for pure PS is shown as the bottom trace in both Figure 6.5 (a) and (b), revealing that in the isotropic region of the ^{1}H MAS spectrum the PS is uniform at 5 kHz but exhibits the expected aromatic:aliphatic ratio at 32 kHz (albeit with broad signals relative to the mobile components of the copolymers). In Figure 6.5 (a), relatively narrow PS aromatic signals are observed only for the two gradient copolymer samples (middle traces), while narrow PB olefinic and aliphatic signals are observed

in all copolymers. The narrow gradient copolymer PS signals become more visible at 32 kHz (Figure 6.5 (b)), while the PB signals are much less sensitive to increased MAS speeds, albeit for slightly better resolution of minor signals arising from 1,2-butadiene and cis enchainments. At 32 kHz, a PS aromatic signal is detected for the PS−PB block copolymer (top trace in Figure 6.5 (b)), similar to that observed for pure PS. Qualitatively, the different aromatic signal widths for PS in the gradient copolymers (middle traces in Figure 6.5 (a)) relative to pure PS and a control PS−PB block copolymer of similar composition indicate that some PS chain segments get incorporated into more mobile regions and that the amount of PS in such an environment may be altered by addition of a Lewis base modifier like THF.

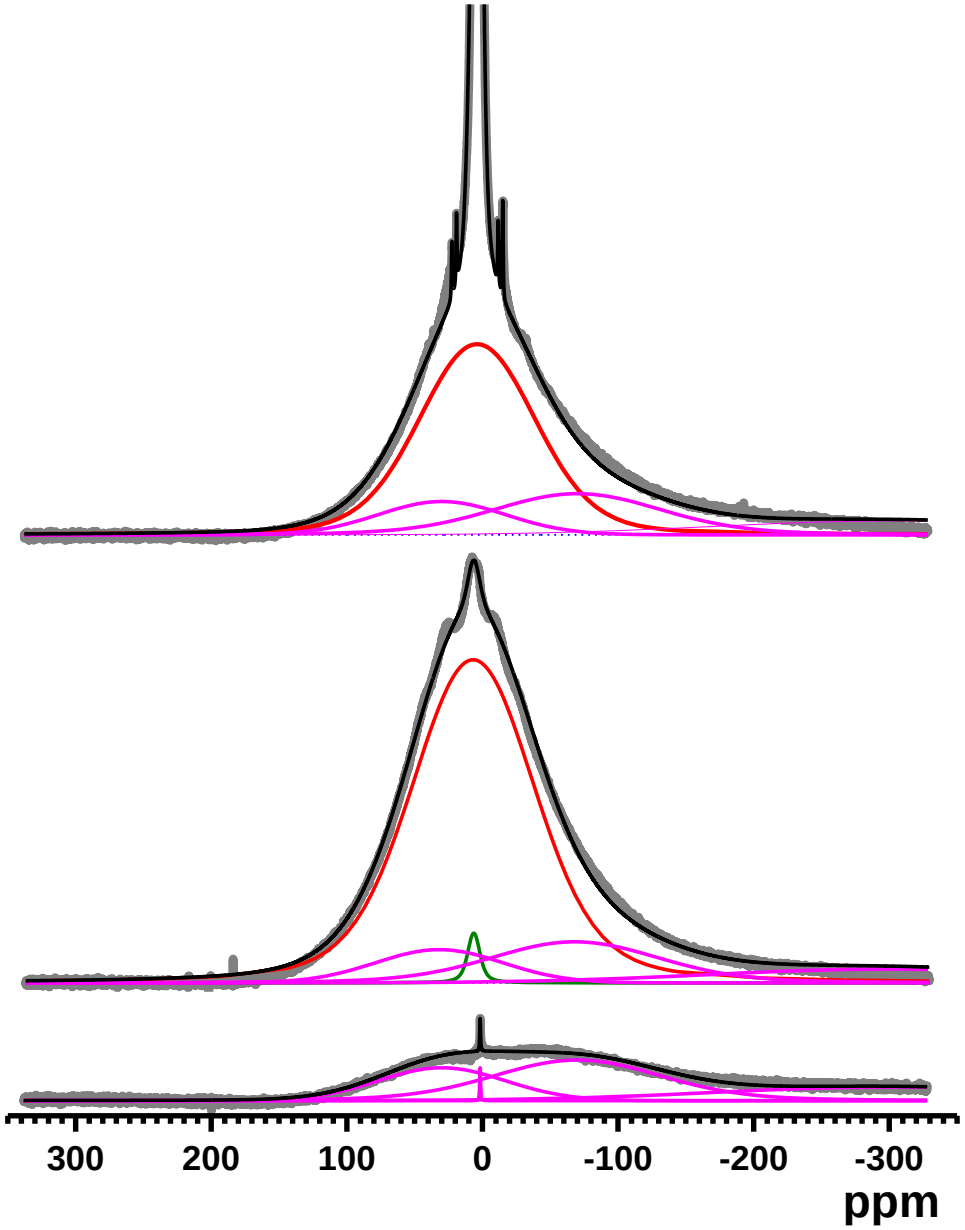

Figure 6.6. Line-shape of PS rigid component and rotor background. ^{1}H MAS NMR spectra for the empty rotor, pure PS, and PS-grad-PB_THF at 5 kHz. The magenta lines in all spectra denote the background contribution, and the red lines in the top and middle spectra are for the rigid PS contribution in the gradient copolymer and pure PS, respectively. Additional contributions corresponding to a narrower, but still rigid, PS component and its sidebands are included in the deconvolution but are too small to show in this figure.

In Figure 6.7(a) the narrow peaks at 5 kHz spectrum are from the mobile region, and the wide peak is for the rigid region of the material. The total integrated area of any narrow liquid-like signals appearing in the isotropic chemical shift region of the spectra acquired at 5 kHz represents the amount of mobile or soft phase present in any copolymer sample. As discussed previously, spectra acquired at 32 kHz should reflect the total signal intensity. A comparison of the total integrated area of all signals acquired at 32 kHz to the intensity of the mobile segment signals at 5 kHz, including spinning sidebands, provides a quantitative definition of the bulk percent rigidity of the sample, corresponding to the percent of ^{1}H signal from the rigid components.

$$\boldsymbol{bulk\ \%\ rigid} = \left[\frac{(\boldsymbol{I_{32}} - \boldsymbol{I_5^{mobile}}}{\boldsymbol{I_{32}}}\right] \times \mathbf{100} \qquad (17)$$

To determine the bulk rigid fraction in these materials, a simple relationship is used as shown in equation-17, where I_{32} represents the total intensity at 32 kHz and I_5^{mobile} denotes only the mobile intensity (sum of all narrow signals) in the 5 kHz spectrum. Intensities were obtained by deconvoluting the spectra using a set of Voigt line shapes to fit both the mobile and broad components of the spectra, as shown in Figure 6.6 and Figure 6.7. A broad but reproducible background signal arising from the rotor-stator is obtained at each spinning speed, as shown in Figure 6.6. The background signal for empty rotor was fitted with three Gaussian lineshapes (shown in magenta line in Figure 6.6), and the fitting parameters of the background signal were used for each deconvolution processes. The magenta lines in the top and the middle trace of Figure 6.6 shows the background signals, which is easily subtracted out from each spectrum after the deconvolution process. The red broad line (top and middle trace in Figure 6.6 and Figure 6.7 (a) and (c)) represents the rigid PS signal. Two green lines of intermediate line-width (shown in Figure 6.7 (c)) accounts for the semi-rigid phase of aliphatic and aromatic PS. The Figure 6.7 (b) and (c)

shows the expanded view of the isotropic region of the deconvoluted spectra. The blue, wine and the purple lines represent the PS (aliphatic and aromatic) mobile signal, 1,4-PB (aliphatic and olefinic), and 1,2-PB (aliphatic and olefinic) signals respectively. Using acquisition conditions described in the Experimental Section, the total overall intensity detected in the 5 kHz spectrum is routinely equal to 97−99% of the total intensity detected in the 32 kHz spectrum. For reference, pure atactic PS (T_g = 100 °C) exhibits no narrow peak at 5 kHz, while the % rigidity in pure PB (T_g = −95 °C) was at most 2% using this method. The control experiments on completely rigid (pure-PS homopolymer) and completely mobile (pure-PB homopolymer) materials show excellent agreement with the expected results, within the error of the experiments. In order to assess the fast/slow MAS NMR method for determination of the percent rigid fraction in gradient copolymers, measurements were made on the PS−PB block copolymer and several gradient copolymers; however, results of only five samples are given in Table 6 – 1. Comparison of the last three samples, where the preparation of the gradient interface is identical but the wt % PS is varied, indicates that increasing the hard segment PS content leads to the expected increase in the bulk % rigid fraction. The PS−PB block copolymer, PS-grad-PB, and PS-grad PB_THF, which have similar wt % PB but different interfacial structures, have a very similar bulk % rigid fraction. Previously published work on some commercial styrene− butadiene copolymers using static NMR methods yielded bulk rigid fractions near 70%, but in those cases, the butadiene content was much lower at 22−25 wt %.[105b]

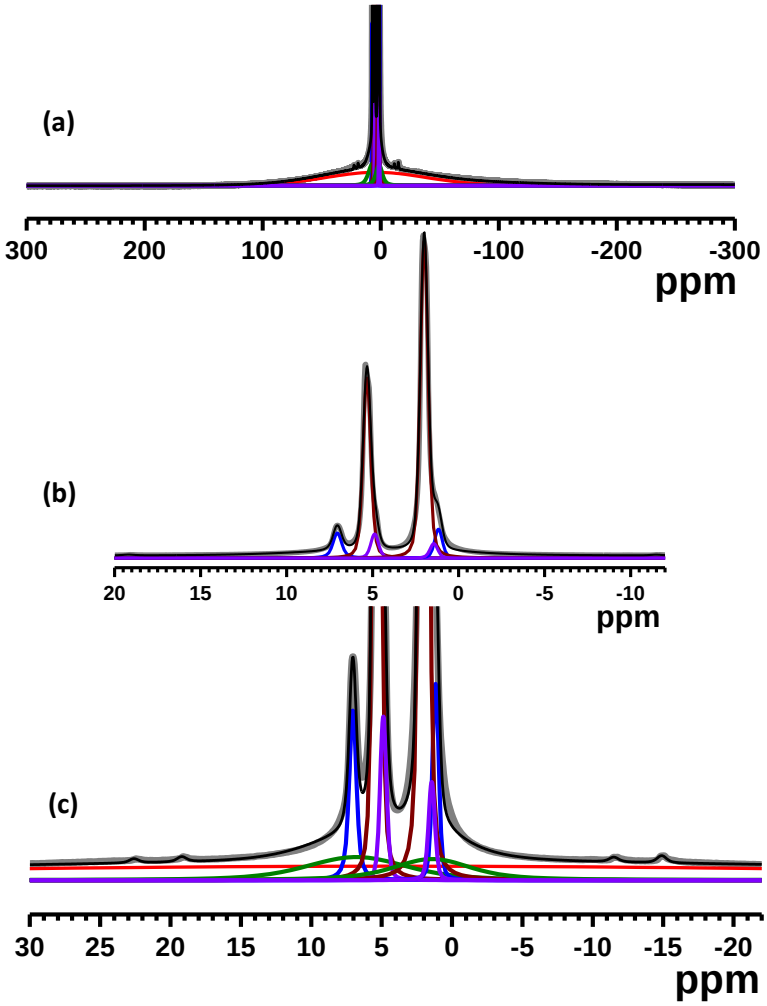

Figure 6.7. Deconvolution of ^{1}H MAS NMR spectrum for the PS-grad-PB_THF sample. (a) Showing representative figure of deconvolution of the ^{1}H MAS NMR spectra of gradient copolymer samples. Note that, the top part of the spectrum is truncated to show the bottom rigid part (red line) properly, (b) showing the deconvolution of the isotropic region (horizontally expanded). Only the narrow components are visible in this figure. The 'blue' lines are for mobile PS, 'wine' lines for 1,4-PB and 'purple' lines are for 1,2-PB, (c) both horizontally and vertically expanded figure, showing the narrow mobile components of PS (blue), 1,2-PB (purple), 1,4-PB (wine) and the relatively wide 'green' line represents semi-rigid component of PS. The 'red' line (almost straight line) shown here represents the rigid-PS components.

Table 6—1. Measured Fast/Slow MAS NMR Results for ^{1}H Bulk Percent Rigid Fraction in the Block and Gradient Copolymers[a].

Sample	wt % PS	mol % PS	^{1}H % PS	^{1}H % rigid
Block	50.8	34.9	41.7	36.9
PS-grad-PB	50.8	34.9	41.7	35.0
PS-grad-PB_THF	49.5	33.7	40.4	38.4
grad_THFb	55.5	39.3	46.3	44.7
grad_THFc	60.3	44.1	51.3	49.3

[a]The last two samples were prepared similar to PS-grad-PB_THF, but with additional styrene monomer feed at the end of the polymerization process. The amount of PS in each copolymer was determined by solution ^{1}H NMR measurements.

The fastest reliable spinning speed in our laboratory is 32 kHz, which explains the choice of this seemingly arbitrary MAS speed. The working assumption for defining “fast” is that the homogeneous dipolar couplings are rendered heterogeneous via spinning, and the broad dipolar line width for strongly coupled protons will be converted to an isotropic spectrum with accompanying sidebands. Figure 6.4 shows that this occurs with 32 kHz MAS for PS−PB copolymers. The preference would be to spin even faster, e.g. 50 kHz, and as more laboratories have access to even faster MAS equipment, this will become routinely accessible. Typical MAS conditions for routine solids experiments are in the “slow” 4−7 kHz range, so 5 kHz was chosen as representative of standard conditions. More importantly, it is well-known that narrow line widths, on the order of the 2 ppm criteria for defining “mobile” or liquid-like resolution discussed later, are only obtained in solid macromolecules when significant isotropic motion is present. The slow MAS data are only used to get the mobile fraction intensity, and this will be the same at any common slow speed; the sample is the primary source of spatial averaging, not the MAS. Therefore, given that all intensity is taken from the fast MAS data, whether that is 30 or 32 or 40 kHz, and only the mobile intensity is taken from the slow data, the results should be invariant to minor deviations in the spinning speeds used as long as the criteria described above are satisfied.

The slow-fast MAS ^{1}H NMR experimental method described above quickly and easily yields the percent rigidity for any polymer or copolymer. Also, it is amenable to variable temperature data collection

so that one can determine how the bulk rigidity changes over temperature ranges relevant to end-use applications. However, the real advantage about other methods lies in the ability to get component specific information. For example, the appearance of mobile PS in the gradient copolymers is readily observed in the spectra. One could determine the area of the narrow PS signals in the 5 kHz spectra of Figure 6.4 or Figure 6.5, and compare that intensity to the total PS signal, yielding the percent of PS that is mobile. This is simply not possible using traditional static wide-line methods. However, fitting the broad, rigid PS at low spinning speeds is more difficult than fitting narrow components, and additional error may be introduced. More importantly, the possibility of rigid PB chains, whose signals are harder to discern than the appearance of a mobile PS peak, would lead to an overestimation of the total PS signal. Further, frictional heating effects at fast MAS speeds could complicate the ability to get accurate difference signals, as the sample temperature is effectively higher relative to the slow MAS condition unless cooling air is applied and controlled (vide infra). This method is attractive due to its simplicity, and the possibility for complete automation, but in this initial study, the need for a complementary validation method exists.

Therefore, an improved determination of the amount of mobile PS and rigid PB can be accomplished in a straightforward manner by employing a quantitative spin-counting internal calibration technique, which makes use of PDMS as an internal standard. PDMS is an attractive standard as it provides a very sharp liquid-like signal at 0.2 ppm, well outside of the spectral region of interest, as evident in Figure 6.8. A known amount of PDMS is added to a known amount of copolymer sample, and both are centralized in the rotor via top and bottom Teflon spacers, to minimize radio frequency field inhomogeneity.[107] Control experiments done using pure HMB, a plastic organic crystal whose static line width is intermediate between that of PS and PB, verifies the confidence of this method by generating yields of 101 ± 4% of the expected theoretical HMB intensity. Comparison of the total integrated intensity of the PDMS signal with

measured PDMS mass allows one to determine the intensity per ^{1}H in the spectra. This provides a means to compare observed signal intensities to expected values based on measured sample mass.

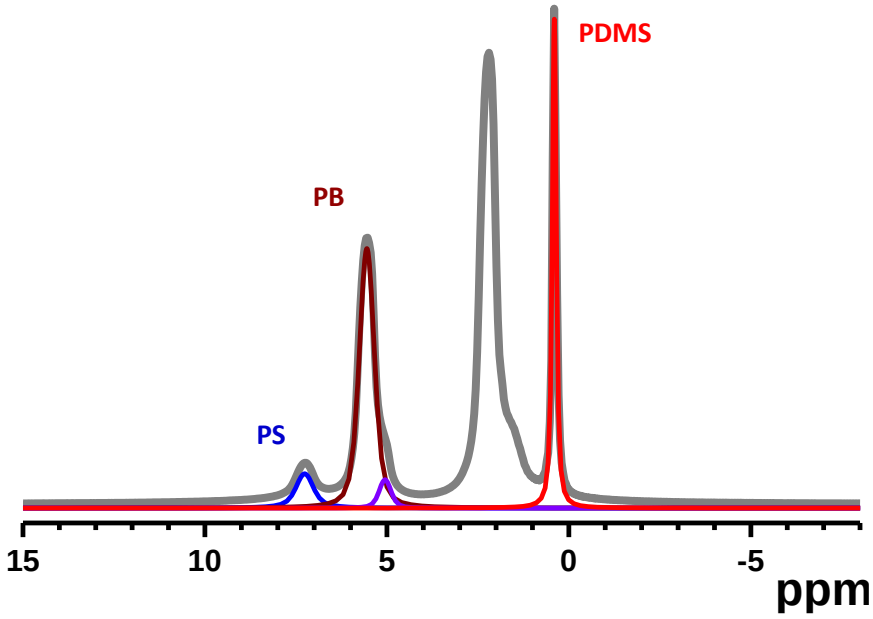

Figure 6.8. The 5 kHz ^{1}H MAS NMR spin-counting spectrum of the PS-grad-PB_THF.[110] The narrow signal at 0.2 ppm (shown in red line) is from the PDMS spin-counting standard. The wine and purple lined components are for the olefinic proton of 1,4-PB and 1,2-PB respectively. The blue line represents intensity for mobile aromatic PS.

Based on the composition of the copolymers derived from solution NMR and the measured sample mass, the expected signal intensity per ^{1}H of the PS and PB components is known. Figure 6.8 shows the deconvoluted spectrum of ^{1}H spin-counting experiment of PS-grad-PB_THF, where the red line at 0.2 ppm shows the integrated area for PDMS, the wine, and purple line represents the integrated area for 1,4-PB and 1,2-PB olefinic signals respectively. The blue line at ca. 7 ppm is for the signal of mobile aromatic PS. The fraction of rigid PB or mobile PS was determined using the spin-counting method. The data were calculated (for rigid PB) using the following equations-

$$\frac{I^{PDMS}}{m^{PDMS}} \times \frac{M_w^{PDMS}}{\#\ proton\ in\ PDMS} = {integrated\ area}/{1\ proton} \tag{18}$$

$$= I^{unit}$$

$$I^{unit} \times \frac{6\ proton}{1\ mole\ of\ PB} \times \frac{m^{PB}}{M_w^{PB}} \tag{19}$$

$$= expected\ intensity\ for\ PB\ (I^{expected})$$

$$\%\ missing\ PB\ signal = \%\ rigid\ PB = \frac{I^{expected} - I^{observed}}{I^{expected}} \times 100 \tag{20}$$

Where, I is for the integrated area, m is for mass and M_w represents molecular weight. Knowing the mass of PDMS, the mass of sample and weight fraction of PB in the sample, the fraction of PB that is in rigid phase can be calculated. As a test, the total observed PB signal of a pure PB sample was measured, giving 102.3% of the expected mobile signal. The higher than expected signal is attributed to the measured intensity of the PDMS peak, which is the largest source of uncertainty in this method. In order to minimize the amount of error, the signal intensities were measured by numerical integration rather than by manual peak fitting techniques. Because of the overlap of the aliphatic PS and PB signals, only the mobile aromatic PS and olefinic PB signals were considered in the calculations to determine the amount of mobile PS and rigid PB, respectively. To provide a more accurate representation of the rigid PB fraction, the 1,2-PB contribution to the PB determined from solution NMR was used to obtain the number of olefinic ^{1}H per unit mass. Non-negligible amounts of 1,2-PB were observed, with ~10% in the block copolymer and PS-grad- PB and ~15% in PS-grad-PB_THF series.

Table 6—2. Summary of Fast/Slow ^{1}H MAS Percent Rigid Measurements and Spin-Counting NMR Measurements for the PS-PB Block Copolymer and the Two PS-grad-PB Samples of Similar Butadiene wt %[a].

sample	block	PS-grad-PB	PS-grad-PB_THF	grad_THFb	grad_THFc
Modifier	no THF	no THF	THF	THF	THF
Wt % PS	50.8	50.8	49.5	55.5	60.3
^{1}H % PS	41.7	41.7	40.4	46.3	51.3
% 1,2-PB	9.8	9.7	14.9	13.3	13.1
% mobile PS (spin count)	0.5	2.8	8.1	7.5	6.1
% rigid PB (spin count)	8.7	13.4	24.5	26.5	26.8
% missing signal (spin count)	-1.1	4.1	4.2	-3.2	-5.7
^{1}H % rigid total	47.2	48.3	52.9	58.6	62.8
^{1}H % rigid total (fast MAS)	36.9	35.0	38.4	44.7	49.3

[a]The weight percent values and percent of PB that is 1,2 PB (% 1,2 PB) reported were obtained by ^{1}H solution NMR. Note that the last two columns, denoted THF_b and THF_c, are the same gradient preparation used for PS-grad-PB_THF, but with an additional PS block appended, hence the overall higher total percent rigid fraction.

Results of spin-counting measurements performed on the block copolymer, PS-grad-PB, PS-grad-PB_THF, and the grad_THFb and THF_c samples are presented in Table 6 – 2. The percent of PS in a mobile phase was found by comparing the intensity in the mobile aromatic PS peak to the total expected aromatic PS intensity based on the sample mass, wt % PS, and intensity per ^{1}H determined by the PDMS standard. Consistent with the observations from the slow and fast MAS measurements depicted in Figure 6.5, the block copolymer is found to contain almost no mobile PS (0.5%), while 8.1% of the PS in PS-grad-PB_THF is mobile. The fraction of rigid PB, whose existence is not easily discerned by simply looking at the spectra, is accounted for by examining the percentage of mobile olefinic PB intensity missing from the expected olefinic intensity. A similar trend to that observed for mobile PS is observed, with the block copolymer having the least rigid PB (8.7%) while PS-grad-PB_THF exhibits the largest fraction of PB in a rigid phase (24.5%). Taken together, these data indicate a heterogeneous distribution of local segmental environments for the gradient materials, the extent of which can be varied based on the synthesis conditions. These results provide quantitative and component-specific evidence for the concept of “PS-softening” and “PB-hardening”. In addition, the results for the grad_THFb and grad_THFc copolymers (last two columns of Table 6 – 2) show the same phase complexity as the PS-grad-PB_THF material, but with a

slightly larger rigid PB fraction and a slightly smaller mobile PS fraction. This result, along with the increased total percent rigidity, is completely consistent with what is expected for appending a larger PS block in the same synthesis used to make the PS-grad-PB_THF copolymer. Since PB accounts for about 60% of the ^{1}H intensity in these 50:50 wt:wt % copolymers, the amount of rigid PB and mobile PS observed by spin-counting MAS would indicate that we should have a net increase in the bulk rigid fraction, in contrast to the fast MAS results shown previously in Table 6 – 1 and reproduced in the last row of Table 6 – 2. In order to understand this discrepancy, the bulk rigid fraction is calculated directly from the spin-counting measurements by replacing the intensity at 32 kHz in equation (1) with the total expected signal intensity as determined from the mass of the copolymer samples. The total missing signal is measured to be less than 5% of the expected signal, which is consistent with the small (~−3%) differences observed between the total intensities at 5 and 32 kHz noted earlier. As shown in Table 6 – 2, the bulk rigid fraction is increased to 48−63% for the four copolymers via the absolute spin-counting method, with all of the gradient copolymers exceeding the block copolymer. While there is a noticeable difference in the bulk rigid fraction measured by the spin-counting versus the fast/slow MAS methods, it appears to be a systematic effect and does not affect any comparison between samples if the same method of determining bulk rigid fraction is used. The reason for the difference is still being studied but is believed to be due to difficulties in correctly phasing the empty rotor background of the 2.0 mm fast MAS, which in turn could lead to a systematic error in the measured total intensity by that method and temperature effects in the sample caused by the frictional heating at 32 kHz. Control experiments on our system show that the frictional heating effect is the largest source of error in the fast MAS method since our fast MAS probe does not have active variable-temperature control capability. Chemical shift thermometry using standard lead nitrate experiments reveals a 50 K difference in sample temperature at 32 kHz versus 5 kHz in our probe, resulting in a measurable but reproducible decrease in total signal intensity at 32 kHz due to thermal population differences. Under active temperature control of the sample, this source of error

will be eliminated, and this method should provide quantitative accuracy comparable to the spin-counting approach described below. In contrast, the spin-counting method is internally calibrated, relies only upon a single spectral acquisition, and its absolute accuracy clearly makes it the gold standard. The key advantage of the spin-counting method compared to the fast MAS approach is that all information can be obtained using standard MAS probes and that difference measurements are not required in order to determine rigid phase contents. However, the fast/slow MAS method is attractive due to its simplicity and potential for complete automation, and for this reason, we report it here and will work to continue to improve its absolute accuracy.

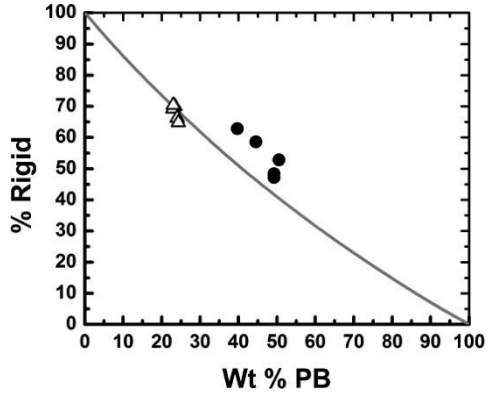

Figure 6.9. Comparison of the bulk percent rigid fraction for styrene-butadiene copolymers versus weight percent butadiene content for materials used in this study (filled symbols analyzed by spin-counting), and prior results from[105b] (open symbols).

A graph of our data, along with these prior results, is given in Figure 6.9. A curved line corresponding to the expected bulk % rigid fraction in the case of no mixing of rigid and mobile components (i.e., PS is completely rigid, and PB is completely mobile) is included in order to provide a point of reference; the curve is not a straight line due to the different proton contents in styrene and butadiene. As shown in Figure 6.9, all three of the gradient copolymers prepared with the THF modifier lie significantly above the predicted line, while the block copolymer is only 2% above the theoretical percent rigid value but below the non-THF gradient copolymer. We would certainly expect that gradient

copolymers, compared to traditional block copolymers, would have a more complex distribution of relevant relaxation times (e.g., T_2) or dynamics (e.g., dipolar or CSA modulation) and that those distributions could affect final mechanical properties. However, the process for tailoring chain interfaces begins with synthesis, and the ability to determine in a straightforward experiment how changes in synthesis, like varying modifier type or amount, impacts where the "low-T_g" and "high-T_g" monomer units ultimately reside in the material is critical. The spin-counting results described above clearly show that the amount of rigid PB and the amount of soft PS in the THF modified gradient copolymers exceeds that expected for block copolymers, and to our knowledge, this component specific chain information cannot be duplicated using any previously described experimental approach. In this way, one can quickly determine which synthesis schemes show the most promise for making high gradient materials and identify which products are worthy of additional experimental evaluation. Future work will focus on using variable temperature methods to extract central correlation time constants and their distributions, which should accurately reflect differential interfacial dynamics in gradient copolymers relative to their block copolymer analogs.

6.4 Conclusions

We have developed a simple and novel experimental approach which can quantitatively reveal the amount of rigid and soft phases in styrene − butadiene gradient copolymers with component specific resolution and proves that differential phase partitioning takes place in gradient copolymers that does not occur in similar block copolymers. The spin-counting strategy, we introduced, accurately determines the amount of the low-T_g, or "soft", butadiene component that is incorporated into the rigid domains of gradient copolymers and simultaneously reveals how much of the high-T_g, or "hard", styrene component is incorporated into the soft phase. Most importantly, we demonstrate that the polymer distributions can be manipulated by varying the gradient copolymer synthesis conditions and that these component

specific distributions change even when the overall chemical composition of the system is constant. The developed experimental method is also applicable to other heterogeneous copolymer systems if the heterogeneity in the chain mobility is large.

CHAPTER 7

7 CONCLUSIONS

7.1 Overall Conclusions

The phase composition of the polyethylene samples was investigated using the developed experimental method. The modified-EASY pulse sequence was found to be useful for morphology studies of polyethylene, as this experiment can provide sufficient information to reveal the distribution of PE chains in different morphological regions in a single experimental acquisition. The developed method is simple, reliable, and can provide quantitative information about the different phases of polyethylenes.

A wide variety of PE samples were analyzed in the first part of this study ranging from the linear samples with different average molecular weight (M_w, 43 – 400 Kg/mole), the PE copolymers with short chain branches of different branch length (SCB), the PE chains with long chain branches (LCB), the chains with long chain branches that contain short chain branches (LCSC), and the ultra-high molecular weight PE (UHMWPE), to understand the effect of chain length and topology on the morphology of polyethylenes. The crystalline and the amorphous content was found to change nearly in a linear fashion with the chain length of linear samples. The similar result was seen for the branched samples, although, for branched samples (especially for LCB samples), we don't have enough data points to draw a conclusion. The individual components of the interface (the mobile all-trans and the constrained amorphous chains) were also found to have a relation with the chain length, although the relationship is not well-defined. However, the total interface, which was calculated by adding the mobile all-trans and the constrained

amorphous chain content, was found to increase almost linearly with the increased molecular weight of PEs of all chain architectures.

The chain topology has a significant effect on the phase composition. The branched sample was found to have significantly higher interface content than that of the linear samples. The increased interface content in short chain branched PE is because of the difficulties in chain folding for the presence of short chain branches, which cannot be incorporated in the crystalline region but protruded in the interface regions. However, the long chain branched sample was found to have lower interface content than that of SCB. The reason behind this is the long chain branch can itself be a part of a crystal domain, which is not possible for short chain branches. As we have analyzed only one LCB sample, a straightforward conclusion cannot be drawn. The highest interface content was found in the LCSC samples.

The effect of thermal history on the polyethylene morphology was also studied for a set of linear PE samples. Linear polyethylenes of the same reactor batch were processed by different thermal treatment. It was found that the sharply cooled (or quenched) samples have higher amorphous and lower crystalline content than that of the untreated and the annealed (or slow-cooled) samples. The total interface content for all three sets of samples was found to increase almost linearly with the molecular weight. However, the annealed samples were less affected by the increased molecular weight of PE. The highest interface content was found in the quenched samples for the same molecular weight.

In the future, more PE samples with different branch size, branch density, and thermal histories will be analyzed for a better understanding of the effect of chain length, architecture and thermal processing on the polyethylene morphology. This knowledge will help to design a particular type of polyethylene of desired properties.

In separate work, the effect of the synthesis conditions on the morphology of styrene-butadiene gradient copolymer was studied. A novel solid-state ^{1}H NMR experimental method, based on slow/fast MAS, was developed to quantitatively determine the rigid and soft phase in styrene-butadiene gradient copolymers. The experiment quantitatively reveals the amount of rigid and mobile phases in the styrene-butadiene gradient copolymers with component specific resolution and proves that differential phase partitioning takes place in the gradient copolymer that does not occur in the similar block copolymers. A spin-counting strategy was also introduced which quantitatively determined that the amount of soft butadiene that is incorporated into the hard phase, and the amount of the hard polystyrene that is incorporated into the mobile phase. Furthermore, we showed that by controlling the polymer synthesis conditions the comonomer distribution in the gradient copolymer chains can be manipulated.

8 REFERENCES

1. Hosoda, S., *Polym. J.* **1988,** *20* (5), 383.

2. (a) Albizzati, E.; Galimberti, M., *Catalysis today* **1998,** *41* (1), 159; (b) Jørgensen, J. K.; Larsen, Å.; Helland, I., *e-Polymers* **2010,** *10* (1), 1596.

3. (a) Spiess, H. W., *Annual Review of Materials Science* **1991,** *21* (1), 131; (b) Yu, T.; Guo, M., *Progress in Polymer Science* **1990,** *15* (6), 825; (c) Frydman, L., *Annual review of physical chemistry* **2001,** *52* (1), 463.

4. (a) Randall, J. C., **1984**; (b) Schmidt-Rohr, K. S., H. W., *Multidimensional Solid-State NMR and Polymer*. Academic Press: San Diego, Ca, 1994; (c) Zhang, L.; Hansen, E. W.; Helland, I.; Hinrichsen, E.; Larsen, Å.; Roots, J., *Macromolecules* **2009,** *42* (14), 5189.

5. (a) Lai, D.; Yakimets, I.; Guigon, M., *Materials Science and Engineering: A* **2005,** *405* (1), 266; (b) Humbert, S.; Lame, O.; Séguéla, R.; Vigier, G., *Polymer* **2011,** *52* (21), 4899.

6. (a) Peacock, A., *Handbook of polyethylene: structures: properties, and applications*. CRC Press: 2000; (b) Pethrick, R. A.; Viney, C., *Techniques for polymer organisation and morphology characterisation*. Wiley Chichester (W. Sx.): 2003; (c) King, S. M.; Pethrick, R. A.; Dawkins, J. V., *Small-angle neutron scattering, John Wiley & Sons Ltd., Chichester* **1999**, 171.

7. Siesler, H. W.; Urban, M. W.; Craver, C. D., *Adv. Chem. Series* **1993,** *236*.

8. Isasi, J. R.; Mandelkern, L.; Galante, M. J.; Alamo, R. G., *Journal of Polymer Science Part B: Polymer Physics* **1999,** *37* (4), 323.

9. (a) Cullity, B. D., *Elements of X-ray Diffraction*. London, 1978; (b) Coufal, H.; Tong, H. M.; Nguyen, L. T., New Characterization Techniques for thin Polymer Films. Wiley, New York: 1990.

10. (a) Sadler, D. M.; Hall, I., Structure of Crystalline Polymers. Elsevier, London: 1984; (b) Higgins, J. S.; Benoît, H., *Polymers and neutron scattering*. Clarendon press Oxford: 1994; (c) Jones, R. A. L.; Richards, R. W., *Polymers at surfaces and interfaces*. Cambridge University Press: 1999.

11. (a) Campbell, D.; Pethrick, R. A.; White, J. R., *Polymer characterization: physical techniques*. CRC press: 2000; (b) Williams, D. B., **1984**.

12. Savage, R. C.; Mullin, N.; Hobbs, J. K., *Macromolecules* **2015,** *48* (17), 6160.

13. (a) Chen, Q.; Kurosu, H., Solid-State NMR Studies on Semicrystalline Polymers. In *Annual Reports on NMR Spectroscopy*, Webb, G., Ed. Elsevier Ltd.: London, 2007; Vol. 61, pp 247; (b) Yamanobe, T.; Uehara, H.; Kakiage, M., **2010,** *70*, 203; (c) Hu, W. G.; Schmidt-Rohr, K., *Polymer* **2000,** *41*, 2979; (d) Spiess, H. W., Deuteron NMR—a new tool for studying chain mobility and orientation in polymers. In *Characterization of Polymers in the Solid State I: Part A: NMR and Other Spectroscopic Methods Part B: Mechanical Methods*, Springer: 1985; pp 23; (e) Uehara, H.; Tanaka, H.; Yamanobe, T., *Polymer Journal* **2012,** *44* (8), 795.

14. Pechmann, H. v., *Ber. dtsch. chem. Ges* **1898,** *31*, 2640.

15. Bamberger, E.; Tschirner, F., *Berichte der deutschen chemischen Gesellschaft* **1900,** *33* (1), 955.

16. Fawcett, E.; Gibson, R.; Perrin, M.; Patton, J.; Williams, E., *British Patent* **1937,** *471590*.

17. (a) Kaminsky, W., *Polyolefins: 50 years after Ziegler and Natta II*. Springer: 2013; (b) Ziegler, K., *Angew. Chem.* **1952,** (64), 323.

18. Natta, G.; Corradini, P.; Bassi, I. W., *1960* **1960,** *15* (9).

19. Malpass, D. B., *Introduction to Industrial Polyethylene: Properties, Catalysts, and Process*.

ed.; Scrivener Publishing LLC.: Salem, MA, 2010.

20. (a) Kawai, F.; Watanabe, M.; Shibata, M.; Yokoyama, S.; Sudate, Y.; Hayashi, S., *Polymer Degradation and Stability* **2004,** *86* (1), 105; (b) Beach, B. L.; Kissin, Y. V., JI Kroschwitz, Encyclopedia of Polymer Science and Engineering, vol. 6. Wiley, New York: 1986; (c) James, D. E., *Mark, HF, Bikales, NM, Overberger, CG, Menges, G., Eds* **1985**, 429; (d) McDaniel, M. P.; Benham, E. A. Linear, very low density polyethylene polymerization process and products thereof. December 28, 1993; (e) Kissin, Y. V., *Kirk-Othmer Encyclopedia of Chemical Technology* **2005**.

21. Doak, K. W., *MARK, HM; BIKALES, NM; OVERBERG, CG; MENGES, G. Encyclopedia of Polymer Science and Engineering. New York: John-Wiley & Sons* **1986,** *6*.

22. (a) Bubeck, R. A., *Materials Science and Engineering: R: Reports* **2002,** *39* (1), 1; (b) Read, D. J.; McLeish, T. C. B., *Macromolecules* **2001,** *34* (6), 1928.

23. Gupta, P.; Wilkes, G. L.; Sukhadia, A. M.; Krishnaswamy, R. K.; Lamborn, M. J.; Wharry, S. M.; Tso, C. C.; DesLauriers, P. J.; Mansfield, T.; Beyer, F. L., *Polymer* **2005,** *46* (20), 8819.

24. Teng, H.-x.; Shi, Y.; Jin, X.-g.; Cheng, S. Z. D., *高分子科学* **2002,** *20* (4), 347.

25. Sarzotti, D. M.; Soares, J. B. P.; Penlidis, A., *Journal of Polymer Science Part B: Polymer Physics* **2002,** *40* (23), 2595.

26. (a) Galland, G. B.; Da Silva, L. F.; Nicolini, A., *Journal of Polymer Science Part A: Polymer Chemistry* **2005,** *43* (20), 4744; (b) Simanke, A. G.; Galland, G. B.; Freitas, L.; da Jornada, J. A. H.; Quijada, R.; Mauler, R. S., *Polymer* **1999,** *40* (20), 5489.

27. Robertson, G. L., Edible, biobased and biodegradable food packaging materials. Chpt. 3 in “Food Packaging: Principles and Practice,” 3rd ed., 49-90. CRC Press, Boca Raton, Fla: 2013.

28. Hashemi, S.; Williams, J. G., *Polymer* **1986,** *27* (3), 384.

29. Choi, K.-Y.; Ray, W. H., *Journal of Macromolecular Science-Reviews in Macromolecular Chemistry and Physics* **1985,** *25* (1), 57.

30. (a) Shamiri, A.; Chakrabarti, M.; Jahan, S.; Hussain, M.; Kaminsky, W.; Aravind, P.; Yehye, W., *Materials* **2014,** *7* (7), 5069; (b) Zakharov, V. A.; Bukatov, G. D.; Yermakov, Y. I., On the mechanism of olefin polymerization by Ziegler-Natta catalysts. In *Industrial Developments*, Springer: 1983; pp 61; (c) Kaminsky, W., *Catalysis Today* **1994,** *20* (2), 257.

31. (a) Kissin, Y., *Studies in Surface Science and Catalysis* **2007,** *173*, 1; (b) Weckhuysen, B. M.; Schoonheydt, R. A., *Catalysis Today* **1999,** *51* (2), 215; (c) McDaniel, M. P., *Advances in catalysis* **2010,** *53*, 123.

32. (a) Wunderlich, B., *Macromolecular physics. vol. 1: Crystal structure morphology, defects*. Academic Press: 1973; (b) Bassett, D. C., *Principles of polymer morphology*. CUP Archive: 1981; (c) Kobayashi, K.; Geil, P. H., *Interscience Publisher, New York, NY* **1963**, 474.

33. (a) Keller, A., *Reports on progress in Physics* **1968,** *31* (2), 623 %@ 0034; (b) Phillips, P. J., *Reports on Progress in Physics* **1990,** *53* (5), 549 %@ 0034; (c) Bassett, D. C., *Developments in crystalline polymers*. Springer: 1982; Vol. 1 %@ 0853341168; (d) Barham, P. J., Materials Science and Technology; Cahn, RW, Haasen, P., Kramer, EJ, Eds. VCH: Weinheim: 1993.

34. Sauter, E., *Z Phys Chem B* **1932,** *18*, 417.

35. Keller, A., *Philosophical Magazine* **1957,** *2* (21), 1171.

36. (a) Petraccone, V.; Allegra, G.; Corradini, P. In *Calculation of minimum potential energy of folds and kinks in polyethylene crystals*, Wiley Online Library: 1972; pp 419; (b) Ungar, G.; Stejny, J.; Keller, A.; Bidd, I.; Whiting, M. C., *Science* **1985,** *229* (4711), 386.

37. Toda, A., *Colloid and Polymer Science* **1992,** *270* (7), 667.

38. Fischer, E. W., *Z. Naturforsch* **1957**, 753.

39. Herrmann, K.; Gerngross, O.; Abitz, W., *Zeitschrift für Physikalische Chemie* **1930,** *10* (Abt. B), 371.

40. (a) Yundt, A. P., *Tappi* **1951,** *34* (2), 89; (b) Schlesinger, W.; Leeper, H. M., *Journal of Polymer Science* **1953,** *11* (3), 203; (c) Keller, A.; Waring, J. R. S., *Journal of Polymer Science* **1955,** *17* (86), 447; (d) Peck, V.; Kaye, W. In *Behavior of Crystallites in Polyethylene*, JOURNAL OF APPLIED PHYSICS, AMER INST PHYSICS CIRCULATION FULFILLMENT DIV, 500 SUNNYSIDE BLVD, WOODBURY, NY 11797-2999: 1954; pp 1465.

41. Till, P., *Journal of Polymer Science* **1957,** *24* (106), 301.

42. Flory, P., *Journal of the American Chemical Society* **1962,** *84* (15), 2857.

43. (a) Muller, A., *Proceedings of the Royal Society of London. Series A, Containing Papers of a Mathematical and Physical Character* **1928**, 437; (b) Müller, A., *Proceedings of the Royal Society of London. Series A, Containing Papers of a Mathematical and Physical Character* **1932**, 514.

44. (a) Hengstenberg, J., *Zeitschrift für Kristallographie-Crystalline Materials* **1928,** *67* (1), 583; (b) Kohlhaas, R.; Soremba, K. H., *Z. Kristallogr* **1938,** *100*, 47; (c) Smith, A. E., *The Journal of Chemical Physics* **1953,** *21* (12), 2229; (d) Shearer, H. M. M.; Vand, V., *Acta Crystallographica* **1956,** *9* (4), 379; (e) Brathovde, J. R.; Lingafelter, E. C., *Acta Crystallographica* **1958,** *11* (10), 729; (f) Vainshtein, B. K.; Pinsker, Z. G. In *Determination of the hydrogen positions in the crystal structure of a paraffin*, 1950; pp 53; (g) Müller, A.; Lonsdale, K., *Acta crystallographica* **1948,** *1* (3), 129; (h) Piper, S. H.; Brown, D.; Dyment, S., *Journal of the Chemical Society, Transactions* **1925,** *127*, 2194; (i) Schoon, T., *Z. Physiol. Chem B* **1938,** *39*, 385.

45. Vand, V., *Acta Crystallographica* **1951,** *4* (2), 104.

46. Schmidt-Rohr, K.; Spiess, H. W., *Macromolecules* **1991,** *24*, 5288.

47. (a) Chaiyut, N.; Amornsakchai, T.; Kaji, H.; Horii, F., *Polymer* **2006,** *47* (7), 2470; (b) Kitamaru, R.; Horii, F.; Murayama, K., *Macromolecules* **1986,** *19*, 636; (c) Kuwabara, K.; Kaji, H.; Horii, F.; Bassett, D. C.; Olley, R. H., *Macromolecules* **1997,** *30* (24), 7516; (d) Mowery, D. M.; Harris, D. J.; Schmidt-Rohr, K., *Macromolecules* **2006,** *39* (8), 2856.

48. Sadler, D. M. t.; Keller, A., *Science* **1979,** *203* (4377), 263.

49. Hoffman, J. D.; Williams, G.; Passaglia, E. In *Analysis of the α, β, and γ relaxations in polychlorotrifluoroethylene and polyethylene: Dielectric and mechanical properties*, Wiley Online Library: 1966; pp 173.

50. Ferry, J. D., *Viscoelastic properties of polymers*. John Wiley & Sons: 1980.

51. (a) Williams, M. L.; Landel, R. F.; Ferry, J. D., *Journal of the American Chemical society* **1955,** *77* (14), 3701; (b) Fox Jr, T. G.; Flory, P. J., *Journal of Applied Physics* **1950,** *21* (6), 581.

52. Cowie, J. M. G., Polymers: Physics and Chemistry of Modern Materials. Chapman and Hall, New York: 1991.

53. Wunderlich, B., *The Journal of Chemical Physics* **1962,** *37* (10), 2429.

54. Krigbaum, W. R.; Roe, R. J.; Smith, K. J., *Polymer* **1964,** *5*, 533.

55. (a) Levitt, M. H., *Spin dynamics: basics of nuclear magnetic resonance*. John Wiley & Sons: 2001; (b) Keeler, J., *Understanding NMR spectroscopy*. John Wiley & Sons: 2011.

56. Purcell, E. M.; Torrey, H. C.; Pound, R. V., *Physical review* **1946,** *69* (1-2), 37.

57. Bloch, F., *Physical review* **1946,** *70* (7-8), 460.

58. (a) Andrew, E. R.; Bradbury, A.; Eades, R. G., **1958**; (b) Andrew, E. R.; Bradbury, A.; Eades, R. G., **1959**; (c) Lowe, I. J., *Physical Review Letters* **1959,** *2* (7), 285.

59. (a) Ernst, R. R.; Richard, R., *Ed Grant DM & Harris RK. Encyclopedia of Nuclear Magnetic Resonance* **1996,** *1*; (b) Ernst, R. R.; Anderson, W. A., *Review of Scientific Instruments* **1966,** *37* (1), 93.

60. Haeberlen, U.; Waugh, J. S., *Physical Review* **1968,** *175* (2), 453.

61. Schaefer, J.; Stejskal, E. O.; Buchdahl, R., *Macromolecules* **1975,** *8* (3), 291.

62. Farrar, T. C., *Analytical Chemistry* **1970,** *42* (4), 109A.

63. (a) Sanders, J. K. M.; Hunter, B. K.; Griesinger, C., *Angewandte Chemie-English Edition* **1994,** *33* (19), 1992; (b) Lynden-Bell, R. M.; Harris, R. K., *Nuclear magnetic resonance spectroscopy*. Appleton-Century-Crofts: 1969.

64. Stejskal, E. O.; Memory, J. D., High Resolution Solid State NMR. Oxford University Press, New York: 1994.

65. Atta ur, R.; Choudhary, M. I., Chapter 1 - The Basics of Modern NMR Spectroscopy. In *Solving Problems with NMR Spectroscopy*, Atta ur, R.; Choudhary, M. I., Eds. Academic Press: San Diego, 1996; pp 1.

66. (a) Ernst, M.; Zimmermann, H.; Meier, B. H., *Chemical Physics Letters* **2000,** *317* (6), 581; (b) Gan, Z.; Ernst, R. R., *Solid state nuclear magnetic resonance* **1997,** *8* (3), 153; (c) Scholz, I.; Hodgkinson, P.; Meier, B. H.; Ernst, M., *The Journal of chemical physics* **2009,** *130* (11), 114510 %@ 0021.

67. (a) McConnell, J., *Press, Cambridge* **1987**; (b) Goldman, M. X., *Quantum description of high-resolution NMR in liquid s*. Clarendon Press. Oxford University Press: 1988.

68. Solomon, I., *Physical Review* **1955,** *99* (2), 559.

69. Hartmann, S. R.; Hahn, E. L., *Physical Review* **1962,** *128* (5), 2042.

70. Sato, H.; Tanaka, Y.; Randall, J. C. In *NMR and Macromolecules*, 1984; p 181.

71. Alpert, N. L., *Physical Review* **1947,** *72* (7), 637.

72. Hall, I. H., *Structure of crystalline polymers*. Elsevier Science Ltd: 1984.

73. (a) Peacock, A. J., *Handbook of Polyethylene*

Marcel Dekker, Inc.: New York, NY, 2000; (b) Gedde, U. W.; Eklund, S.; Jansson, J. F., *Polymer* **1983,** *24* (12), 1532; (c) Hosoda, S.; Nozue, Y.; Kawashima, Y.; Utsumi, S.; Nagamatsu, T.; Wagener, K.; Berda, E.; Rojas, G.; Baughman, T.; Leonard, J., *Macromolecular Symposia* **2009,** *282* (1), 50.

74. Herglotz, H. K., Structure of Crystalline Polymers, edited by IH HALL. London: Elsevier: 1984.

75. Chiang, R.; Flory, P. J., *Journal of the American Chemical Society* **1961,** *83* (13), 2857.

76. Hagemann, H.; Snyder, R. G.; Peacock, A. J.; Mandelkern, L., *Macromolecules* **1989,** *22* (9), 3600.

77. (a) Kitamaru, R.; Horii, F.; Zhu, Q., *Polymer* **1994,** *35*, 1187; (b) Yao, Y.; Jiang, S.; Rastogi, S., *Macromolecules* **2014,** *47* (4), 1371.

78. Litvinov, V. M.; Kurelec, L., *Polymer* **2014,** *55* (2), 620.

79. Earl, W. L.; VanderHart, D. L., *Macromolecules* **1979,** *12*, 762.

80. VanderHart, D. L., *Journal of Magnetic Resonance (1969)* **1981,** *44* (1), 117.

81. Bloembergen, E. M. P., R. V. Pound, *Physical Review* **1948,** *73* (7), 679.

82. (a) Alamo, R. G.; Blanco, J. A.; Carrilero, I.; Fu, R., *Polymer* **2002,** *43* (6), 1857; (b) Axelson, D. E., *VCH Verlagsgesellschaft, High Resolution NMR Spectroscopy of Synthetic Polymers in Bulk* **1986**, 157; (c) Axelson, D. E.; Mandelkern, L.; Popli, R.; Mathieu, P. d., *Journal of Polymer Science: Polymer Physics Edition* **1983,** *21* (11), 2319.

83. (a) Kuwabara, K.; Kaji, H.; Horii, F., *Macromolecules* **1997,** *30*, 7516; (b) Crist, B.; Peterlin, A., *Journal of Polymer Science Part A-2: Polymer Physics* **1969,** *7* (7), 1165.

84. Jaeger, C.; Hemmann, F., *Solid State Nucl. Magn. Reson.* **2014,** *57-58*, 22.

85. Tapash, A.; DesLauriers, P. J.; White, J. L., *Macromolecules* **2015,** *48* (9), 3040.

86. Simanke, A. G.; De Lemos, C.; Pires, M., *Polymer Testing* **2013,** *32* (2), 279.

87. (a) Stevens, J. C., *Studies in Surface Science and Catalysis* **1996,** *101*, 11; (b) Wu, L.; Wanke, S. E., *Handbook of Transition Metal Polymerization Catalysts* **2010**, 261; (c) Shamiri, A.; Chakrabarti, M. H.; Jahan, S.; Hussain, M. A.; Kaminsky, W.; Aravind, P. V.; Yehye, W. A., *Materials* **2014,** *7* (7), 5069.

88. (a) Guichon, O.; Seguela, R.; David, L.; Vigier, G., *Journal of Polymer Science Part B: Polymer Physics* **2003,** *41* (4), 327; (b) Chuu, K.-J.; Ha, J.-W.; Park, T.-H., *Materials Letters* **1997,** *30* (1), 115.

89. Kitamaru, R.; Horii, F.; Murayama, K., *Macromolecules* **1986,** *19* (3), 636.

90. (a) Mead, W. T.; Desper, C. R.; Porter, R. S., *Journal of Polymer Science: Polymer Physics Edition* **1979,** *17* (5), 859; (b) Phillips, T. L.; Hanna, S., *Polymer* **2005,** *46* (24), 11035; (c) Lee, S.; Rutledge, G. C., *Macromolecules* **2011,** *44* (8), 3096; (d) Ghazavizadeh, A.; Rutledge, G. C.; Atai, A. A.; Ahzi, S.; Rémond, Y.; Soltani, N., *Journal of Polymer Science Part B: Polymer Physics* **2013,** *51* (16), 1228.

91. Hosoda, S.; Nozue, Y.; Kawashima, Y.; Utsumi, S.; Nagamatsu, T.; Wagener, K.; Berda, E.; Rojas, G.; Baughman, T.; Leonard, J. In *Perfectly controlled lamella thickness and thickness distribution: a morphological study on ADMET polyolefins*, Wiley Online Library: 2009; pp 50.

92. (a) Doskočilová, D.; Schneider, B.; Jakeš, J.; Schmidt, P.; Baldrian, J.; Hernández-Fuentes, I.; Alonso, M. C., *Polymer* **1986,** *27* (11), 1658; (b) Eckman, R. R.; Henrichs, P. M.; Peacock, A. J., *Macromolecules* **1997,** *30* (8), 2474; (c) Hansen, E. W.; Kristiansen, P. E.; Pedersen, B., *The Journal of Physical Chemistry B* **1998,** *102* (28), 5444; (d) Kaji, A.; Ohta, Y.; Yasuda, H.; Murano, M., *Polymer Journal* **1990,** *22* (6), 455; (e) Kitamaru, R.; Horii, F.; Zhu, Q.; Bassett, D. C.; Olley, R. H., *Polymer* **1994,** *35* (6), 1171; (f) Cheng, J.; Fone, M.; Reddy, V. N.; Schwartz, K. B.; Fisher, H. P.; Wunderlich, B., *Journal of Polymer Science Part B: Polymer Physics* **1994,** *32* (16), 2683; (g) Kuwabara, K.; Kaji, H.; Horii, F., *Macromolecules* **2000,** *33* (12), 4453; (h) Zhang, L.; Hansen, E. W.; Helland, I.; Hinrichsen, E.; Larsen, Å.; Roots, J., *Macromolecules* **2009,** *42* (14), 5189.

93. (a) Chen, Q.; Kurosu, H., *Annual Reports on NMR Spectroscopy* **2007,** *61*, 247; (b) Yamanobe, T.; Uehara, H.; Kakiage, M., *Annual Reports on NMR Spectroscopy* **2010,** *70*, 203.

94. (a) Kiho, H.; Peterlin, A.; Geil, P. H., *Journal of Applied Physics* **1964,** *35* (5), 1599; (b) Hu, W. G.; Schmidt-Rohr, K., *Polymer* **2000,** *41* (8), 2979.

95. Chaiyut, N.; Amornsakchai, T.; Kaji, H.; Horii, F., *Polymer* **2006,** *47* (7), 2470.

96. (a) Schmidt-Rohr, K.; Spiess, H. W., *Macromolecules* **1991,** *24* (19), 5288; (b) Hu, W. G.; Boeffel, C.; Schmidt-Rohr, K., *Macromolecules* **1999,** *32* (5), 1611.

97. Yu, Y.; DesLauriers, P. J.; Rohlfing, D. C., *Polymer* **2005,** *46* (14), 5165.

98. Randall, J. C., *Journal of Macromolecular Science—Reviews in Macromolecular Chemistry and Physics* **1989,** *29* (2-3), 201.

99. (a) Earl, W. L.; VanderHart, D. L., *Macromolecules* **1979,** *12* (4), 762; (b) Tonelli, A. E. X., *NMR spectroscopy and polymer microstructure: the conformational connection*. Titles Supplied by John Wiley & Sons Australia: 1989.

100. Bärenwald, R.; Goerlitz, S.; Godehardt, R.; Osichow, A.; Tong, Q.; Krumova, M.; Mecking, S.; Saalwächter, K., *Macromolecules* **2014,** *47* (15), 5163.

101. (a) Beginn, U., *Colloid and polymer science* **2008,** *286* (13), 1465; (b) Wang, J.-S.; Matyjaszewski, K., *Macromolecules* **1995,** *28* (23), 7901; (c) Jakubowski, W.; Juhari, A.; Best, A.; Koynov, K.; Pakula, T.; Matyjaszewski, K., *Polymer* **2008,** *49* (6), 1567; (d) Gallow, K. C.; Jhon, Y. K.; Tang, W.; Genzer, J.; Loo, Y. L., *Journal of Polymer Science Part B: Polymer Physics* **2011,** *49* (9), 629; (e) Mok, M. M.; Pujari, S.; Burghardt, W. R.; Dettmer, C. M.; Nguyen, S. T.; Ellison, C. J.; Torkelson, J. M., *Macromolecules* **2008,** *41* (15), 5818; (f) Tito, N. B.; Milner, S. T.; Lipson, J. E. G., *Macromolecules* **2010,** *43* (24), 10612.

102. (a) Mok, M. M.; Ellison, C. J.; Torkelson, J. M., *Macromolecules* **2011,** *44* (15), 6220; (b) Mok, M. M.; Kim, J.; Wong, C. L. H.; Marrou, S. R.; Woo, D. J.; Dettmer, C. M.; Nguyen, S. T.; Ellison, C. J.; Shull, K. R.; Torkelson, J. M., *Macromolecules* **2009,** *42* (20), 7863; (c) Mok, M. M.; Masser, K. A.; Runt, J.; Torkelson, J. M., *Macromolecules* **2010,** *43* (13), 5740; (d) Jiang, R.; Jin, Q.; Li, B.; Ding, D.; Wickham, R. A.; Shi, A.-C., *Macromolecules* **2008,** *41* (14), 5457.

103. Yuan, W.; Mok, M. M.; Kim, J.; Wong, C. L. H.; Dettmer, C. M.; Nguyen, S. T.; Torkelson, J. M.; Shull, K. R., *Langmuir* **2009,** *26* (5), 3261.

104. Ribaut, T.; Oberdisse, J.; Annighofer, B.; Fournel, B.; Sarrade, S.; Haller, H.; Lacroix-Desmazes, P., *The Journal of Physical Chemistry B* **2011,** *115* (5), 836.

105. (a) Mauri, M.; Thomann, Y.; Schneider, H.; Saalwächter, K., *Solid state nuclear magnetic resonance* **2008,** *34* (1), 125; (b) Thomann, Y.; Thomann, R.; Hasenhindl, A.; Mülhaupt, R.; Heck, B.; Knoll, K.; Steininger, H.; Saalwächter, K., *Macromolecules* **2009,** *42* (15), 5684; (c) Saalwächter, K., *Progress in Nuclear Magnetic Resonance Spectroscopy* **2007,** *51* (1), 1.

106. Litvinov, V. M.; Penning, J. P., *Macromolecular Chemistry and Physics* **2004,** *205* (13), 1721.

107. Wang, X.; Coleman, J.; Jia, X.; White, J. L., *The Journal of Physical Chemistry B* **2002,** *106* (19), 4941.

108. Jouenne, S.; Gonzalez-Leon, J. A.; Ruzette, A.-V.; Lodefier, P.; Tence-Girault, S.; Leibler, L., *Macromolecules* **2007,** *40* (7), 2432.

109. White, J. L.; Beck, L. W.; Ferguson, D. B.; Haw, J. F., *Journal of Magnetic Resonance (1969)* **1992,** *100* (2), 336.

110. Andrew Clough, J. L. S., Arifuzzaman Tapash, Lance Gill, Nitin V. Patil, Joe Zhou, and Jeffery L. White, *Macromolecules* **2014,** *47* (8), 2625.

9 APPENDICES

In this appendix, the original EASY, modified-EASY (version 1) and modified-EASY (version 2) pulse program is included. In addition, the method of finding the best TPPM decoupling conditions is also briefly discussed.

9.1 Original EASY Pulse Program:

The pulse program code for the EASY experiment is given here-

```
;EASY_2d_NOESup.rel
;Stator background suppresion program with decoupling for X nuclei
;by Jaeger and Hemmann (Solid State NMR, Vol 57-58, p 22-28, 2014)
;zg with background and ringing removal
;uses double buffering, set 2D experiment with TD1 = 2
;set NBL=2 (use two buffers)
;l4: additional scans: total number of scans: 2*NS times l4
;pl1: X power level
;p1: X 90 pulse
;pl13: decoupling power
```

```
#include <Avance.incl>
#include <preamp.incl>
                        ;protects HP preamps during pulse
#include <powswi.incl>
                        ;enables HP transmitter gain switching
                        ;if new style 400V boards are available
#include <trigg.incl>
                        ;this provides a trigger output from
                        ;HP router BNC NMR5-13
#include <observe.incl>
                        ;this is only necessary for 3 channel
                        ;SE-451 and uxnmr versions before
                        ;vs. xwin-nmr.a.9
;the following lines are not necessary starting with xwin-nmr.a.9
;obsf1                  ;remove semicolon for X-observation on F1
;obsf2                  ;remove semicolon for 1H observation on F2
;obsf3                  ;remove semicolon for F3 observation
10u pl1:f1              ;set pl1 for F1 (default)
1 ze                    ;set RCU to replace mode
 10m pl13:f2            ;set decoupling power
2 1m do:f2
```

```
;#include <praq.prot>
 10u st0                ;set first buffer as current
 d1                     ;delay before the first acquisition pulse (τ1)
3 1u protect            ;protect all preamps
 trigg                  ;provide a scope trigger at HP router
 3u:f1 ph1              ;this line is not necessary if phaspr is set to
                        ;3u in edscon
 (p1 ph1):f1            ;the first acquisition pulse
;-------------------------------
;  scan 1
;-------------------------------
 1u cw:f2               ;turn on CW proton decoupling at power pl2
 d3:f1 ph0              ;reset the RF phase for detection, dead time delay
 goscnp ph31
 1m do:f2               ;make sure the adc is finished
 10u st                 ;set second buffer as current
 d7                     ;delay before the second acquisition pulse (τ2)
;-------------------------------
;  scan 2
;-------------------------------
 (p1 ph1):f1            ;the second acquisition pulse
```

```
 1u cw:f2                ;turn on CW proton decoupling at power pl2
 d3:f1 ph0               ;reset the RF phase for detection, dead time delay
 go=2 ph31               ;complete phase cycle
 1m do:f2
 10m wr #0               ;write buffer to memory after NS scans
 lo to 2 times l4
HaltAcqu, 1m
exit
ph0= 0                   ;constant phase for acquisition
ph1= 0 2 2 0 1 3 3 1     ;excitation pulse phase list
ph31=0 2 2 0 1 3 3 1     ;signal routing corresponds to pulse phase list
```

9.2 Modified-EASY (version 1)

The modified-EASY (version-1) pulse program code is given below-

```
;EASY_2d_NOESup_5plstrn(version1).rel
;Modified from stator background suppresion program with decoupling ;for X nuclei
;by Jaeger and Hemmann (Solid State NMR, Vol 57-58, p 22-28, 2014)
;zg with background and ringing removal
;uses double buffering, set 2D experiment with TD1 = 2
;set NBL=2 (use two buffers)
;l4: additional scans: total number of scans: 2*NS times l4
```

```
;pl1: X power level
;p1: X 90 pulse
;pl13: decoupling power
#include <Avance.incl>
#include <preamp.incl>
                        ;protects HP preamps during pulse
#include <powswi.incl>
                        ;enables HP transmitter gain switching
                        ;if new style 400V boards are available
#include <trigg.incl>
                        ;this provides a trigger output from
                        ;HP router BNC NMR5-13
#include <observe.incl>
                        ;this is only necessary for 3 channel
                        ;SE-451 and uxnmr versions before
                        ;vs. xwin-nmr.a.9
;the following lines are not necessary starting with xwin-nmr.a.9
;obsf1                  ;remove semicolon for X-observation on F1
;obsf2                  ;remove semicolon for 1H observation on F2
;obsf3                  ;remove semicolon for F3 observation
```

```
10u pl1:f1              ;set pl1 for F1 (default)
1 ze                    ;set RCU to replace mode
 10m pl13:f2            ;set decoupling power
2 1m do:f2
;#include <praq.prot>
 10u st0                ;set first buffer as current
 d1                     ;delay before the first acquisition pulse (τ1)
3 1u protect            ;protect all preamps
 trigg                  ;provide a scope trigger at HP router
 3u:f1 ph1              ;this line is not necessary if phaspr is set to
                        ;3u in edscon
 (p1 ph1):f1            ;the first acquisition pulse
;-------------------------------
;  scan 1
;-------------------------------
 1u cw:f2               ;turn on CW proton decoupling at power pl2
 d3:f1 ph0              ;reset the RF phase for detection, dead time delay
 gosc ph31
 1m do:f2               ;make sure the adc is finished
 10u st                 ;set second buffer as current
 d7                     ;delay after the first acquisition
```

```
;-------------------------------
;  scan 2
;-------------------------------
 3u:f1 ph1                ;this line is not necessary if phaspr is set to
                          ;3u in edscon
;-----Spoiler pulse train starts here----------------------------
;-----Spoiler pulse=1-----------------------------------------
 (p2 ph2):f1              ;90 degree spoiler pulse at carbon channel
  d2                      ;delay between two spoiler pulses, set d2=1 sec
;-----Spoiler pulse=2-----------------------------------------
 (p2 ph2):f1              ;90 degree spoiler pulse at carbon channel
  d2                      ;delay between two spoiler pulse, set d2=1 sec
;-----Spoiler pulse=3-----------------------------------------
 (p2 ph2):f1              ;90 degree spoiler pulse at carbon channel
  d2                      ;delay between two spoiler pulse, set d2=1 sec
;-----Spoiler pulse=4-----------------------------------------
 (p2 ph2):f1              ;90 degree spoiler pulse at carbon channel
  d2                      ;delay between two spoiler pulse, set d2=1 sec
;-----Spoiler pulse=5-----------------------------------------
 (p2 ph2):f1              ;90 degree spoiler pulse at carbon channel
  d2                      ;delay before the second acquisition pulse (τ2)
```

```
;-----Spoiler pulse train ends here------------------------------

 (p1 ph1):f1            ;the second acquisition pulse

 1u cw:f2               ;turn on CW proton decoupling at power pl2

 d3:f1 ph0              ;reset the RF phase for detection, dead time delay

 go=2 ph31              ;complete phase cycle

 1m do:f2

 10m wr #0              ;write buffer to memory after NS scans

 zd

 lo to 2 times l4

HaltAcqu, 1m

exit

ph0= 0                  ;constant phase for acquisition

ph1= 0 1 2 3            ;excitation pulse phase list

ph2= 0 1 2 3            ;phase list for spoiler pulse

ph31=0 1 2 3            ;signal routing corresponds to pulse phase list
```

9.3 Modified-EASY (version 2)

The pulse program of modified-EASY (version -2) is given here

```
;EASY_cpd_1spoilerpulse_tapash(version2).rel

;Modified from stator background suppresion program with decoupling ;for X nuclei
```

```
;by Jaeger and Hemmann (Solid State NMR, Vol 57-58, p 22-28, 2014)

;zg with background and ringing removal

;NOE suppression pulse added before both acquisition pulse, remove ;semicolone if NOEsup required

;uses double buffering, set 2D experiment with TD1 = 2

;set NBL=2 (use two buffers)

;l4: additional scans: total number of scans: 2*NS times l4

;pl1: X power level

;p1: X 90 pulse

;pl13: decoupling power

#include <Avance.incl>

#include <preamp.incl>

                    ;protects HP preamps during pulse

#include <powswi.incl>

                    ;enables HP transmitter gain switching

                    ;if new style 400V boards are available

#include <trigg.incl>

                    ;this provides a trigger output from

                    ;HP router BNC NMR5-13

#include <observe.incl>

                    ;this is only necessary for 3 channel
```

```
                        ;SE-451 and uxnmr versions before
                        ;vs. xwin-nmr.a.9
;the following lines are not necessary starting with xwin-nmr.a.9
;obsf1                  ;remove semicolon for X-observation on F1
;obsf2                  ;remove semicolon for 1H observation on F2
;obsf3                  ;remove semicolon for F3 observation
10u pl1:f1              ;set pl1 for F1 (default)
1 ze                    ;set RCU to replace mode
 10m pl13:f2            ;set decoupling power
2 1m do:f2
;#include <praq.prot>
 10u st0                ;set first buffer as current
 d1                     ;delay before the first acquisition pulse (τ1)
3 1u protect            ;protect all preamps
 trigg                  ;provide a scope trigger at HP router
 3u:f1 ph1              ;this line is not necessary if phaspr is set to
                        ;3u in edscon
 (p1 ph1):f1            ;the first acquisition pulse
;-------------------------------
;  scan 1
;-------------------------------
```

```
 1u cpd2:f2 ph4          ;turn on tppm(composite pulse decoupling) proton
                         ;decoupling at power pl13

 d3:f1 ph0               ;reset the RF phase for detection, dead time delay

 goscnp ph31

 1m do:f2                ;make sure the adc is finished

 10u st                  ;set second buffer as current

 d7                      ;delay between the first acquisition and the spoiler ;pulse

;-------------(90 pulse to saturate crystal intensity------------

 (p2 ph2):f1             ;spoiler pulse to avoid NOE enhancement

 d2                      ;delay before the second acquisition pulse (τ2)

;----------------------------------------------------------------

;-------------------------------

;  scan 2

;-------------------------------

 (p1 ph1):f1             ;second acquisition pulse

 1u cpd3:f2 ph4          ;turn on tppm(cpd3) proton decoupling at power pl13

 d3:f1 ph0               ;reset the RF phase for detection, dead time delay

 go=2 ph31               ;complete phase cycle

 1m do:f2

 10m wr #0               ;write buffer to memory after NS scans

 lo to 2 times l4
```

```
HaltAcqu, 1m

exit

ph0= 0                  ;constant phase for acquisition

ph1= 0 2 2 0 1 3 3 1    ;excitation pulse phase list

ph2= 0 2 2 0 1 3 3 1    ;phase list for spoiler pulse

ph4= 0                  ;phase list for cpd decoupling

ph31=0 2 2 0 1 3 3 1    ;signal routing corresponds to pulse phase list
```

9.4 Optimization of TPPM Conditions

The data presented in Chapter 5 were acquired using the modified-EASY (version 2) pulse program with TPPM decoupling. As the TPPM decoupling conditions are sensitive to various experimental conditions, and can change from experiment to experiment, the best conditions were optimized before each of the experiments. The method of optimizing the best TPPM conditions is briefly described here:

In TPPM decoupling two parameters need to be optimized for the best decoupling, 1) the phase angle (ϕ), and 2) the duration of the composite decoupling pulse (pcpd). For the best decoupling efficiency, the 'pcpd' should be near to 180° pulse but shouldn't be equal to 180°. For the different experiments, the proton decoupling power was not exactly the same, so, the pcpd need to be optimized every time before each of the experiments.

The TPPM decoupling gives a better result only at high spinning speed and at high decoupling power. The MAS speed should be at least 12 kHz and the proton decoupling power should be high enough to get the ν_{1H} at least 100 KHz. For our experiments, we spun our samples at ca. 12 kHz at MAS and the

proton nutation frequency was 100 kHz. The only method of determining the best TPPM decoupling is to run experiments with changing conditions and compare the line-width (or peak height) of the spectra. As the direct polarization experiment is too long (due to very long T_1 relaxation time), cross-polarization method was utilized for the TPPM decoupling condition optimization.

The cross-polarization experimental parameters or CP conditions (carbon channel power level for the contact pulse (pl1), proton 90° pulse duration (p3), proton power level for the contact pulse (pl2) and proton decoupling power for CP experiment (pl12)) were optimized first to get the Hartmann-Hahn condition ($\gamma_H B_{1H} = \gamma_C B_{1C}$) using hexamethylbenzene (HMB) standard sample.

To find the TPPM conditions, several CP experiments were run on the specific sample. The starting phase angle value for the TPPM decoupling was taken as 15°, and the starting pcpd was ca. 180° pulse for proton at a specific decoupling power. Several experiments with different pcpd were run keeping the phase angle same, and the best pcpd value was determined from the peak intensity. Then using that pcpd, phase angle was optimized in a similar way. After getting the optimized phase angle, the pcpd value was again tested for that specific phase angle. This procedure was done before running every sample.

VITA

Arifuzzaman Tapash

Candidate for the Degree of

Doctor of Philosophy

Thesis: A NEW SOLID-STATE NMR METHOD REVEALS THE INFLUENCE OF CHAIN STRUCTURE AND THERMAL HISTORY ON THE CRYSTAL-AMORPHOUS INTERFACE IN POLYETHYLENES

Major Field: Chemistry

Biographical:

Education:

Completed the requirements for the Doctor of Philosophy in Chemistry at Oklahoma State University, Stillwater, Oklahoma in May 2016.

Completed the requirements for the Master of Science in Applied Chemistry & Chemical Engineering at University of Dhaka, Dhaka in 2006.

Completed the requirements for the Bachelor of Science in Applied Chemistry & Chemical Technology at University of Dhaka, Dhaka in 2005.

Experience: Worked as a graduate research assistant at Oklahoma State University from August 2010 to present under Dr. Jeffery L. White.

Professional Memberships: American Chemical Society